UCL
Université catholique de Louvain

École polytechnique de Louvain (EPL)

epl

Hybridization of combustion power plants with concentrated solar power

Dissertation presented by
Axel Gérard

for obtaining the Master's degree in
Mechanical Engineering

Supervisors
Hervé Jeanmart, Jean Snoeck

Readers
Yann Bartosiewicz, Gauthier Limpens

Academic year 2017-2018

Aknowledgements

I express my profound gratitude to my supervisors, Prof. Hervé Jeanmart and Mr. Jean Snoeck for their availability, their continuous guidance and their interest in my work. I also highly appreciated the freedom I had to propose and develop my own master thesis subject.

I would also like to thank Mr Bernard Marié, my supervisor in Tractebel Engineering, for the opportunity I had to do an internship linked with my master thesis and for the guidance throughout the year. In addition, I especially appreciated the collaboration with the team I have been part of during my internship for their help and for sharing their experiences. Finally, I thank Mr. Jan Vermeir (Engie) who devoted time to help me for the economical part of my work.

Moreover, I am grateful to Prof. Yann Bartosiewicz and Mr. Gauthier Limpens for accepting to read this document, for spending time to assess my work and also for giving me the opportunity to build the basis of my Master thesis through the project of the course Thermal cycles, which was my favourite project of my studies. In this respect, I would also like to give a special thanks to Maxime Lejeune, with whom I set up the program.

Last but not least, I thank my family, my friends and the secretary of the IMMC division, Mrs Isabelle Hennau, for their continuous support and encouragement.

Contents

Nomenclature

Acronyms

Symbol	**Description**
$SAGT_{cc}$	Hybridized gas turbine integrated in a combined cycle
BE	break-even
CAPEX	capital expenditures in [$]
CSP	Concentrated solar power
DB	Duct burner
DNI	Direct normal irradiance in $[W/m^2]$
HRGT	Heat recovery gas turbine
HRSG	Heat recovery steam generator
ISCC	Integrated solar combined cycle
LCOE	Levelized cost of energy in [$/kWh]
LHV	Low heating value of the fuel in [MJ/kg] or [kJ/kg]
NGCC	Natural gas combined cycle
NGT	Natural gas turbine
NTU	Number of transfer units, characterising the heat transfer.
OPEX	Operating expenses in [$]
SAGT	Solar aided gas turbine
SAHRGT	Solar aided heat recovery gas turbine
SHX	Solar heat exchanger

Definitions

Symbol	**Description**
$\dot{Q}$	heat load in kW
$Q = \Delta h$	specific heat load in kJ/kg

Parameters

Symbol	Description
$\dot{Q}_{sol}$	solar heat flux injected in the power plant in [MW]
η_{conc}	Concentration efficiency of solar radiation between the aperture collector area and the solar receiver area
η_{it}	isentropic efficiency of the steam turbines
η_{mec}	mechanical efficiency of the cycle, modelling the mechanical losses in the turbine
η_{piC}	polytropic efficiency of the air compressor modelling irreversibilities and aerodynamic losses
η_{piT}	polytropic efficiency of the gas turbine modelling irreversibilities and aerodynamic losses
ϕ_{in}	relative humidity of the ambient air
dta	difference between the HP superheater outlet temperature and the gas inlet temperature in the recovery boiler
$Fuel$	type of fuel burned in the combustion chamber, it may be CH4 or C12H23
k_{cc}	pressure ratio modelling the pressure losses in the combustion chamber
k_{mec}	fraction of the sum of the motor power at the compressor and the turbine, absorbed by the auxiliaries and dissipated by the mechanical friction
nfh	number of feed heater (with steam extraction from the turbine) in the steam cycle
p_{HP}	high pressure in the steam cycle
Pe	effective power produced by the cycle
$pinch$	lowest temperature difference between the flue gas and the water/steam in the heat recovery steam generator (at the evaporator water inlet)
$pinch_{sol}$	temperature pinch between the outlet fluid temperature of the solar heat exchanger and the solar receiver temperature
$postcomb$	allows to activate or deactivate the post combustion between the gas turbine outlet and the HRSG gas inlet
$quality$	vapor fraction at the steam turbine outlet
r_c	gas turbine compression ratio between the atmospheric pressure and the outlet pressure of the compressor
T_H	maximum temperature allowed at the outlet of the combustion chamber (= at the inlet of the turbine)
T_{air}	ambient air temperature
T_C	condenser temperature in the steam cycle
C	Concentration ratio between the aperture collector area and the solar receiver area

Chapter 1

Foreword

In a world where power generation produces a lot of greenhouse gases, where the demand for energy is growing and where the economy is strongly linked to energy, the energy sector is facing gigantic challenges. This work will focus on one possible solution to these challenges: the hybridisation of thermal combustion power plants with concentrated solar power (CSP). Indeed, this integration provides synergies between these two technologies of power generation because both technologies provide a source of high temperature heat. In fact, despite the growing development of renewable energy sources, an ongoing role for fossil fuels is anticipated. This need of both energy sources leads to several advantages to integrate them. Actually, what are the incentives of integrating a solar field in a combustion power plant ? The advantages of the hybridization are firstly listed regarding the combustion power plants and then concerning the CSP power plants.

The main goal for the combustion power plant is obviously to reduce the CO_2 emissions by using the CO_2 free solar energy in order to limit greenhouse gases and therefore to limit the global warming of our planet. Indeed, countries are increasingly looking toward renewable sources to meet their energy requirements and to reduce their carbon footprint. From an economic point of view, this hybridisation seems not interesting compared to a standalone combustion power plant because of the higher investment cost of the solar field (than combustion power plants). Nevertheless, one may expect the appearance in more and more countries of a tax on CO_2 high enough to make the hybrid economically interesting. In addition, one may expect an increase in the price of fuel in the future due to the demand growth and due to the increasing difficulty to extract fuels from the earth. Consequently, it has to be established if the reduction in fuel consumption due to the use of "free" solar energy would be sufficient to make the hybrid more profitable. To conclude, the development of such a technology is driven by the potential to provide cost-effective CO_2 mitigation.

On the CSP side, as renewable energies are really intermittent because they depend on the weather, they cannot be used alone to supply the electricity grid. Storage or other energy sources are needed to compensate for the intermittency of renewable energies. This interconnection can be done on the grid level but also on the plant level. The latter case consists of directly backup the concentrated solar power generation with fuel-based power generation on the same geographical site. By doing that, the power plant is able to provide dispatchable power (power available on demand). Therefore, the hybridisation ensures a better reliability and flexibility of the power plant, which is very important because the frequency on the grid must stay constant in order to avoid damage to the grid. In addition, this intermittency results in low plant capacity factor (the ratio of the total actual energy produced or supplied over a definite period, to the energy that would have been produced if the plant had operated continuously at the maximum rating) in order to reduce the probability of an unscheduled reduction in output power and thus it decreases the efficiency of standalone CSP.
Moreover, CSP suffers from a very high investment cost, higher than conventional combustion

power plants. Consequently, the hybridisation with the cheaper and more efficient combustion power generation is very interesting. The consequence is that hybridisation will also enable CSP plants to be established in regions with moderate direct normal irradiance (because profitable even with a lower DNI), thereby moving it away from arid regions and closer to load centres, where energy demand is the highest.
Another indirect advantage is that hybridisation offers to CSP to increase the cost effectiveness of thermal energy storage by enabling the capacity of the storage to be optimised independent of any commitments to meet supply. Indeed, the maximum economic utilisation of the storage occurs at much smaller storage capacities than that needed to maintain firm supply.
As a conclusion, hybridisation will enable earlier and deeper penetration of solar thermal renewable source into the energy market by increasing the efficiency and the reliability and by reducing the cost of the power plant.

Another question that can be asked is **"Why choose solar energy and no other renewable energies?"** As mentioned previously, the choice of this renewable energy (solar energy) offers many synergies with the combustion energy as these two technologies are technically compatible. Indeed, both power generation processes follow the same process. A working fluid is pressurised, heated, and then expanded through a turbine. This compatibility allows the equipment sharing. Typically for the strongly synergistic hybrids only the heat generation and the heat exchanger are separated, the rest is shared. This reduces drastically the investment cost. Another advantage is that this compatibility allows operation optimisation. For example, it is well known that the efficiency of a turbine decreases when the turbine is turned down. If the renewable plant is totally separated from the combustion plant, an increase of the power generated by the solar plant will result in a decrease of the power generated by the combustion plant and so in a decrease in efficiency of the combustion power plant. On the contrary if the energy sources are totally compatible, they shared the turbine and so the decrease in power from one source of energy can be compensated by an increase in power of the other energy source, which results in a constant turbine efficiency. In addition, the solar energy storage can also be shared with the combustion power plant as both technologies are temperature compatible, i.e. both technologies can achieve the temperature required at the turbine inlet.

A last question would be **"Why not use solar photovoltaic (PV) technologies in order to hybridise combustion power plant or why not use PV standalone?"** Actually, PV is a promising technology with falling costs in recent years and is really simple but its variable power output makes it necessary to use fossil fuel backup or storage. The problem for the first case is that there is no synergy between PV and combustion power plant, so it is not really interesting to combine these two technologies, as explained in the previous paragraph. For the second case, the storage used to maintain a firm supply is the expensive battery technology. The problem is that the electricity storage is much more expensive than the thermal storage, that is why using PV panels is not interesting in power plants that have to maintain a firm supply. Furthermore, the cost of material extraction for the batteries is expected to increase in the future.

To conclude, this work attempts firstly to provide a general view of the possible hybridization systems in the next chapter (chapter 2). At the end of the chapter 2, one category of hybridization process is chosen and is analysed thermodynamically in the Chapters 3 and 4 in order to determine the most efficient solution. Subsequently, an economic analysis is carried out with a view to determine the most profitable system. Finally, as this Master thesis was realised in partnership with Tractebel Engineering (where an internship was achieved), the company allowed the use of a well-developed heat and mass balance software, Thermoflow. Therefore, this enabled the application of the theory developed in the chapters 3, 4 and 5 through the modelling of an existing hybridized power plant, as explained in the chapter 6.

Chapter 2

Hybrid power plants: a review

Before studying in detail such hybridization option, it is very important to review what exists currently on the market. That is exactly what is done in this section. This review is based on the following papers [23, 2, 26, 27, 7]. In order to assess the type and the quality of the hybridization, a classification is proposed.

2.1 Classification

2.1.1 Classification by solar share

The solar share is defined as the fraction of the total input energy to the plant, that is supplied by the sun. It is important to consider an annually averaged value.

- Solar aided Combustion Generation: solar share is below 33%.
- Balanced Solar-Combustion Generation: solar share is between 33% and 66%.
- Combustion Aided Solar Generation: solar share is above 66 %.

This work will be focused on Solar aided combustion generation because it is the cheaper, the more efficient and the more reliable case.

2.1.2 Classification by extent of integration

Here, the criterion assesses the extent of integration (synergy) between CSP and combustion. Thus, this evaluates also the potential to reduce capital cost and energy losses through hybridization.

- Auxiliary: shares only the supporting infrastructure, such as electrical cabling and control systems.
- Indirect: transfers chemical stuff from a solar thermochemical cycle to a power cycle or vice versa. Shares also auxiliaries.
- Semi-direct: shares the major non-solar components of the solar and combustion power cycle (e.g. turbine, condenser, pump). Shares also the auxiliaries.
- Direct: shares the solar and combustion thermal harvesting equipment (e.g. receiver and combustor), together with the semi direct and auxiliary components.

This work will be focused on Semi-direct solutions because the direct solutions are in the research state and the other are not synergistic enough.

2.1.3 Classification by comparison with the best alternative options

Here, the hybrid performance is compared with the state-of-the-art stand-alone technology.

- Solar positive - combustion negative hybrid: A system efficiency that equals or exceeds the efficiency of the best stand-alone solar plant, but not of the best stand-alone combustion plant.
- Solar negative - combustion positive hybrid: A system efficiency that equals or exceeds the efficiency of the best stand-alone combustion plant, but not of the best stand-alone solar plant.
- Solar positive - Combustion positive hybrid: A system efficiency that equals or exceeds the efficiency of both best solar plant and best combustion plant.

Unfortunately, at the present, the hybridised power plants are only solar positive - combustion negative hybrids from the thermodynamic point of view because of the high radiation intensity of the sun and the low efficiency of the energy transformation to heat. However, hybrids can be solar positive - combustion positive from the economical point of view thanks to the free solar energy.

2.2 Solar field

It is very important to understand how the solar field works in order to evaluate the attractiveness of the different hybridization solutions.

2.2.1 Different CSP technology families

The solar field consists of collectors that concentrate solar energy on receivers. At present, there are four main ways of arranging the collectors and the receivers.

Parabolic troughs: This system consists of parallel rows of mirrors curved in one dimension to focus the sun's rays on an absorber tube. The mirrors and the absorber tubes move in tandem with the sun as it crosses the sky. The working fluid that passes through the tubes is synthetic oil. The oil preheats, evaporates and superheats water in a heat exchanger. Therefore, it is an indirect steam generation. Parabolic troughs are the most mature of the CSP technologies and form the bulk of the current commercial plants.

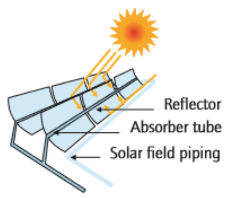

Figure 2.1: Parabolic troughs [2]

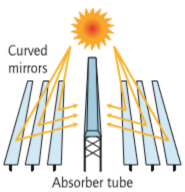

Figure 2.2: Linear fresnels [2]

Linear Fresnel reflectors. Here the mirrors are flat or slightly curved and the sun's rays are concentrated on a downward-facing linear, fixed receiver. The main advantage is thus the simple design that requires lower investment. Indeed, it facilitates the direct steam generator (water directly preheated evaporated and superheated in the tubes). This allows also higher temperatures and a second fluid which would have to be pumped is not needed (reduces heat transfer losses too). However, this system is less efficient in converting solar energy to electricity than parabolic troughs.

The parabolic dish concentrates the sun's rays at a focal point propped above the centre of the dish. The dish and the receiver move in tandem with the sun. This system is mostly a direct steam generator. Dishes offer the highest solar-to-electric conversion performance of any CSP system. The compact size and the low compatibility with thermal storage put this system in competition with photovoltaic panels.

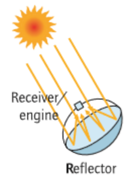

Figure 2.3: Parabolic dish [2]

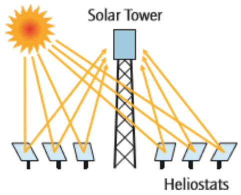

Figure 2.4: Solar tower [2]

Solar towers. This system uses hundreds or thousands of small reflectors to focus the sun's rays on a central receiver placed atop a fixed tower. Direct and indirect steam generation are possible. This concept achieves very high temperatures and is highly flexible but is quite expensive.

In order to summarize, the line focus receiver (the first two ones) track the sun along a single axis, making the device more simple than the point focus receiver (the last two ones) which tracks the sun along two axis but which allows higher temperatures. Furthermore, the Linear Fresnels and the towers are fixed, which ease the transport of collected heat to the power block, compared to the mobile receiver (parabolic receiver) which is able to collect more energy.

2.2.2 General considerations

In order to assess the total efficiency of the solar field integration in the combustion power plant, a good indicator is the efficiency of the solar thermal power generation. It is the ratio between the effective power obtained at the turbine and the solar flux. This latter is equal to the product of the aperture collector area and the direct solar normal irradiance of the sun, the DNI, expressed in $\mathrm{W\,m^{-2}}$. This efficiency is also equal to the product of

- the efficiency of absorption of the high temperature heat by the solar receiver, $\eta_{en,\,sol-field}$. This efficiency is equal to the difference between the efficiency of concentrating the direct normal irradiance, η_{conc}, and the heat loss coefficient of the receiver, ϵ_{loss}.
- the efficiency of the heat conversion into power by the heat engine $\eta_{en,\,sol-heat}$.

Therefore, the solar radiation-to-electrical efficiency is equal to

$$\eta_{en,\,sol-rad} = \frac{\Delta Pe_{SC}}{A_{coll}DNI} = \eta_{en,\,sol-field} \cdot \eta_{en,\,sol-heat} = (\eta_{conc} - \epsilon_{loss}) \cdot \eta_{en,\,sol-heat} \tag{2.1}$$

where ΔPe_{SC} is the difference between the power produced by the integrated solar combined cycle and the stand-alone combined cycle without solar field but with exactly the same parameters. (same fuel consumption).

In this section, only the maximum theoretical solar radiation-to-electrical energy conversion efficiency is considered, which means that are considered an ideal solar concentrator (no reflectivity or spillage losses), thus $\eta_{conc} = 1$, an ideal solar receiver (only radiation losses modelled as blackbody absorption, no convection/conduction heat losses), and an ideal heat engine (Carnot). Thus:

$$\eta_{en,\,sol-rad,\,ideal} = \left[1 - \left(\frac{\sigma T_H^4}{C \cdot DNI}\right)\right] \cdot \left[1 - \left(\frac{T_L}{T_H}\right)\right] \tag{2.2}$$

where C is the concentration ratio, the ratio between the collector area and the receiver area. $\sigma = 5,67 <, 10^{-8}\,\mathrm{W\,m^{-2}\,K^{-4}}$ is the Stefan-Boltzmann constant. T_H and T_L are expressed in

Kelvin and are respectively the upper and lower operating temperature of the equivalent Carnot heat engine. Note that the receiver temperature is approximated to T_H by considering that the solar heat exchanger is in parallel with the combustion chamber/boiler (in practice this approximation is not often true). Below is the graph of the solar radiation-to-electrical efficiency with respect to T_H, for different concentration ratios.

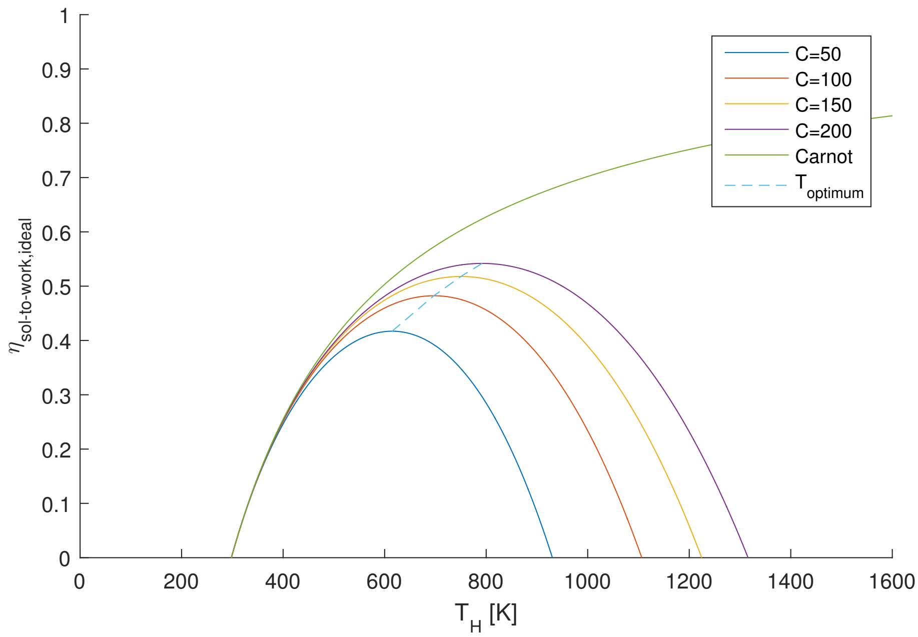

Figure 2.5: $\eta_{rad-to-elec,ideal}$ with respect to T_H

As it can be seen on the graph it is desirable to operate the heat engine at the highest possible temperature from the perspective of the Carnot cycle. On the other side, from the perspective of the receiver it is desirable to lower T_H in order to minimise the radiation losses. As a result, the compromise between these two effects leads to an optimum temperature. As a consequence, there is an incentive to put the combustion downstream, rather than upstream from the receiver. By doing that it is possible to minimise the receiver temperature and in the same time to maximise the high temperature of the power cycle. Moreover, by increasing T_H, the increase in efficiency must be weighed against the additional cost of high temperature materials. (when air is the working fluid, the enthalpy does not need to be transferred through a wall offering the potential to mitigate this limitation).

In addition, it can be observed that the optimal temperature is higher for higher concentration ratio's. This is because radiation losses can be reduced by increasing the concentration ratio of the concentrating optics. Nevertheless, the associated increase in efficiency must be weighed against the additional cost of high precision concentrating optics.

An important consequence of these considerations is the shape of the receivers. Indeed, it can be a tubular receiver surrounded by low emissivity material, allowing radiation to be collected from all directions maximising the economies of scale. This configuration is used for low receiver temperature. For higher temperatures, a cavity receiver is preferable because this lower the radiation losses. Nevertheless, this configuration has a lower thermal capacity due to the need to limit the collection angle from the collectors.

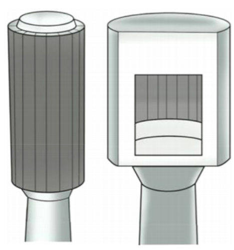

Figure 2.6: [23]

2.3 Hybridization with coal

First of all, coal has the advantage to be abundant, prevalent, and low-cost. It also produces high amounts of CO_2. Therefore, it is a good opportunity to use solar energy to retrofit existent power plants and mitigate CO_2 emissions. In addition, coal power plants have multiple possible points for injecting solar heat, as it will be described below. A summary table can be found in the appendices with the performance of the hybrids described below.

2.3.1 Solar-aided steam generation

The first solution is to use a solar field in parallel with a coal-fired boiler to supplement its heat, as it can be seen on the Figure 3.2. As seen in the previous section, it is interesting to minimise the solar receiver temperature while keeping a higher turbine inlet temperature. That is why the steam coming from the solar field is mixed to superheated steam in excess coming from the boiler in order to increase the steam cycle's efficiency. The problem with this dual source boiler configuration, is that the addition of solar generated steam may cause imbalances in the steam cycle. A high percentage of steam delivered by the solar field would reduce the coal generated steam and therefore would lead in less heat available for superheating, resulting in a lower steam cycle's efficiency. That is why solar fraction is limited with this configuration ($< 10\%$).

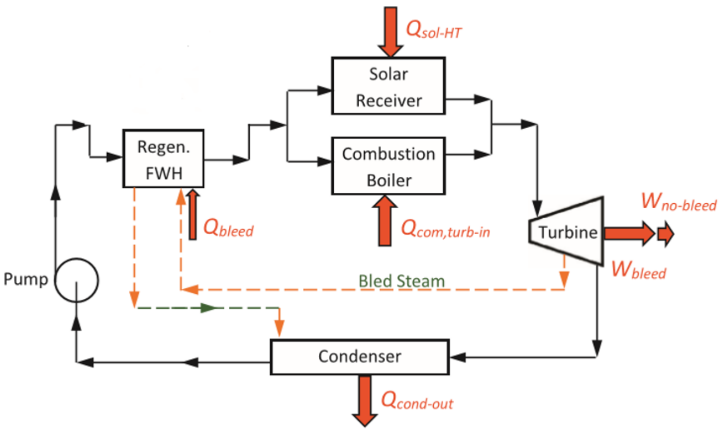

Figure 2.7: Solar aided steam generation in a Rankine cycle [23]

New designs are therefore required for achieving higher solar fractions, as shown on the figure below. Here the location of combustion heat input can be changed via the combustion gas bypass, allowing if needed, additional heat input after solar steam injection in order to superheat this solar steam.

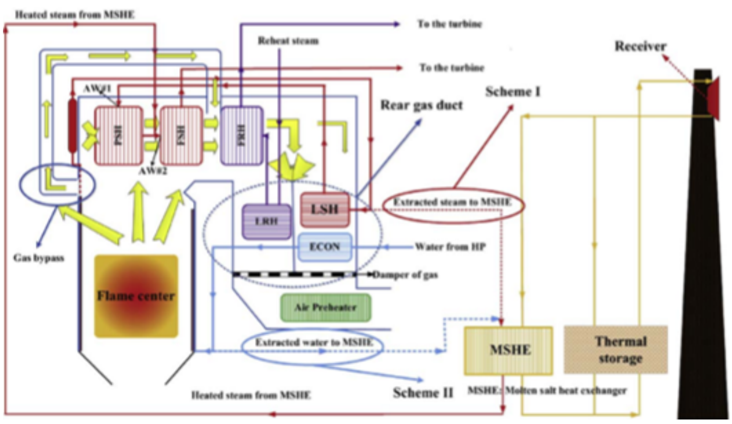

Figure 2.8: Dual-source boiler conguration [26]

To conclude, this type of hybridization is semi-direct and achieves higher efficiencies than standalone solar power plant due to the lower receiver temperature. Nevertheless, the receiver temperature stays quite high because of the need to produce high temperature steam to maximise the cycle's efficiency. The major advantage of this high temperature hybridization is its compatibility with thermal storage as the energy density is high. Zhang et al [34] demonstrated a solar radiation-to-electrical efficiency of 27.8% while stand alone parabolic troughs may achieve 15-20% efficiency with a maximum solar share of 6.1%.

2.3.2 Solar-aided boiler feedwater and air preheating

This type of hybridization is more often used than the previous system. Here the principle is to use solar energy to preheat feedwater upstream from the boiler. The water will then be evaporated and superheated by the boiler. The solar heated steam displaces high temperature steam that is otherwise extracted from the turbine to heat the feedwater. This result in increasing the power output. Another advantage is that the solar heat is collected at a low temperature, which reduces the radiation losses, while relying on combustion to provide high temperature steam in order to achieve high efficiency. However, due to the low energy density, the cost of low temperature thermal storage is high and thus the solar share is lower than for high temperature hybridization like in the previous section. Another advantage of this configuration is its flexibility as combustion is used to keep a stable electricity production despite the DNI fluctuation.

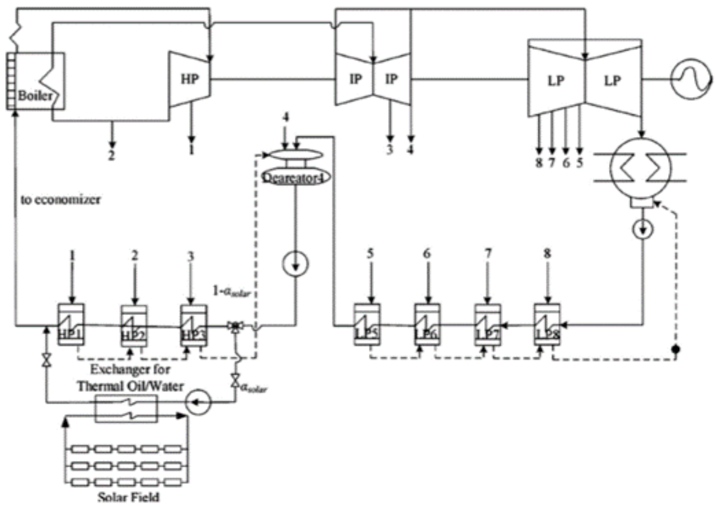

Figure 2.9: solar aided Rankine cycle in which feed water is heated by a solar field [23]

.

Another preheating concept is a system in which particles circulate in a central receiver configuration to collect solar heat. Then this heat is used to preheat the air injected in the boiler, needed for the combustion. The air can also be directly heated by the solar receiver.

To conclude, this solution is semi-direct and achieves higher efficiencies than standalone solar power plants due to its lower receiver temperature. An interesting fact is that the more this temperature is decreased, the more the efficiency difference between the hybrid and the standalone solar power plant is high. This is because the high temperature of the hybrid cycle remains constant thanks to the boiler. Thus higher is the gap between the solar receiver temperature and the inlet turbine temperature, higher is the gain in cycle's efficiency over the standalone solar power plant with the same solar receiver temperature. Yann et al. demonstrated for the feedwater preheating a solar radiation-to-electrical efficiency of 40.3% (max) with a solar share (max) of 10.3% [32] while Prosin et al. proposed a solar air preheating based system with a radiation-to-electrical of 22.3 % and a solar share of 7.8% [28].

2.3.3 Solar-aided post combustion CO_2 capture

Post-combustion carbon capture process is based on the use of solar energy to remove CO_2 from the exhaust gas in order to reduce the carbon footprint of the power plant. In the predominant technology, the flue gas is fed to an absorber column where a solvent is used to absorb CO_2. After that, the CO_2 rich solvent is sent to a stripper column where heat is used to remove the absorbed CO_2 from the solvent, which regenerates the solvent. Then this solvent is recycled back to the absorber column. By using heat coming from the solar field, extraction of steam from the turbine is no more needed, and so the power output is increased. Furthermore, this process does not require high temperatures, allowing high efficiency for the solar field. Another advantage of this system is that it is very easy to retrofit an existing plant as it only needs a connection to the flue gas stream from the boiler. Economically, this solution enables to sell the captured CO_2. A radiation-to-elec. efficiency of 27% with a solar share of 27.6% is observed by Zhao et al. [35].

2.3.4 Solar aided coal gasification with combined cycle

The coal is solid and therefore it has to be burn in a boiler. That is why the three previous hybrids are based on the less efficient Rankine cycle than gas/liquid-combustion based cycle. The cycle which achieves the highest efficiency is the combined cycle but the fuel used in this cycle has to be in the gaseous phase. That is why it can be advantageous to gasify the coal in order to be able to use it in a more efficient cycle than the Rankine cycle. The gasification of coal combines the efficiency benefits of a combined cycle power plant with an abundant fuel source in coal. Here the solar energy is used to partially oxidate carbonaceous fuel by exposing it to a limited amount of oxygen in a high temperature and high pressure environment. The reaction produces a CO and H_2 syngas that can be used in gas turbine for example.

2.4 Hybridization with natural gas

Natural gas is in fact the transition fuel because it provides dispatchability, low cost and reliability of fossil fuels, but has much lower CO_2 emissions than coal due to its low carbon-to-hydrogen ratio. Nevertheless, as natural gas is commonly used in gas turbines, it is more difficult to capture CO_2 than in a Rankine cycle because CO_2 is more diluted in the exhaust. Finally, natural gas is easily transportable through pipelines. A summary table can be found in the appendices with the performance of the different hybrids below.

2.4.1 Solar aided gas turbines

The principle here is to heat air by means of the solar field between the compressor and the turbine. Indeed, the preheating before the compressor is not efficient because by doing that, the work required for the compression would be much higher. The solar thermal energy injected after the compressor is actually employed together with the combustion to provide the heat needed before introduction of the gas to the gas turbine, as depicted in the figure below. The solar heat injection can be both direct or indirect and the solar field technology employed is point focus because of the high temperature needed. The challenge is that gas turbines operate at significantly high temperatures (higher than steam turbines), therefore injecting heat via solar requires high temperatures which presents some technical challenges on the collector end. On the other and, by replacing high temperature heat that is provided by the combustion of natural gas, the solar aided gas turbine has the potential to achieve high solar shares (higher than the Rankine cycles) and has a high compatibility with thermal storage. However, it was seen in the solar field section that a high temperature on the solar receiver is not desirable. As a consequence, the gas turbine hybridization suffers from the decrease in efficiency because of the high receiver temperature. That is why the best option is to inject solar heat before the

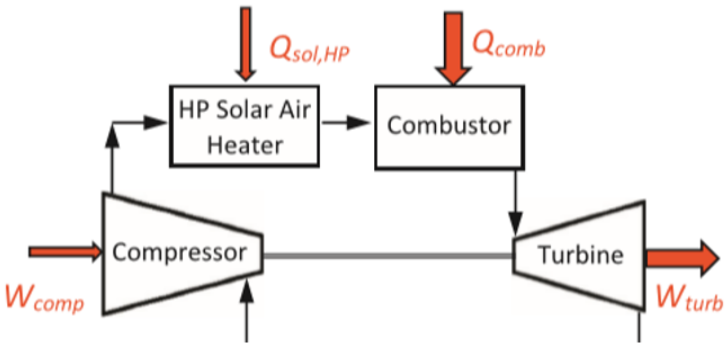

Figure 2.10: Solar aided gas turbine (SAGT) [23]

combustion chamber, allowing a lower temperature on the solar receiver and allowing the fuel combustion to assure that the system can reach adequate operating temperatures, regardless of the available amount of sunlight. In fact, it is thanks to inlet guide vanes that adjust the natural gas and air flows to solar conditions. As a conclusion, the hybrid gas turbine is highly flexible. The advantage of this hybridization option is that the gas turbine can be connected to a bottoming steam cycle and achieve higher efficiencies. Semprini et al. proposed a simple micro solar aided gas turbine with a radiation-to-electrical efficiency of 17% (annual) and a solar share of 52.6% (annual) [29] while Aichmayer et al. demonstrated an overall efficiency of 38.2% with a solar share of 32% (annual) for a solar aided gas turbine connected to a steam cycle. [5].

A similar configuration to the previous one is to use at the same time the solar field and the recuperation of the heat in the flue gas to preheat the air before the combustion chamber.

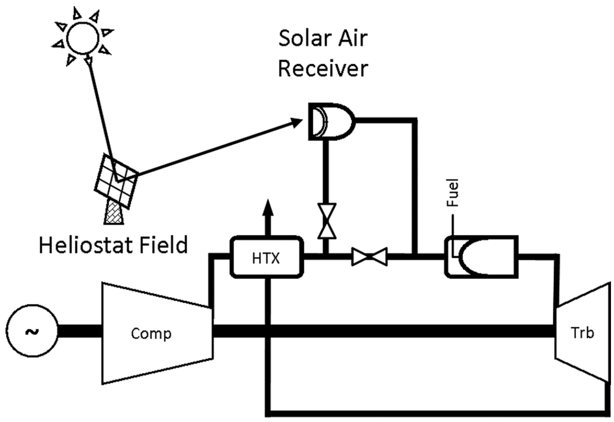

Figure 2.11: Solar aided heat recovery gas turbine (SAHRGT) [26]

The advantage of the recuperation is the increase in efficiency by reducing the fuel consumption thanks to the remaining heat in the flue gas. This solution concerns only small power capacities because the flue gas recuperation is only possible for small powers. Two options are possible. The first one is to inject the heat coming from flue gas before the heat coming from the solar field, as it can be seen on the figure. The other option is to do the contrary by introducing the solar heat before the recuperated heat. This results in a lower receiver temperature (good for $\eta_{en,\,sol-field}$) but also in a lower recuperation efficiency as the flue gas temperature is fixed. Aichmayer et al. determined an overall efficiency of 29.1% with a solar share of 68% [4].

2.4.2 Steam injection gas turbines with solar

This configuration consists in injecting steam in the combustion chamber. Water is thus preheated, evaporated and superheated thanks to the flue gas and the solar heat, as it can be observed in the Figure 3.7. The advantage of this hybrid is the relatively low temperature required for the steam production (even at high pressure) compared to the air temperature required in a typical gas turbine. The low temperature allows one's more to reduce the radiation losses. The other advantage of the low solar receiver temperature is that linear concentrators, which are simpler and less expensive than point concentrators, can be used. However, the key limitation is that the cycle's efficiency decreases with the solar share for a same fuel consumption. Indeed, the steam temperature is lower than the operating inlet turbine temperature and so the cycle relies on combustion to reach this temperature. Finally, this hybridization would require minimal modifications to the power block itself, facilitating the retrofitting. Power plant retrofitting refers to the addition of new technology to the existing older power plant. Polonsky et al. demonstrated for this system a radiation-to-electrical efficiency of 20.1% (annual) with a solar share of 35.2% (annual) [25].

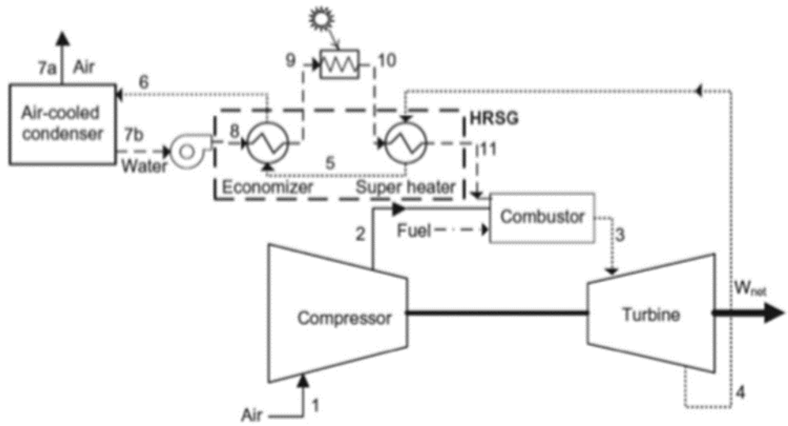

Figure 2.12: Solar hybrid steam injection gas turbine (STIG) [27]

2.4.3 Integrated solar combined cycle (ISCC)

The main advantage of the combined cycle is its efficiency, higher than other cycles. That is the reason why this technology is widely used for new power plants. Integrated combined cycles seek to improve this cycle by integrating solar heat into the bottoming steam cycle. The goal is to replace partially the steam production in the HRSG. In fact, a water bypass is created in order to preheated and/or evaporated and/or superheated water thanks to the solar heat and then can be reintroduced in the HRSG. In addition, for a 3 pressure combined cycle for example, this bypass can be done in the high pressure circuit, medium pressure circuit or high pressure circuit. The solar steam production can be both direct or indirect, the indirect way allowing thermal storage. This results in a lot of possible configurations for the combined cycle hybridization. This hybrid has the advantage to allow low receiver temperature while keeping a very good efficiency thanks to the flue gas and the efficient cycle technology. Furthermore, in order to achieve a better solar share and a better flexibility, the hybridization of the bottoming cycle can be combined with the hy-

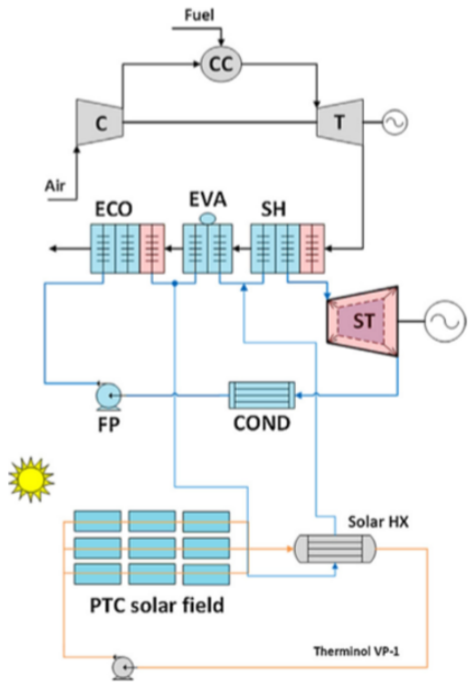

Figure 2.13: Integrated solar combined cycle [27]

bridization of the gas turbine. Manente et al. demonstrated for the ISCC a radiation-to-electrical efficiency of 29.7% with a solar share of 12.8% [20].

2.4.4 Solar methane steam reforming

This technology uses an endothermic chemical reaction to convert methane and steam to syngas.

$$CH_4 + H_2O_{(g)} + heat \rightleftharpoons CO + H_2$$

The solar field is used to provide the required heat for the reaction. The LHV of syngas is chemically 27% higher than the LHV of natural gas. That is why this reaction can also be used to store chemically solar energy. The syngas can be then burned in a gas turbine or a combined cycle. If it is used in a gas turbine, the flue gas can be used to heat water and to provide steam to the endothermic reaction.

2.5 Other hybrid power plants

Another way to hybridize a power plant is to use biofuels. The main incentive to use hybridization with biofuels is that the power generation can be 100% renewable. This type of hybridization is also very flexible. Indeed, biofuels can be used in combustion power plants, in engines to be used for transportation, and they are actually a very good energy storage as high temperatures do not have to be maintained.
The first hybrid technology relies on solar energy and biomass combustion in parallel or in series to inject heat in the steam cycle. This type of hybridization is typically the same as the hybridization with coal but biofuels have the advantage to be renewables. Therefore, the different solar heat injection points are the same as in the section "hybridization with coal".
The second concept is different from the previous one. The hybridization consists here of gasifying the biomass via high temperature solar thermal processes. Indeed, gasification needs a heat source and usually, a part of the biomass feedstock is burned to provide the required heat. The use of solar thermal energy allows to preserve the feedstock and to reduce CO_2 emissions of the gasification process. The main issue is that gasification requires effective heat distribution throughout the reactor to ensure a good efficiency.
The last biofuel hybridization technology uses syngas produced in a conventional gasifier to supply a solar aided gas turbine or an integrated solar combined cycle. This is exactly the same technology as for the hybridization with natural gas except that the fuel is here 100% renewable.

Finally, another hybridization concept is currently emerging. It is the hybrid solar chemical looping combustion (Fig. A.2). It has a strong potential to achieve efficient CO_2 capture with low energy penalty. Actually, it is an oxidation-reduction reaction. The fuel is oxidised in the fuel reactor, thus avoiding direct contact between the fuel and the nitrogen in the air. A metal, called oxygen carrier is employed as the oxidiser and is reduced during the oxidation of the fuel. This reduced metal is then oxidised in a second reactor, the air reactor, using oxygen in the air. The reaction in the fuel reactor is endothermic, that is why solar heat is needed. Another incentive of this cycle is the inherent use of thermochemical storage, which is required to provide firm supply.

2.6 Emerging hybrids

There are many emerging hybrid cycles but one of them is particularly interesting in this context. It is a new patented concept that integrates the combustion system within a solar cavity receiver, as shown beside. Thus, it is a direct integration of solar energy in the cycle, while all hybrids presented previously were indirect integrated solar cycles. The Hybrid Solar Receiver Combustor,

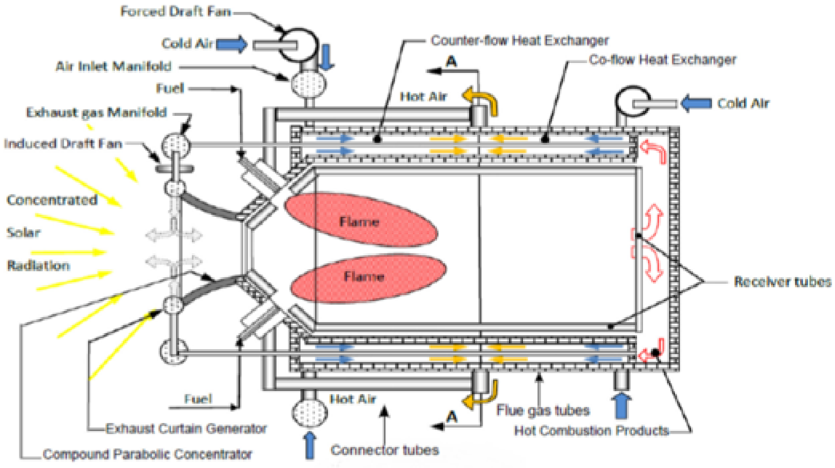

Figure 2.14: direct hybridization between a solar cavity receiver and a combustor [23]

HRSC, can be operated in three modes: solar-only, combustion-only and mixed mode. The main advantages are the reduced losses from both start-up/shut-down and heat exchange surface area, and greater capacity to manage heat flux during periods of rapid change in solar radiation.

2.7 Conclusion

A summary of the advantages and disadvantages of the different hybrids is presented below.

A summary of the advantages and disadvantages of hybridizing CSP with other energy sources.

	Advantages	Disadvantages
Coal	• Uses common, low cost linear concentrator technologies • Can retrofit existing coal plants • Low cost, abundant fuel • Many possible injection points for solar at different temperatures • Coal provides dispatchability • Capital cost savings from shared equipment	• High emission fuel • Equipment age mismatch may be • issue for retrofit • Efficiency limited by Rankine cycle power block • High temp. gasification needs tech. development
Natural Gas	• Low cost, abundant fuel • Low emission fuel • Many possible configurations • Many possible injection points for solar at different temperatures • Efficient ISCC operation possible • NG provides dispatchability • Capital cost savings from shared equipment	• High temperature solar technology still needs development • Efficient ISCC has relatively low solar share
Biofuels	• Potential for purely renewable power generation • Many possible configurations • Many possible injection points for solar at different temperatures • Biofuel provides dispatchability • Capital cost savings from shared equipment	• Limited biofuel availability may require other fuel sources • High temp. gasification needs tech. development

Figure 2.15: Summary table of the advantages and disadvantages of the different hybrids [26]

As a conclusion, it can be said that the Integrated solar combined cycle is currently the best option for new power plants for these reasons:

- natural gas is the transition fuel, it is abundant, cheap and it is a low emission fossil fuel.
- the combined cycle is currently the most efficient power cycle.
- many configurations are possible, there is the possibility to hybridise the gas turbine, the bottoming cycle or both of them. And for each case there are a lot of possible solar heat injection points. Different solar receiver technologies are also compatible.

For these reasons, this option will be further analysed in order to determine the best configuration from the thermodynamic and the economic points of view.

Chapter 3

Integrated solar combined cycle

As mentioned in the previous chapter, there are many injection points for solar heat in a combined cycle. This chapter is focused on the hybridization of the bottoming cycle and the aim is to determine the best injection point from the thermodynamic point of view. An energy and exergy analysis are performed to explain why some configurations reach higher conversion efficiencies in the utilization of solar energy. In this respect, a Matlab model of a triple pressure level integrated solar combined cycle is set up (more efficient than double or single pressure level). This model is based on the article [20] and on the Matlab code built for the course "Thermal cycles" [17]. This model can be used (in attached file Appendix3) through a graphical interface (Fig. A.28).

3.1 Description of the integrated solar combined cycle model

3.1.1 Combined cycle

The flowsheet of the stand-alone combined cycle used for the Matlab model is the following, coming from the book [21].

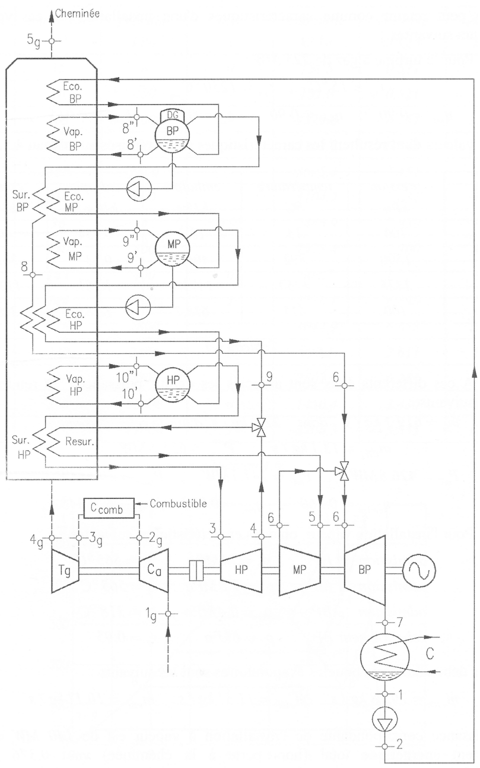

Figure 3.1: Combined cycle flowsheet [21]

The cycle parameters are the same as those used for the project of the course "Thermal cycle". [17] (report in Appendix5). The input parameters for the gas turbine are:

$$P_e = 225\ [MW] \quad T_{air} = 15\ [°C] \quad T_H = 1250\ [°C] \quad r_c = 15\ [-] \quad \eta_{piC} = \eta_{piT} = 0.9\ [-]$$

$$k_{cc} = 0.85 \quad k_{mec} = 0.015\ [-] \quad \phi_{in} = 0.8\ [-]$$

The input parameters for the bottoming cycle are:

$$T_C = 36[°C] \quad quality = 0.95 \quad p_{HP} = 110[bar] \quad n_{fh} = 0 \quad \eta_{mec} = 0.98 \quad Fuel = CH_4$$

$$\eta_{it} = 0.88 \quad dta = 50[°C] \quad pinch = 10[°C] \quad postcomb = off$$

These parameters are described in the nomenclature. Below is the T-S diagram of the combined cycle.

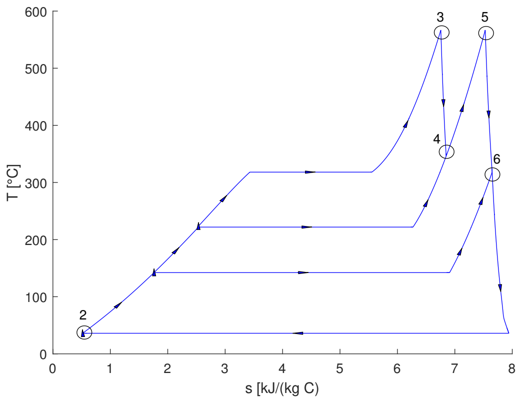

Figure 3.2: T-S diagram of the combined cycle

3.1.2 Solar field

The solar field considered in the model is composed of parabolic trough collectors because it is currently the most mature solar field technology. The main output parameter of the solar field is the solar field efficiency, which was introduced in the previous chapter (Eq 2.1).

$$\eta_{en,\,sol-field} = \frac{\dot{Q}_{sol}}{A_{coll}\,DNI} \tag{3.1}$$

where A_{coll} is the product of the collector longitudinal length and the collector aperture width, which is the distance between the two rims of the curved mirror, as depicted in the figure below. $\dot{Q}_{sol}$ is the heat flux transferred to the solar fluid and is also the heat transferred to the water because no heat transfer losses are taken into account for simplification.

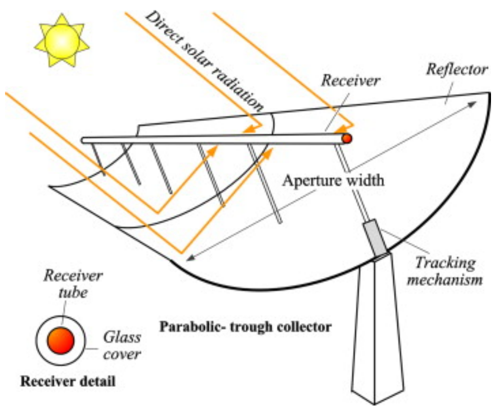

Figure 3.3: Parabolic trough collector representation [8]

As it can be seen in the Figure 3.3, the detailed mechanism of solar heat absorption is the following:

- First, the sun rays collide with the mirror, perpendicular to the aperture area (A_{coll}), with a radiation flux DNI.
- Then, the sun rays are concentrated on the receiver tube (of surface $\frac{A_{coll}}{C}$) with a concentration efficiency η_{conc}. C is in fact the ratio between the collector aperture width and the receiver outside diameter.
- A part of the concentrated radiation flux is lost by radiation. A black body radiation loss is considered.
- Finally, the remaining solar heat flux transferred through a secondary fluid is absorbed by the water in a solar heat exchanger. In this model, no heat transfer losses are taken into account.

From this mechanism, the solar heat flux transferred to the water is derived:

$$\dot{Q}_{sol} = \eta_{conc}\, DNI\, A_{coll} - \frac{A_{coll}}{C} \sigma\, T_{rec}^4 \tag{3.2}$$

The input parameters of the parabolic troughs solar field are the following [20]:

$$\eta_{conc} = 0.75\ [-] \quad C = 80\ [-] \quad DNI = 800\ [-]$$

The receiver temperature, T_{rec}, is defined for simplification as the the sum of the upper water temperature in the solar exchanger and the pinch, $Pinch_{sol}$, which depends on the heat exchanger type.

$$Pinch_{sol,\,economizer} = 5\ [°C] \quad Pinch_{sol,\,evaporator} = 50\ [°C] \quad Pinch_{sol,\,superheater} = 10\ [°C]$$

From the exergy point of view, the solar field efficiency is defined as follows:

$$\eta_{ex,\,sol-field} = \frac{\Delta \dot{E}x_{water,\,sol}}{\dot{E}x_{sol}} \tag{3.3}$$

where $\Delta \dot{E}x_{water,\,sol}$ is the exergy increase of water/steam in the solar heat exchanger. $\dot{E}x_{sol}$ is the exergy of solar radiation calculated according to Petela [24]:

$$\dot{E}x_{sol} = A_{coll}\, DNI \left(1 - \frac{4}{3}\frac{T_0}{T_S} + \frac{1}{3}\left(\frac{T_0}{T_S}\right)^4\right) \tag{3.4}$$

where $T_S = 5792K$ is the Sun temperature and $T_0 = 298.15K$ is the reference ambient temperature. The exergy of solar radiation is close but lower than the energy of solar radiation. Indeed, from the second thermodynamic principle $ds = d_e s + d_i s = \frac{dq}{T} + d_i s$, thus due to a really high Sun temperature, the entropy of solar radiation is very low but is not zero. As a result, the exergy of solar radiation is lower than its energy content because the exergy is defined as $e = h - T_0\, s$.

3.1.3 Hybridization mode

There are two modes of hybridization. The first one is the power boosting mode. It results in additional power being generated when the solar source is available, without fuel consumption change. The second one is the fuel saving mode ant it consists of maintaining a constant power output by reducing the fuel consumption.

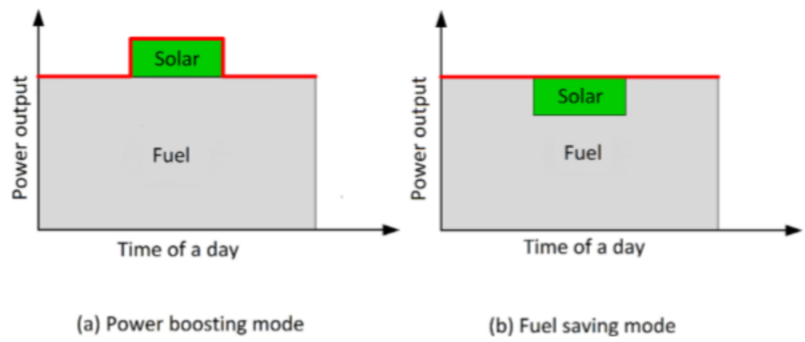

Figure 3.4: Hybridization modes [23]

In the Matlab model, the power boosting mode is much more easy to implement because the fuel saving mode would require to iterate on the gas turbine to find the right fuel mass flow that results in a constant power output. Therefore, the power boosting mode is chosen and thus the input parameter in the Matlab model is the power output of the gas turbine and not the total power output of the combined cycle.

In addition to that, there is an economic incentive to choose the power boosting mode. Indeed, this mode offers the opportunity to sell more electricity during periods of high demand, during which the power price is higher. It also reduces the need to install additional generating capacity. Finally, the extent of fuel savings in the fuel saving mode may be less than the solar input because the efficiency of the turbines reduces with turn-down.

Accordingly, by considering a constant $\dot{Q}_{sol}$, the constant parameter between all hybridization configurations is the solar share, mathematically defined as:

$$sol\,share = \frac{\dot{Q}_{sol}}{\dot{Q}_{sol} + \dot{m}_{fuel}\,LHV} \tag{3.5}$$

$\boxed{\dot{Q}_{sol} \text{ is set to 70 MW}}$ for all configurations. This results in a solar share of 10.2%. This can seem low but without storage, the solar share has to be limited to ensure a sufficient reliability and flexibility in order to provide firm supply. Finally, by fixing $\dot{Q}_{sol}$, the equation 3.2 gives the collector aperture area, A_{coll}.

3.2 Main hybrid output parameters

In order to assess the best hybridization system, three main output parameters are used to evaluate the performance of the solar field integration into the combustion cycle.

The first output parameter is the solar radiation-to-electrical efficiency (Eq 2.1) which was already defined in the previous chapter (the ratio between the incremental power output, due to the solar input, and the thermal solar heat flux injected in the power cycle). It measures the conversion efficiency of solar radiation in electricity. The equivalent exergy efficiency is:

$$\eta_{ex,\,sol-rad} = \frac{\Delta Pe_{SC}}{\dot{E}x_{sol}} \tag{3.6}$$

In addition, the solar radiation-to-electrical efficiencies are linked with the solar field efficiencies by the equation 2.1 (energy) and the following one (exergy):

$$\eta_{ex,\,sol-rad} = \eta_{ex,\,sol-field} \cdot \eta_{ex,\,sol-heat} \tag{3.7}$$

Therefore, the energy conversion efficiency of the heat transferred to water in electricity and the equivalent exergy efficiency are:

$$\eta_{en,\,sol-heat} = \frac{\Delta Pe_{SC}}{\dot{Q}_{sol}} \tag{3.8}$$

$$\eta_{ex,\,sol-ex.conv} = \frac{\Delta Pe_{SC}}{\Delta \dot{E}x_{water,\,sol}} \tag{3.9}$$

The second output parameter is the combined cycle efficiency, which is used to assess the performance of the whole cycle and not just of the integration of solar heat, as it is the case for the previous parameter. The energetic combined cycle efficiency is the ratio between the total power output produced by the cycle and the total heat flux injected in the cycle (the sum of the fuel energy content and the solar radiation energy). This efficiency is defined as:

$$\eta_{toten} = \frac{Pe_{GT\,\&\,SC}}{\dot{m}_{fuel}\,LHV + A_{coll}\,DNI} \tag{3.10}$$

The equivalent exergy efficiency is the ratio between the total effective power and the exergy flux input of the cycle. It is defined as:

$$\eta_{totex} = \frac{Pe_{GT\,\&\,SC}}{\dot{m}_{fuel}\,e_c + \dot{E}x_{sol}} \tag{3.11}$$

with e_c, the exergy of the fuel. It is the corresponding free enthalpy of the complete oxidation reaction of the fuel with the oxygen available in the standard atmosphere. The atmospheric air is considered at the reference temperature, T_0. More details can be found in the book [21].

Another key output parameter is the CO_2 emissions production, $CO_{2,\,prod}$. It is defined as the ratio between the mass flow of CO_2 in [g/h] and the effective power of the ISCC.

$$CO_{2,prod} = \frac{\dot{m}_{CO_2}}{Pe_{GT\,\&\,SC}} \tag{3.12}$$

A similar CO_2 parameter takes into account the life cycle specific CO_2 emissions of the solar field (100 gCO_2/kWh [20]).

$$CO_{2,prod\,tot} = \frac{\dot{m}_{CO_2} + 100 \cdot \Delta Pe_{SC}}{Pe_{GT\,\&\,SC}} \tag{3.13}$$

These two later parameters are not directly linked to η_{toten} despite what it could be guessed. Indeed, η_{toten} depends on $A_{coll}DNI$ which depends directly on the receiver temperature, contrary to $CO_{2,prod\,tot}$ and $CO_{2,prod}$.

3.3 Optimum pressure level to inject solar heat

From the energy point of view, the goal of the hybridization optimisation is to maximize the incremental solar radiation-to-electrical efficiency (Eq 2.1). Therefore, ΔPe_{SC} has to be maximized and thus the solar-heat efficiency (Eq. 3.8) has to be maximized. This results in optimizing the heat conversion efficiency of the steam cycle. In a 3 level combined cycle, the specific enthalpy at the condenser inlet is fixed (because the *quality* is fixed in order to prevent damage at the steam turbine exit). Therefore, condenser losses can only be minimized by minimizing the total feed water mass flow (maximizing the steam cycle efficiency). The heat flux transferred to water in the HRSG being almost fixed (because of the flue gas properties), the only way to minimize the feed water mass flow in the HRSG is to maximize the specific heat load (Δh in kJ/kg) in the HRSG because $\dot{Q} = \dot{m}\Delta h$. As a consequence, the optimal pressure level for hybridisation is the highest pressure level because the specific heat load in the high pressure circuit is the biggest compared to the other pressure levels. Indeed, in the Fig. 3.2:

$$(h_3 - h_2) + (h_5 - h_4) > h_5 - h_2 > h_6 - h_2$$

That is why solar heat is optimally injected in the HP circuit (confirmed by [16]) with a view to proportionally increase the HP mass flow compared to the IP and LP mass flows, and thus to raise the water average specific heat load of the cycle. In addition to that, the heat transfer coefficient increases with the pressure, reducing heat losses in the solar heat exchanger (even though this loss is not taken into account in the Matlab model). On the other hand, it can be noticed that the minimization of the total feed water mass flow induces the minimization of the heat flux transferred to water in the LP economizer (and thus in the whole HRSG) but this negative effect is less important than the beneficial effect of the condenser losses mitigation.

From the exergy point of view, the solar exergy conversion efficiency has to be maximized (3.9). Here, even if the heat loss in the solar heat exchanger (SHX) is neglected, there is an exergy loss in this exchanger. The exergy loss associated to the heat transfer between a heating fluid (the solar fluid) and a heated fluid (the steam) is according to [21]:

$$de = -\frac{T_0}{T_{rec}}(T_{rec} - T_w)ds_v \tag{3.14}$$

Considering this equation, the increase of T_{rec} lowers the exergy loss. As T_{rec} depends highly on T_w (water temperature in the SHX), it is therefore optimal to maximize T_w. In addition, the conversion efficiency of the exergy transferred to water in work follows the same reasoning as for the energetic analysis. However, the highest T_w is in the HP circuit, that is why it is favourable to increase the HP mass flow by injecting solar heat flux in the high pressure level.

It can be noticed that the optimization of $\eta_{en,\,sol-heat}$ and $\eta_{ex,\,sol-ex.conv}$ involves the maximization of the steam temperature and thus also of the solar receiver temperature. However, it was seen before that the receiver temperature increase results in the radiation losses increase and thus in the $\eta_{en,\,sol-field}$ and $\eta_{ex,\,sol-field}$ decrease. This implies the existence of an optimal temperature, as it was described with a simplified case in the Figure (2.5). Actually, regarding the pressure level, the solar receiver temperature is, in the case of the combined cycle, in the range for which the beneficial effects of the temperature rise on $\eta_{en,\,sol-heat}$ and $\eta_{ex,\,sol-ex.conv}$ are more important than the detrimental effects on $\eta_{en,\,sol-field}$ and $\eta_{ex,\,sol-field}$, resulting in a positive effect on $\eta_{en,\,sol-rad}$ and $\eta_{ex,\,sol-rad}$.

3.4 Hybridization possibilities

Now that the high pressure level has been identified as the most suitable solar heat injection point, a choice has still to be done concerning the most efficient injection point in the high pressure circuit itself. It can be a combination of the 3 different heat exchanger bypass (from the HRSG to SHX): the HP economizer, the HP evaporator and the HP superheater. From the energy point of view, the mass flows are the key parameter while the temperature mismatch on the graph (3.5) is the key parameter from the exergy point of view. (note: HT means high temperature and LT means low temperature)
Indeed, the exergy loss is proportional to the temperature mismatch between the flue gas and the steam as shown in the equation (3.14). The solar mass flow that passes through the solar heat exchanger is:

$$\dot{m}_{sol} = \frac{\dot{Q}_{sol}}{\Delta h_{econo-sol} + \Delta h_{evapo-sol} + \Delta h_{superh-sol}}\,[kg\,s^{-1}] \tag{3.15}$$

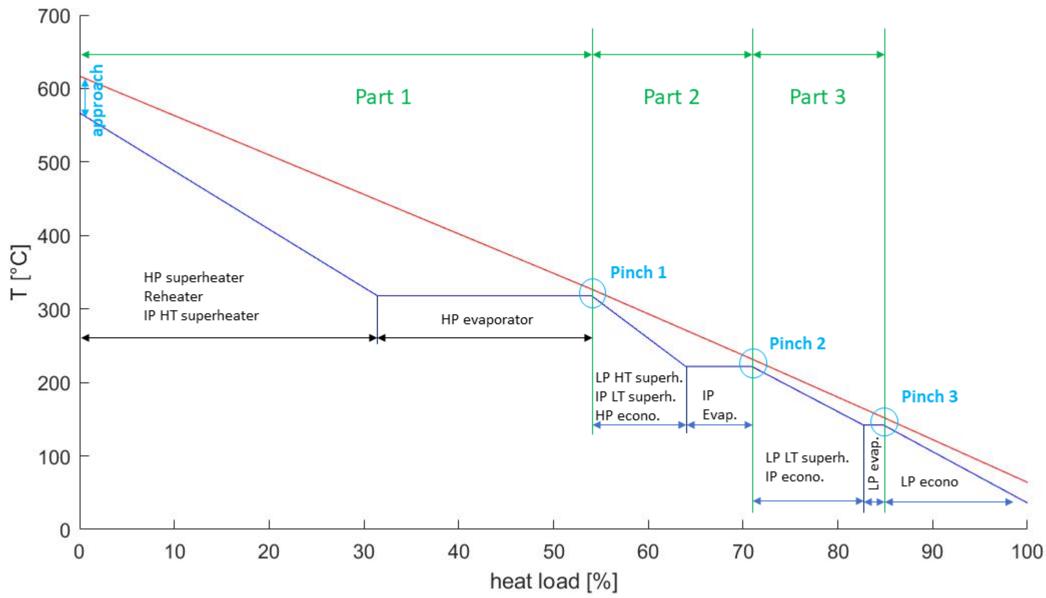

Figure 3.5: Temperature with respect to the heat load (in%) in the HRSG

where Δh is the specific enthalpy difference in $[MJ\,kg^{-1}]$. A very important issue to understand is that $\dot{m}_{LP}$ (mass flow evaporated at low pressure), $\dot{m}_{IP}$ (mass flow evaporated at intermediate pressure) and $\dot{m}_{HP}$ (mass flow evaporated at high pressure, both in the HRSG and in the SHX) are constrained by the input parameters. Indeed, with the layout depicted in the figure (3.1), the HRSG is split in 3 parts in which the heat flux and the temperatures are constrained by the 3 pressure levels, the 3 evaporator pinches (ΔT_{min} between the saturated liquid water and the flue gas in the HRSG evaporator), the approach (ΔT between the HRSG exit superheated steam and the HRSG inlet flue gas) and the flue gas mass flow.

	mass flow
HP turbine	$\dot{m}_{HP}$
IP turbine	$\dot{m}_{HP} + \dot{m}_{IP}$
LP turbine	$\dot{m}_{HP} + \dot{m}_{IP} + \dot{m}_{LP}$
HP superheater	$\dot{m}_{HP}$
IP HT superheater	$\dot{m}_{IP}$
Reheater	$\dot{m}_{HP} + \dot{m}_{IP}$
HP evaporator	$\dot{m}_{HP}$
LP HT superheater	$\dot{m}_{LP}$
IP LT superheater	$\dot{m}_{LP}$
HP economizer	$\dot{m}_{HP}$
IP evaporator	$\dot{m}_{IP}$
LP LT superheater	$\dot{m}_{LP}$
IP economizer	$\dot{m}_{HP} + \dot{m}_{IP}$
LP evaporator	$\dot{m}_{LP}$
LP economizer	$\dot{m}_{HP} + \dot{m}_{IP} + \dot{m}_{LP}$

Table 3.1: Mass flows in the HRSG exchangers

Hence, a heat & mass balance, made of 3 equations (for the 3 HRSG parts) with 3 unknowns is required to compute $\dot{m}_{LP}$, $\dot{m}_{IP}$ and $\dot{m}_{HP}$, depending on the input parameters. As a consequence, the solar heat injection point influences the mass flow distribution between the low, intermediate and high pressure levels. Above is a table summarizing the mass flows in the HRSG components.

Besides, five configurations are tested in order to find the best one. Below are the descriptions of the five studied heat injection points and the guessed relative performance of each hybrid because it is possible to already determine a trend at this stage. It must to be kept in mind that the maximization of the HP mass flow is wanted.

- **ISCC1: HP economizer hybridized**. A fraction of HP water is preheated outside the HRSG in a solar heat exchanger. HP water is split into streams: the first stream is preheated in the solar heat exchanger and the remaining flow is preheated in the HP economizer of the HRSG. Both streams are then mixed and injected in the HRSG evaporator.

  A guess can be done in relation to the mass flows. As it can be seen in the figure (3.5), by displacing part of the HP mass flow of the HP economizer (in part 2) into the solar heat exchanger, the IP mass flow is increased in order to guarantee the decrease of the flue gas enthalpy and of the flue gas temperature between pinch 1 and pinch 2. Consequently, in order to counterbalance the increase in IP mass flow in part 1, the HP mass flow is decreased. With the same reasoning, the LP mass flow is also decreased. To conclude, this type of hybridization seems energetically not very interesting because the HP mass flow diminishes. In addition, the heat load ($\dot{Q}$ in [kW]) is expected to decrease a lot in the HP economizer and a bit in the HP superheater and HP evaporator while heat loads in the IP circuit are expected to increase. It can be concluded that from the exergy point of view, this type of hybridization seems not very interesting because it displaces heat loads from high temperature (HP circuit) to intermediate temperature (IP circuit), which increases the total irreversibilities in the HRSG, as explained with (Eq. 3.14).

- ISCC2: **HP evaporator hybridized**. A fraction of HP steam is evaporated outside the HRSG in a solar steam generator. HP saturated liquid water leaving the HP economizer is split into two streams: the first stream is evaporated in the solar heat exchanger and the remaining flow is evaporated in the HP evaporator of the HRSG. Both streams are then mixed and superheated in the HRSG.

  By displacing part of the HP mass flow of the HP evaporator (in part 1) into the solar heat exchanger, the HP mass flow is much increased in order to guarantee the required decrease of the flue gas enthalpy in part 1. Therefore, $\dot{m}_{IP}$ and $\dot{m}_{LP}$ decrease in order to ensure the decrease of the flue gas enthalpy in part 2 and 3. Moreover, the heat load of the HP evaporator diminishes and as $\dot{m}_{IP}$ and $\dot{m}_{LP}$ are lower, the irrersibilities in the lowest temperature part decrease also. As a consequence, the main sources of irreversibility in the HRSG are much decreased. To conclude, this solar heat injection point seems very interesting from the energy and exergy points of view.

- ISCC3: **HP economizer and evaporator hybridized**. A fraction of HP feed water is preheated and evaporated outside the HRSG in a solar heat exchanger. HP feed water coming from the HP pump is split into two streams. The first stream is preheated and evaporated in the solar heat exchanger while the remaining flow undergoes the same process in the HRSG. The two streams are then mixed and injected in the HP superheater.

  This case is between the two previous cases. By displacing part of the HP mass flow of the HP evaporator (in part 1) into the solar heat exchanger, the HP mass flow is increased but less than in the ISCC2 because HP mass flow is also displaced from the economizer of the HRSG into the solar heat exchanger. Therefore, the IP mass flow increases (but less than in the ISCC1) to ensure the decrease of the flue gas enthalpy in part 2 and the LP mass flow decreases to guarantee the flue gas enthalpy drop in part 3. Besides, the heat load of the HP evaporator decreases, but contrary to the ISCC2, the heat load of the IP evaporator increases (due to the increase of $\dot{m}_{IP}$). To conclude, this type of hybridization seems better than the ISCC1 but less efficient than the ISCC2.

- ISCC4: **HP economizer, evaporator and superheater hybridized**. A fraction of the HP mass flow is preheated, evaporated and superheated outside the HRSG. HP feed water coming from the HP pump is split into two streams. The first stream is preheated, evaporated and superheated in the solar heat exchanger while the remaining flow undergoes the same process in the HRSG. Both streams are then mixed and injected directly in the HP steam turbine.

  The difference with the previous case is that both HP mass flows of the HP evaporator and HP superheater are displaced into the solar heat exchanger. Accordingly, the system has no choice but to further increase the HP mass flow compared to the ISCC3 with the aim of compensating for the additional heat load loss in the HRSG HP superheater. Therefore, the IP and LP mass flows decrease to ensure the enthalpy drop in part 2 and 3. Thus, the heat load of the IP evaporator decreases. However, as here a part of the HRSG superheater heat load is also displaced into the solar heat exchanger (not only evaporator in the part 1), a higher heat load of the HRSG evaporator can be guessed compared to the ISCC3. To conclude, from the energy point of view, compared to the ISCC3, the advantage of the higher HP mass flow has to be weighed against the disadvantage of the higher solar receiver temperature. From the exergy point of view, the advantage of the lower heat load of the IP evaporator has to be weighed against the disadvantage of the higher receiver temperature. Anyway, this option is expected to be less efficient than the ISCC2.

- ISCC5: **HP evaporator and superheater hybridized**. A fraction of HP mass flow is evaporated and superheated outside the HRSG. HP feed water coming from the HP economizer is split into two streams. The first stream is evaporated and superheated in the solar heat exchanger while the remaining flow undergoes the same process in the HRSG. The two streams are then mixed and injected directly in the HP steam turbine.

  Compared to the ISCC2, the mass flows are expected to be in the same order of magnitude because the whole heat load is displaced from the same part, the part 1, but the solar receiver temperature being higher, the energy solar field efficiency is expected to be lower. From the exergy point of view, the heat load of the HP evaporator is expected to be greater than in the ISCC2 because of the smaller HP superheater heat load, in the same part of the HRSG. To conclude, this type of hybridization is expected to be less interesting than the ISCC2. Nevertheless, the ISCC5 is expected to be slightly better than the ISCC4 because for the same solar receiver temperature, the HP mass flow is higher and the IP mass flow is lower.

A last ISCC could have been analysed, by only hybridizing the HP superheater, but the too high solar receiver temperature and the fact that the evaporator has been identified as the most suitable component to be hybridized (highest heat load) led to not consider this case.
It can be also noticed that the increase of the total mass flow of the ISCC compared to the stand-alone combined cycle allows the flue gas to exit the HRSG at a lower temperature. More heat is thus transferred from the flue gas to water, increasing the power output. Nevertheless, the dew point has to be taken into account. Indeed, if the exit flue gas temperature falls under the dew point, condensation appears in the HRSG, causing damage because of the corrosion of the tubes.

3.5 Other interesting hybrid output parameters

In order to evaluate and quantify more deeply the ins and outs of the 5 hybridization types described above, other output parameters than the main output parameters are needed. They are required in order to understand precisely where such hybrid is more interesting than another one. Below are the energetic and exergetic steam cycle efficiencies.

$$\eta_{toten,\,SC} = \frac{Pe_{SC}}{\dot{Q}_{hrsg} + A_{coll}\,DNI} \tag{3.16}$$

where $\dot{Q}_{hrsg}$ is the total heat flux transferred to water in the HRSG.

$$\eta_{totex,\,SC} = \frac{Pe_{SC}}{\dot{E}x_{fg} + \dot{E}x_{sol}} \tag{3.17}$$

where $\dot{E}x_{fg}$ is the exergy available from the exhaust gases of the gas turbine, cooled down to ambient temperature. These efficiencies are useful because they allow the assessment of the bottoming cycle without taking into account the gas turbine. They also allow the introduction of new important output parameters by being split into a product of two efficiencies.

$$\eta_{toten,\,SC} = \eta_{mec} \cdot \eta_{cyclen,\,SC} \cdot \eta_{gen,\,SC} = \frac{Pe_{SC}}{\dot{W}_{SC}} \cdot \frac{\dot{W}_{SC}}{\dot{Q}_{hrsg} + \dot{Q}_{sol}} \cdot \frac{\dot{Q}_{hrsg} + \dot{Q}_{sol}}{\dot{Q}_{hrsg} + A_{coll}\,DNI} \tag{3.18}$$

$$\eta_{totex,\,SC} = \eta_{mec} \cdot \eta_{cyclex,\,SC} \cdot \eta_{gex,\,SC} = \frac{Pe_{SC}}{\dot{W}_{SC}} \cdot \frac{\dot{W}_{SC}}{\Delta\dot{E}x_{water,\,tot}} \cdot \frac{\Delta\dot{E}x_{water,\,tot}}{\dot{E}x_{fg} + \dot{E}x_{sol}} \tag{3.19}$$

where $\Delta\dot{E}x_{water\,tot} = \Delta\dot{E}x_{water,\,hrsg} + \Delta\dot{E}x_{water,\,sol}$ is the total exergy gain of water in the HRSG and in the solar heat exchanger.

3.6 Results & Discussion

The results provided by the Matlab model are presented in this section. Firstly, the $\dot{Q}_{sol}$-T diagrams and the exergy pie-charts of each ISCC are depicted and then a comparative table is shown. Finally a critical comparison is made. The energy pie-charts can be found in the appendices.

3.6.1 Results

NGCC (natural gas combined cycle):

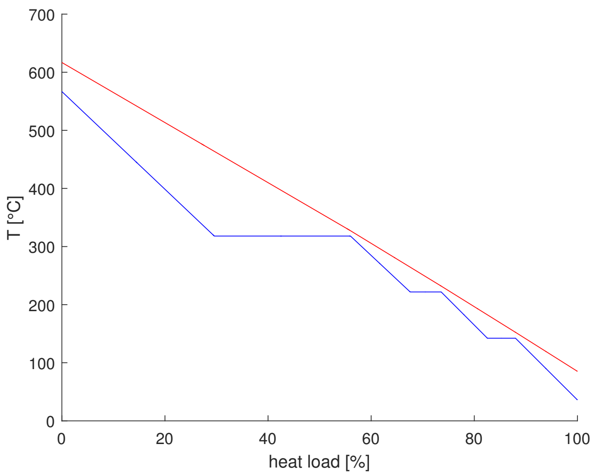

Figure 3.6: $\dot{Q}$-T diagram

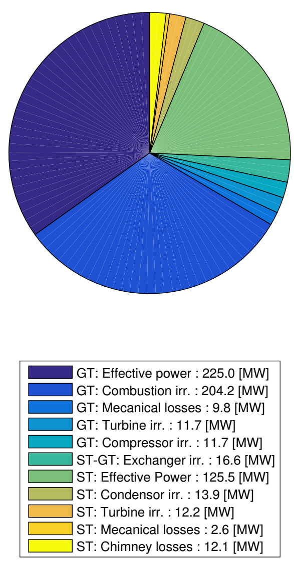

Figure 3.7: Exergy pie-chart

ISCC1: It is noted that the first type of hybridization produces an inconsistent result as it can be seen in the figure below. Actually, the problem is that a negative HP mass flow is observed in part 2 of the HRSG. Indeed, as explained in the previous section, the displacement of heat load from the HRSG HP economizer into the solar exchanger induces an increase of the IP mass flow in order to satisfy the pinches 2. This leads to a decrease of the total HP mass flow in order to satisfy the pinch 1. However, in this case, the solar heat flux transferred to HP water ($70MW$) is so high that dividing this heat flux by the specific enthalpy difference in the HP economizer, a higher solar HP mass flow relative to the required total HP mass flow is obtained. This results in a negative HP mass flow in part 2 without what a heat flux increase in part 2 would appear and would prevent the difference between the flue gas temperature and the HP water saturation temperature from reaching the pinch 1.

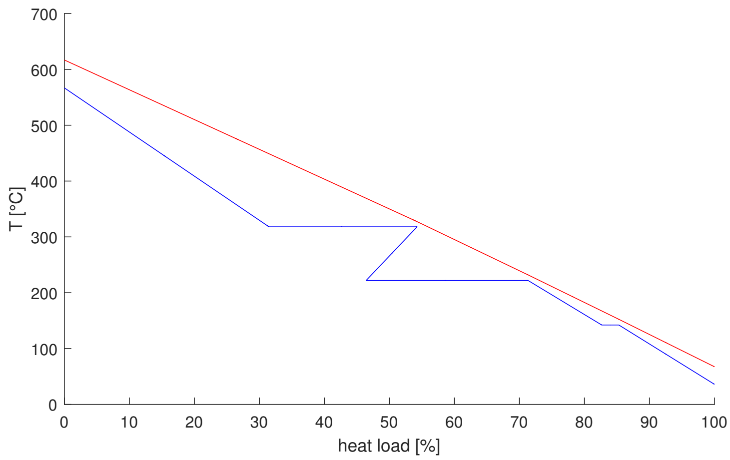

Figure 3.8: $\dot{Q}_{sol}$-T diagram

The solution would be to decrease $\dot{Q}_{sol}$ (at a lower value than 32 MW) but this results in a decrease of the solar share, which is disadvantageous for the hybridization. As a conclusion, it can be said that the hybridization of only the HP economizer is not a good idea.

ISCC2: evaporator hybridized

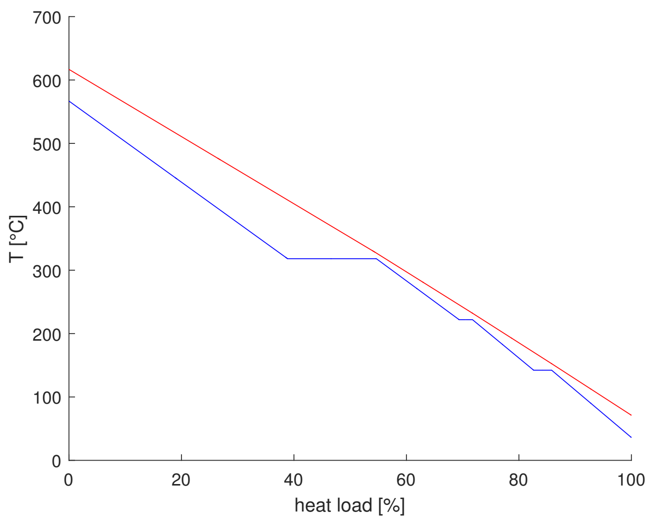

Figure 3.9: $\dot{Q}$-T diagram

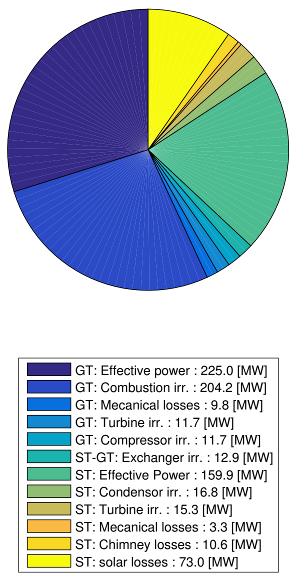

Figure 3.10: Exergy pie-chart

ISCC3: economizer and evaporator hybridized

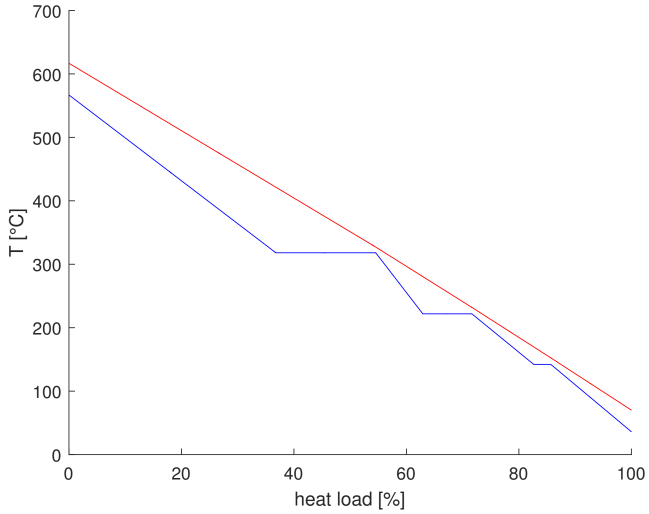

Figure 3.11: $\dot{Q}$-T diagram

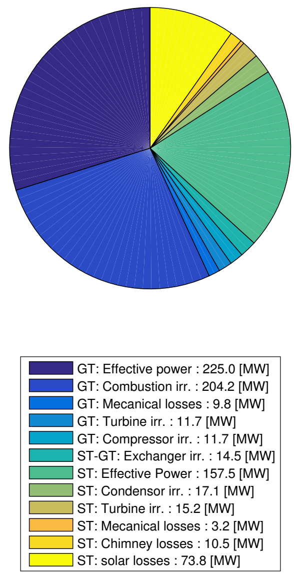

Figure 3.12: Exergy pie-chart

ISCC4: economizer, evaporator and superheater hybridized

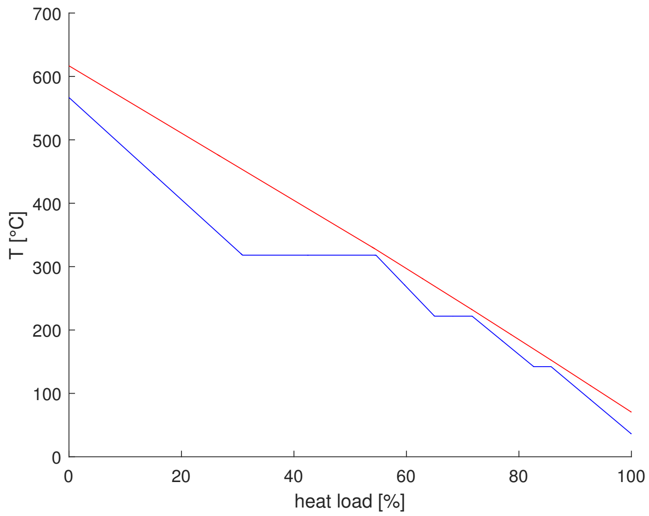

Figure 3.13: $\dot{Q}$-T diagram

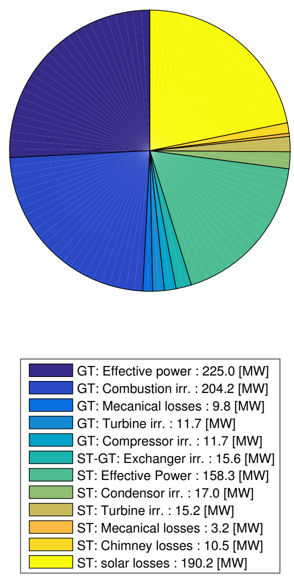

Figure 3.14: Exergy pie-chart

ISCC5 evaporator and superheater hybridized

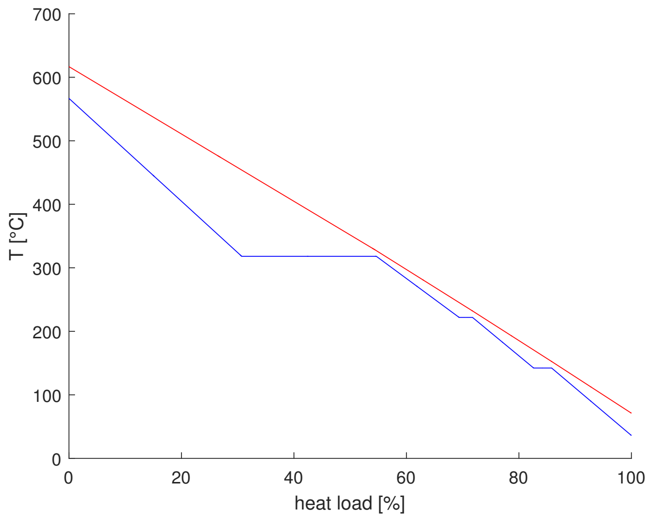

Figure 3.15: $\dot{Q}$-T diagram

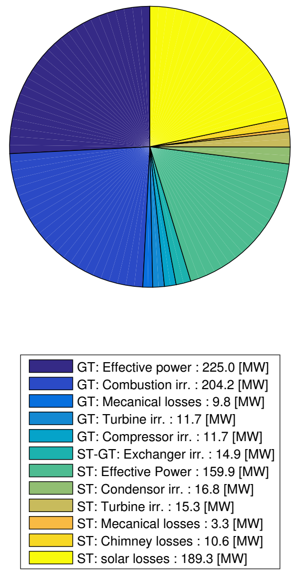

Figure 3.16: Exergy pie-chart

summary table:

	NGCC	ISCC2	ISCC3	ISCC4	ISCC5
Pe_{SC} $[MW]$	125.5	159.9	157.5	158.3	159.9
$\dot{m}_{LP}$ $[kg/s]$	8	5	5	5	5
$\dot{m}_{IP}$ $[kg/s]$	11	4	16	12	4
$\dot{m}_{HP,tot}$ $[kg/s]$	70	99	88	92	99
$\dot{m}_{HP,sol}$ $[kg/s]$	/	56	40	27	34
$\eta_{\mathbf{toten}}$	**0.567**	**0.524**	**0.52**	**0.445**	**0.447**
$\eta_{\mathbf{totex}}$	**0.543**	**0.51**	**0.507**	**0.439**	**0.441**
$\eta_{toten,\,SC}$	0.377	0.349	0.344	0.271	0.274
$\eta_{gen,\,SC}$	1	0.8982	0.8983	0.7037	0.7034
$\eta_{cyclen,\,SC}$	0.3845	0.3968	0.3903	0.3924	0.3968
$\eta_{totex,\,SC}$	0.686	0.548	0.54	0.386	0.39
$\eta_{gex,\,SC}$	0.8431	0.6694	0.6615	0.4725	0.4763
$\eta_{cyclex,\,SC}$	0.8307	0.8355	0.8330	0.8338	0.8355
$\eta_{\mathbf{en,\,sol-rad}}$	/	**0.295**	**0.275**	**0.135**	**0.141**
$\eta_{en,\,sol-field}$	/	0.6	0.6	0.288	0.288
$\eta_{en,\,sol-heat}$	/	0.491	0.457	0.468	0.491
$\eta_{\mathbf{ex,\,sol-rad}}$	/	**0.3157**	**0.2941**	**0.1443**	**0.1513**
$\eta_{ex,\,sol-field}$	/	0.33	0.322	0.162	0.166
$\eta_{ex,\,sol-ex.conv}$	/	0.9576	0.9127	0.8882	0.9089
A_{coll} $[m^2]$	/	145 781	145 781	304 188	304 188
solar share	0	0.102	0.102	0.102	0.102

	NGCC	ISCC2	ISCC3	ISCC4	ISCC5
$CO_{2,prod}$ [g/kWh]	**346**	**315**	**317**	**316**	**315**
$T_{exhaust}$ $[^\circ C]$	85.2	71.1	70.1	70.4	71.1
$T_{dew\,point}$ $[^\circ C]$	44.4	44.4	44.4	44.4	44.4

Table 3.2: performance summary table

3.6.2 Discussion

First of all, the mass flows are analysed because they are the most important parameters with the purpose of assessing the 3 main hybrid output parameters. These main output parameters are then construed based on the results. It is advised to look at the table in the same time as to read the discussion.

Mass flows

Concerning the mass flows, it can be noticed that the results expected in the previous section are confirmed. In general, it can be said that the hybridization in part 1 of the $\dot{Q} - T$ diagram (ISCC2 and ISCC5) provides the highest HP mass flows (higher than the NGCC) and the lowest IP & LP mass flows (lower than the NGCC), as explained previously. The LP, IP and HP mass flows of the ISCC2 and the ISCC5 are exactly the same because in both cases, only part 1 is hybridized. Only the solar mass flow is different because the specific enthalpy difference in the solar exchanger is higher for the ISCC5 (due to the hybridization of the superheater in the ISCC5). On the other hand, the hybridization of the economizer (ISCC3 and ISCC4), as it is performed in part 2 of the $\dot{Q} - T$ diagram, leads to a higher IP mass flow than the NGCC. The difference between the ISCC3 and the ISCC4 is that in the ISCC4, the heat load displaced in part 1 is proportionally more important than in the ISCC3, due to the hybridization of the superheater, resulting in a higher HP mass flow and thus in a lower IP mass flow than the ISCC3.

Combined cycle performance

The gas turbine parameters are constant, therefore the variation of η_{toten} and η_{totex} depend on the variation of $\eta_{toten,\,SC}$ and $\eta_{totex,\,SC}$. It can be observed that the energy and exergy total steam cycle efficiencies are lower for the ISCCs compared to the NGCC. It is mainly due to the lower energy and exergy generation efficiencies as illustrated by $\eta_{gen,\,SC}$ and $\eta_{gex,\,SC}$ despite higher cycle efficiencies, as shown by η_{cyclen} and η_{cyclex}. There are thus two effects:

- $\eta_{gen,\,SC}$ and $\eta_{gex,\,SC}$: these two efficiencies are lower for the ISCCs compared to the NGCC because of the low conversion efficiency of solar radiation into solar heat or solar exergy, as represented by $\eta_{en,\,sol-field}$ and $\eta_{ex,\,sol-field}$. In addition, $\eta_{gen,\,SC}$ and $\eta_{gex,\,SC}$ are better for the ISCC2 and 3 than for the ISCC4 and 5 and they are very similar between the ISCC2 and 3 , and between the ISCC4 and 5. Indeed, $\eta_{en,\,sol-field}$ and $\eta_{ex,\,sol-field}$ depend mainly on the solar receiver temperature which is higher for the ISCC4 and 5 than for the ISCC2 and 3. The very small difference of $\eta_{gen,\,SC}$ and $\eta_{gex,\,SC}$ between the ISCC2 and 3 and between the ISCC4 and 5 comes from the different flue gas exhaust temperature of the HRSG, which is due to a different total water mass flow. Indeed, lower is the exhaust temperature, lower are the exhaust losses (as depicted in the pie-charts) and thus higher are $\eta_{gen,\,ST}$ and $\eta_{gex,\,ST}$.

- $\eta_{cyclen,\,SC}$ and $\eta_{cyclex,\,SC}$: here, the ISCC efficiencies are better than the NGCC efficiency. As explained in the section 3.3, this comes from the higher HP mass flow. Indeed, from the energy point of view, bigger is the HP mass flow, smaller are the condenser losses. That is why $\eta_{cyclen,\,SC}$ is the same between the ISCC2 and 5 because HP, IP and LP mass flows are the same, and that is also why $\eta_{cyclen,SC}$ of the ISCC2 and 5 is higher than $\eta_{cyclen,SC}$ of the ISCC4, which is higher than $\eta_{cyclen,SC}$ of the ISCC3 due to different HP mass flows (condenser losses can be seen from the energy pie-charts in the appendices). The same reasoning can be applied to Pe_{SC}. From the exergy point of view, $\eta_{cyclex,SC}$ of the ISCC2 and 5 is higher than $\eta_{cyclex,SC}$ of the ISCC4, which is higher than $\eta_{cyclex,SC}$ of the ISCC3, because of the higher thermal matching between water and the flue gas in the HRSG, as it can be seen in the $\dot{Q} - T$ diagrams. Indeed, this reduces the irreversibities in the HRSG as it can be observed from the exergy pie-charts.

To conclude, the dominant efficiency allowing to compare energetically the ISCC2 and 3 with the ISCC4 and 5 is $\eta_{gen,SC}$ and the dominant efficiency needed to compare energetically the ISCC2 with the ISCC3 and the ISCC4 with the ISCC5 is $\eta_{cyclen,SC}$, while $\eta_{gex,SC}$ is sufficient to compare exergetically all ISCCs. Finally, the hybridization type that provides the best total performance is the ISCC2.

Solar performance

Solar radiation efficiencies, $\eta_{en,sol-rad}$ and $\eta_{ex,sol-rad}$ assess the capacity of converting solar radiation into electricity. On the one hand, they depend on the solar field efficiencies and on the other hand, they depend on the ability of the steam cycle to transform the heat/exergy flux given by the solar heat exchanger into work.

- $\eta_{en,sol-field}$ and $\eta_{ex,sol-field}$: From the energy point of view, $\eta_{en,sol-field}$ depends on the concentration efficiency and on the radiation loss coefficient (Eq. 2.1), and thus on the solar receiver temperature. That is why $\eta_{en,sol-field}$ of the ISCC2 and 3 is the same but is higher than that of the ISCC4 and 5, because the solar receiver temperature depends on the outlet steam temperature of the SHX (radiation losses can be observed in the energy pie-charts in the appendices). An indirect effect of the radiation losses increase is that the collector area has to increase in order to maintain $\dot{Q}_{sol} = 70MW$, resulting in higher concentration losses. From the exergy point of view, the influence of the solar receiver temperature is the same except that $\eta_{ex,sol-field}$ is not exactly the same between the ISCC2 and 3 and between the ISCC4 and 5. Indeed, the average water temperature in the solar heat exchanger in higher in the ISCC2 and 5, resulting in a decrease of the solar irreversibilies (due to Eq 3.14), as it can be seen in the exergy pie-charts.

- $\eta_{en,sol-heat}$ and $\eta_{ex,sol-ex.conv}$: the reasoning is almost the same as the one described for the steam cycle efficiencies ($\eta_{cyclen,SC}$ and $\eta_{cyclex,SC}$). However, $\eta_{en,sol-heat}$ and $\eta_{ex,sol-ex.conv}$ do not depend directly on the exact values of the mass flows. They depend on the incremental change (between hybridized and not hybridized) in mass flows, which is not the same thing. On the other hand, $\eta_{en,sol-heat}$ is higher than $\eta_{cyclen,SC}$ because solar heat is injected only in the HP circuit and $\eta_{ex,sol-ex.conv}$ is higher than $\eta_{cyclex,SC}$ because solar exergy is injected at higher temperature than the average temperature of the steam cycle working fluid.

To conclude, the best solar performance is observed for the ISCC2. In addition, the collector aperture area is highly dependent on the radiation losses and thus on the solar receiver temperature, that is why A_{coll} of the ISCC4 and 5 is more than two times bigger than A_{coll} of ISCC2 and 5, which is a negative feature regarding the investment cost and also the land area needed to install the solar field. Finally, the solar share is constant through all ISCCs because $\dot{Q}_{sol}$ is constant.

exhaust

Concerning the exhaust, the most important output parameter is the CO_2 emissions. As the fuel consumption is constant through all configurations, $CO_{2,prod}$ only depends on Pe_{SC}, that is why both ISCC2 and ISCC5 achieve the best performance, as the power output is the same. It is also needed to verify that the flue gas exhaust temperature is above the dew point and it is the case for all configurations. Finally, as explained previously, the exhaust flue gas temperature depends on the total feed water mass flow because this temperature is fixed by the heat flux through the LP economizer, which is crossed by $\dot{m}_{HP} + \dot{m}_{IP} + \dot{m}_{LP}$.

Conclusion

As a conclusion, regarding the 3 main hybrid output parameters, the best hybridization configuration is the one for which only the evaporator is hybridized. Furthermore, it is noted that the solar field efficiency of the ISCC2 (and 3) is independent of the addition of post combustion because the solar receiver temperature is computed from the HP saturation temperature of water. On the contrary, the solar receiver temperatures of the ISCC4 and 5 are computed from the exhaust steam temperature of the HRSG. Therefore, by adding for example post combustion such that the flue gas temperature reaches 750 $°C$ at the HRSG inlet, the radiation losses on the solar receiver are so high that a theoretical negative solar field efficiency is observed. Accordingly, the ISCC2 (and 3) is more flexible than the ISCC4 and 5, which is a very good advantage on the electricity market.
Finally, the Matlab program is free of access to the reader in attached files (Appendix3) if he wants to play with the parameters. A graphical interface allows an easy use. Screen shots of the Matlab graphical interfaces can be seen at the end of the appendices.

3.7 Parameter study

Now that the solar heat injection point has been chosen, a parameter study can be performed. This parameter study is done on the ISCC2. The studied input parameters are the DNI, the solar share, the highest pressure of the steam cycle and the solar field type. Only the energy analysis is performed because the relative trend would be the same with the exergy analysis and because only an energy analysis is possible with Thermoflow.

3.7.1 DNI

It is important to analyse this parameter as it represents the solar radiation intensity. Indeed, the DNI varies according to the year, to the season and to the hour of the day. The hypothesises are the following:

- the solar field size remains constant, i.e. $A_{coll} = 145781\, m^2$.
- the solar concentration efficiency remains constant, i.e. $\eta_{conc} = 0.75$
- the solar receiver temperature remains constant.
- therefore, the free variable is $\dot{Q}_{sol}$, which is computed thanks to 3.2

This DNI parameter study actually analyses the change in performance relative to the solar conditions variation of one particular geographical site because the solar field hardware is fixed (A_{coll}) (temporal analysis). Another DNI parameter study could have been done by keeping $\dot{Q}_{sol}$ constant and by computing A_{coll} to analyse the change in performance relative to the design solar conditions of different geographical sites (geographical analysis). Nevertheless, the results of this study are in the appendices (Fig. A.5 & A.6) because a positive effect is expected on all output parameters (except for CO_2 emissions for which there is no effect because $\dot{Q}_{sol}$ remains constant).
The 3 main hybrid output parameters are obtained as it can be seen in the graphs below. It can be observed that the graph of the solar radiation-to-electrical efficiency has a horizontal

asymptote. Actually, the solar heat-to-electrical efficiency remains constant because it depends only on the type of hybridization, which is independent of the DNI. Therefore, the asymptotic behaviour comes from the solar field efficiency that has a horizontal asymptote in 0.75, which is in fact the concentration efficiency. This can be explained by the following equation (thanks to Eq. 3.2):

$$\eta_{en,\,sol-field} = \frac{\dot{Q}_{sol}}{A_{coll} DNI} = \eta_{conc} - \frac{\sigma\, T_{rec}^4}{C\, DNI} \tag{3.20}$$

As a consequence, if the DNI tends to infinity, $\eta_{en,\,sol-field}$ tends to η_{conc}. In addition, for low values of DNI, the radiation loss coefficient is higher than η_{conc}, that is why the solar field efficiency is positive only for DNI values above 160 W/m^2.
That is also why a steeper decrease in η_{toten} is observed for values below 160 W/m^2. More generally, η_{toten} decreases with the DNI because the degradation of $\eta_{gen,\,SC}$ with the DNI is higher than the improvement of $\eta_{cyclen,\,SC}$ (in other words, it is also due the fact that $\eta_{en,\,sol-rad} < \eta_{toten}$). The graph seems to be a line, but in fact the graph of η_{toten} has the same shape than the graph of CO_2. Indeed, η_{toten} tends theoretically to $\eta_{en,\,sol-rad}$ for infinite values of DNI. Accordingly, the "degradation speed" of the total efficiency decreases (very slightly) with the DNI.

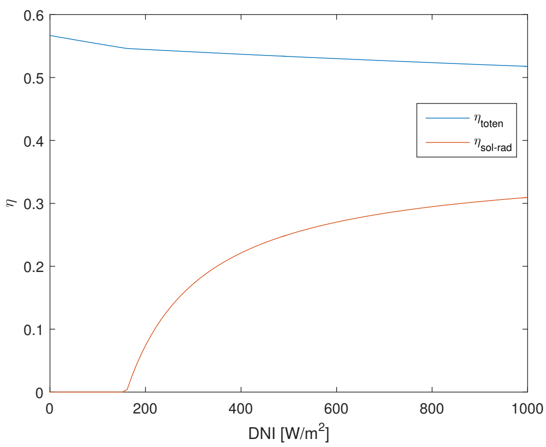

Figure 3.17: η_{toten} & $\eta_{en,\,sol-rad}$ according to the DNI

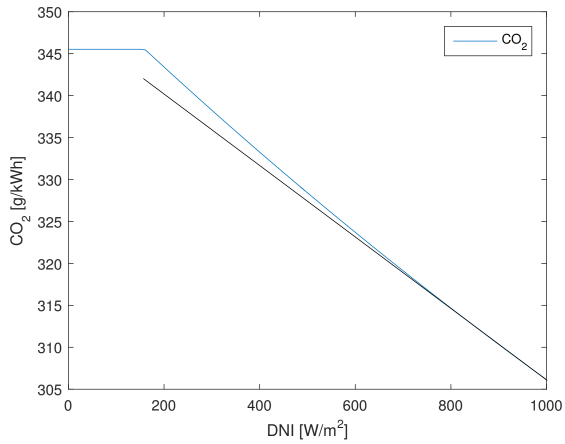

Figure 3.18: CO_2 emissions according to the DNI

Regarding the CO_2 emissions, the positive effect of the increase in DNI can be seen in the graph above. This is not a line because the CO_2 production tends to 0 for infinite values of DNI.

3.7.2 $\dot{Q}_{sol}$

It is also interesting to analyse the performance changes when the solar share is changed. The studied input parameter is thus $\dot{Q}_{sol}$. In other words, the variable is here the size of the solar field. Is it desirable to have a big solar field or a small solar field ? The hypothesises are this time the following:

- the DNI remains constant, i.e. $DNI = 800\, W/m^2$.
- the solar concentration efficiency remains constant, i.e. $\eta_{conc} = 0.75$
- the solar receiver temperature remains constant.
- therefore, the free variable is A_{coll}.

Contrary to the DNI variation, the $\dot{Q}_{sol}$ variation induces a constant solar field efficiency. Indeed, the aperture collector area varies proportionally with $\dot{Q}_{sol}$(Eq. 3.2), therefore, the solar field

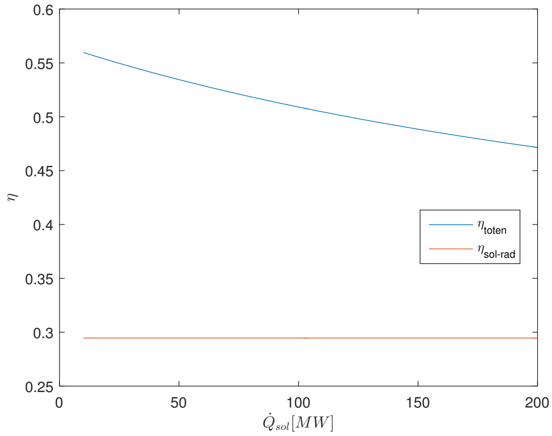

Figure 3.19: η_{toten} & $\eta_{en,\,sol-rad}$ according to $\dot{Q}_{sol}$

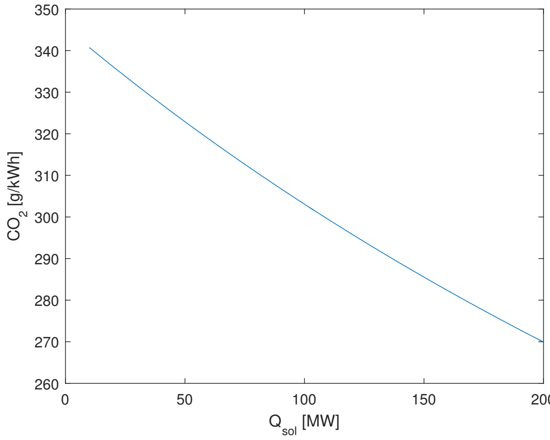

Figure 3.20: CO_2 emissions according to $\dot{Q}_{sol}$

efficiency (Eq. 3.1) remains constant. In addition, the solar heat to electrical efficiency remaining constant, the solar radiation-to-electrical efficiency is constant, as it can be seen in the graph above. The relative effect of the $\dot{Q}_{sol}$ variation on η_{toten} is the same than the effect of the DNI variation on η_{toten} because the DNI variation results in the $\dot{Q}_{sol}$ variation. As a conclusion, increasing the solar share results in lower CO_2 emissions and constant solar performance but results also in a lower total energy efficiency of the cycle.

3.7.3 p_{HP}

While the previous parameter studies concern the solar conditions and the solar field, this parameter study concerns the combined cycle itself. Indeed, the highest pressure of the steam cycle is analysed. The aim of this study concerns the case for which a new power plant is built and an optimal high pressure is sought. This do not concern any retro fitting of an existent power plant, as the highest pressure is a critical input parameter taken into account before the construction of the power plant. Below are the graphs of the main efficiencies. The maximum pressure taken into account is 180 bars because above this pressure, the mass flows are inconsistent.

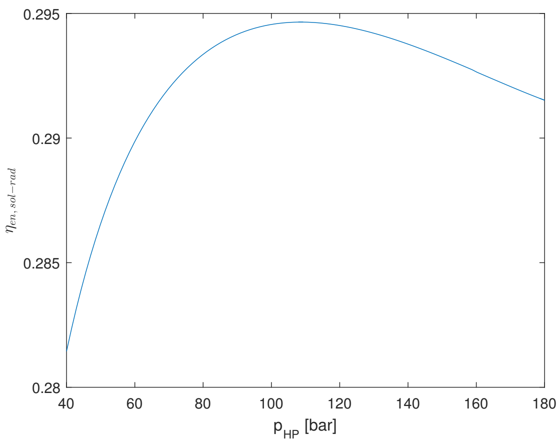

Figure 3.21: $\eta_{en,\,sol-rad}$ with respect to p_{HP}

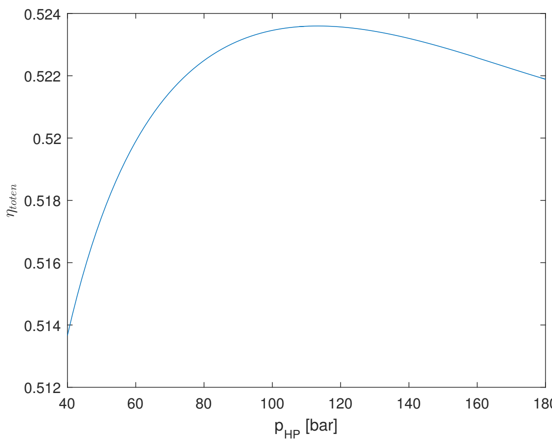

Figure 3.22: η_{toten} with respect to p_{HP}

As it can be seen in the graphs, there is an optimal high pressure. This can be explained with two trends. Firstly, the increase of the highest pressure improves $\eta_{cyclen,SC}$, thus also $\eta_{en,\,sol-heat}$, because the specific heat load in the HP circuit increases, (due to the increase of $(h_5 - h_4)$ in

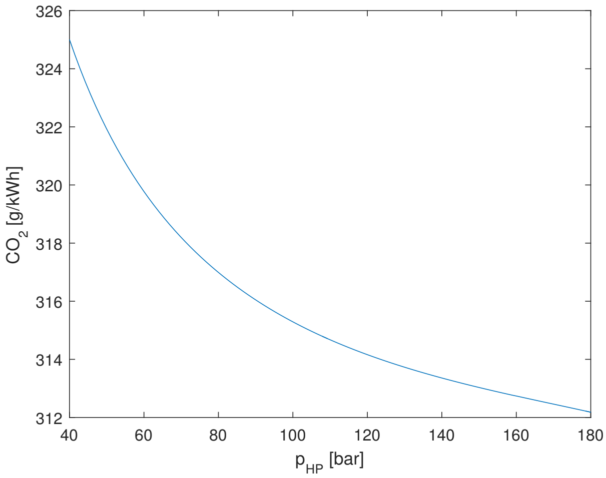

Figure 3.23: CO_2 emissions with respect to p_{HP}

the Figure 3.2), reducing the total feed water mass flow and therefore lowering the condenser losses. However, the increase of the highest pressure induces the increase of the HP saturation temperature of water and thus also of the solar receiver temperature. Therefore, the radiation losses in the solar field increase. This reduces the solar field efficiency $\eta_{en,\,sol-field}$ and thus also $\eta_{gen,SC}$. The radiation losses are a function of T_{rec}^4, that is why the increase of the highest pressure is firstly advantageous and becomes more and more disadvantageous for high values of p_{HP}. As a conclusion, it can be noticed that the optimal pressure is around 110 bar, which is precisely the default highest pressure of the studied combined cycle. That is thanks to the good design of the solar field. Indeed, as it can be seen in the Figure 2.5, for each concentration ratio there is an optimal solar receiver temperature for which the solar radiation-to-electrical efficiency is the highest. As a consequence, as p_{HP} is linked to T_{rec}, the concentration ratio has been chosen in order that the highest solar radiation-to-electrical efficiency is achieved at 110 bars. That is why parabolic troughs with $C = 80$ is the optimal solar field technology in this case.

Moreover, it is observed that the CO_2 emissions decrease with the increase of the highest pressure because CO_2 emissions depend in this case only on the total power output, which is highly dependent on $\eta_{cyclen,ST}$, more than on $\eta_{en,\,sol-field}$. That is the reason why even if the decrease speed of the CO_2 emissions diminishes with respect to p_{HP}, the CO_2 emissions continue to decrease for very high values of p_{HP}.

3.7.4 Solar field

Other valuable input parameters to study are the solar field parameters, i.e. η_{conc} and C. Therefore, the goal is here to change the type of solar field. For example, the cheaper Linear Fresnels (than parabolic troughs) are studied. The new parameters are then [20]:

- $\eta_{conc} = 0.65$
- $C = 171.4$

The solar field efficiency becomes 0.58 compared to 0.6 for the parabolic troughs. This results in lower overall performance. The aperture collector area becomes 150 839 m^2 compared to 145 781 m^2 with the parabolic troughs. In the end, it can be concluded that the parabolic troughs are in this case more efficient than the Linear Fresnels.

Chapter 4

Gas turbine and overall combined cycle hybridization

As mentioned in the review, it is also possible to hybridizide the gas turbine by pre heating the air between the compressor and the combustion chamber. Firstly, the stand-alone gas turbine performance is studied in order to focus on the understanding of the gas turbine hybridization process. After that, the possible combinations of hybridizing a combined cycle are analysed.

4.1 Description of the solar aided gas turbine

The stand-alone gas turbine used for the Matlab model was modelled according to the book [21]. The input parameters taken into account are the same as the gas turbine parameters of the combined cycle used in the previous chapter (they are described in the nomenclature). Therefore:

$$P_e = 225\ [MW] \quad T_{air} = 15\ [^\circ C] \quad T_H = 1250\ [^\circ C] \quad r_c = 15\ [-] \quad \eta_{piC} = \eta_{piT} = 0.9\ [-]$$
$$k_{cc} = 0.85 \quad k_{mec} = 0.015\ [-] \quad \phi_{in} = 0.8\ [-]$$

where Pe is the gas turbine power output without any solar heat addition. An additional parameter is needed in order to analyse another type of gas turbine: the exhaust heat recovery gas turbine. This is the Number of Transfer Units, defined as the ratio of the heat exchanger's ability to transfer heat to the fluid's minimum ability to absorb heat [19]. In this model, the NTU is set to:

$$NTU = 4$$

This type of gas turbine allows the use of the exhaust flue gas energy in order to preheat the air before entering the combustion chamber. Thanks to that, the fuel consumption is reduced and thus the total gas turbine efficiency is improved. For more information about the gas turbine model, the report of the project of the course "Thermal cycle" is in attached documents (Appendix5). Below are the T-S diagrams of the simple natural gas turbine (NGT) and of the exhaust heat recovery gas turbine (HRGT).

In addition, the solar aided steam injection gas turbine is not studied in this work because steam produced thanks to the exhaust flue gas of a gas turbine and a solar field, is better transformed into work in a combined cycle than in a steam injection gas turbine. Indeed, as already mentioned in the review, the steam injection in a gas turbine lowers the gas turbine efficiency. Therefore, the reason why this hybridization type is not further analysed in this work is that if steam is wanted to be produced thanks to the exhaust flue gas of a gas turbine, it is better to inject this steam in a combined cycle than in the gas turbine itself from the thermodynamic point of view.

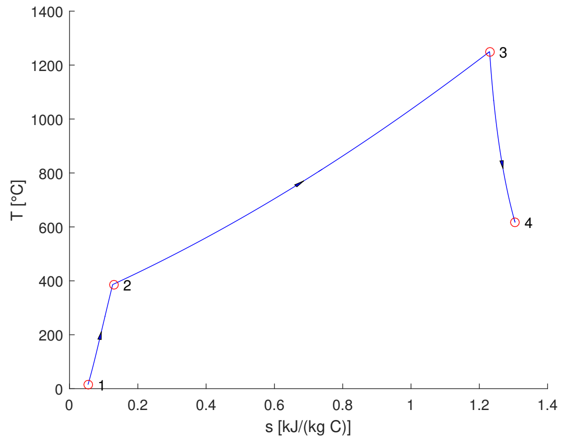

Figure 4.1: T-S diagram of the simple gas turbine

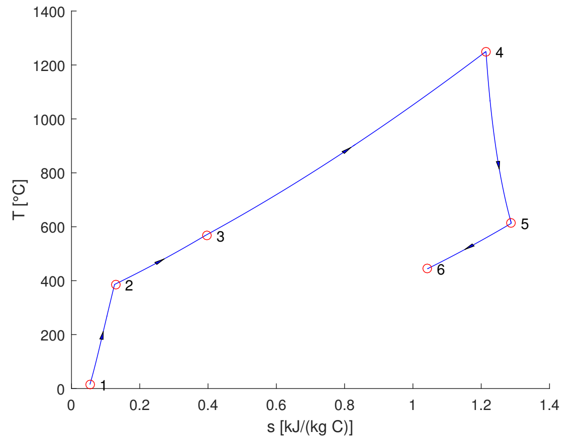

Figure 4.2: T-S diagram of the exhaust heat recovery gas turbine

Concerning the solar field, as the inlet temperature of the turbine (T_H) is very high, a central tower is used. Indeed, the central receiver can achieve higher receiver temperatures than parabolic troughs and thanks to a much higher concentration ratio, the optimal solar receiver temperature is also higher, as it can be seen in the graph 2.5. The heat transfer between air and the receiver is direct, without any solar fluid. Actually, without considering any exhaust heat recovery, air at high pressure coming from the compressor enters the solar receiver exchanger at low temperature and exits the solar receiver exchanger at high temperature before being injected in the combustion chamber. The pressure is considered constant in the solar heat exchanger. Furthermore, the solar field hypothesises are the same as in the previous chapter. The solar input parameters are the following [13, 9, 11]:

$$\eta_{conc} = 0.6\,[-] \quad C = 800\,[-] \quad DNI = 800\,[-] \quad Pinch_{sol} = 5\,[°C] \quad \dot{Q}_{sol} = 70\,[MW]$$

Regarding the hybridization mode, similarly to the hybridization of the bottoming part of the combined cycle, the power boosting mode is used in this model. The fuel saving mode was nevertheless implemented but is not presented in this work. Indeed, it allows an easier comparison and combination with the previous chapter. Moreover, the power boosting mode has some thermodynamic and economical advantages already described in the previous chapter.

4.2 Interesting parameters

The main hybrid output parameters are the same than in the previous chapter. The only difference is of course that ΔPe_{SC} in the equations (3.1), (3.6), (3.8), (3.9) and (3.13) is replaced by ΔPe_{GT} and that $Pe_{GT\,\&\,SC}$ in the equations (3.10), (3.11), (3.12) and (3.13) is replaced by Pe_{GT}. ΔPe_{GT} is the difference between the power produced by the solar aided gas turbine (SAGT) and the gas turbine without solar field, but with exactly the same parameters (same fuel consumption). Therefore, while the unknown for the non-hybridized gas turbine is the fuel mass flow (because the power is imposed), the unknown for the solar aided gas turbine is actually the power output. Accordingly, a first calculation is performed through the non-hybridized gas turbine, which gives the fuel mass flow. Then, this fuel mass flow is used in the calculation of the solar aided gas turbine in order to compute the power output.

In order to better understand the total efficiencies, they are developed in a product of efficiencies:

$$\eta_{toten,\,GT} = \frac{Pe_{GT}}{\dot{m}_{fuel}\,LHV + A_{coll}\,DNI} \tag{4.1}$$

$$\eta_{totex,GT} = \frac{Pe_{GT}}{\dot{m}_{fuel}\, e_c + \dot{E}x_{sol}} \tag{4.2}$$

$$\eta_{toten,GT} = \eta_{mec} \cdot \eta_{cyclen,GT} \cdot \eta_{gen,ST} = \frac{Pe_{GT}}{\dot{W}_{GT}} \cdot \frac{\dot{W}_{GT}}{\dot{Q}_{comb} + \dot{Q}_{sol}} \cdot \frac{\dot{Q}_{comb} + \dot{Q}_{sol}}{\dot{m}_{fuel}\, LHV + A_{coll}\, DNI} \tag{4.3}$$

$$\eta_{totex,GT} = \eta_{mec} \cdot \eta_{cyclex,GT} \cdot \eta_{gex,GT} = \frac{Pe_{GT}}{\dot{W}_{GT}} \cdot \frac{\dot{W}_{GT}}{\Delta\dot{E}x_{comb} + \Delta\dot{E}x_{sol}} \cdot \frac{\Delta\dot{E}x_{comb} + \Delta\dot{E}x_{sol}}{\dot{m}_{fuel}\, e_c + \dot{E}x_{sol}} \tag{4.4}$$

4.3 Hybridization possibilities

Three hybridization cases are modelled in the Matlab program. Two of them include an exhaust heat recovery exchanger.

- SAGT (solar aided gas turbine): Regarding the case without exhaust heat recovery, the hybridization consists of adding a solar heat exchanger between the compressor outlet and the combustion chamber inlet.

- SAHRGT1 (solar aided heat recovery gas turbine): Considering an exhaust heat recovery, there are two possibilities. The first possibility is to inject solar heat at the outlet of the exhaust heat recovery exchanger. This injection point seems very relevant for the gas turbine cycle efficiency, $\eta_{GT,cyclen}$ (Eq. 4.3). Indeed, it maximizes the heat transfer between the exhaust flue gas and the compressed air because the temperature difference between the exhaust flue gas and the compressor outlet is high, higher than the case for which the solar heat is injected before the exhaust recovered heat. In fact, the heat transfer performance is constrained by the NTU parameter, from which the air outlet temperature of the exhaust heat recovery exchanger is derived. (T_3) [21]. State numbers refer to Figure 4.7.

$$NTU = \frac{T_3 - T_2}{T_6 - T_3} \Rightarrow T_3 = \frac{NTU}{1 + NTU}(T_6 - T_2) + T_2 \tag{4.5}$$

  It can be seen that greater is the temperature difference ($T_6 - T_2$), greater is T_3, thus smaller is the temperature difference in the combustion chamber ($T_5 - T_4$), and smaller is the fuel consumption. However, this injection point lowers the solar field efficiency due to the fact that the solar heat exchanger is placed after the exhaust heat recovery exchanger, making the required solar receiver temperature very big.

- SAHRGT2: The other possibility is to place the solar heat exchanger just after the compressor. This solution is expected to raise the solar field efficiency compared to the previous injection point because the solar receiver temperature is lower. Nevertheless, the cycle gas turbine efficiency ($\eta_{GT,cyclen}$) is expected to be smaller than for the previous case because less heat is recovered from the exhaust flue gas. Indeed, the temperature difference ($T_6 - T_3$) in the graph 4.9 (SAHRGT2) is smaller than ($T_6 - T_2$) in the graph 4.7 (SAHRGT1), thus the temperature difference in the solar heat exchanger is lower for the SAHRGT2 according to the NTU equation.

Therefore, simulations have to be performed in order to assess which effect is more dominant relative to the overall performance.

4.4 Results & Discussion

4.4.1 Results

Are presented in this section the results of the three hybridization types described above, and the results of the following non-hybridized gas turbines.

- NGT (natural gas turbine): without exhaust heat recovery
- HRGT (heat recovery gas turbine): with exhaust heat recovery.

The T-S diagrams of the NGT and the HRGT are depicted in the Figures 4.1 and 4.2. Below are the exergy pie-charts of these two power plants.

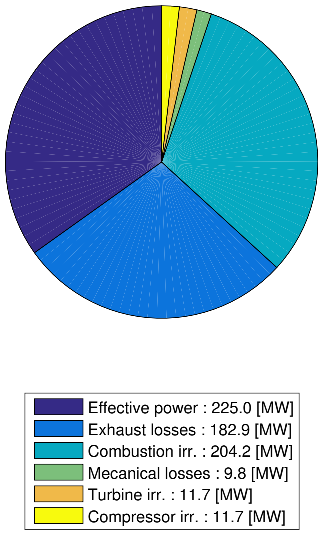

Figure 4.3: Exergy pie-chart of the NGT

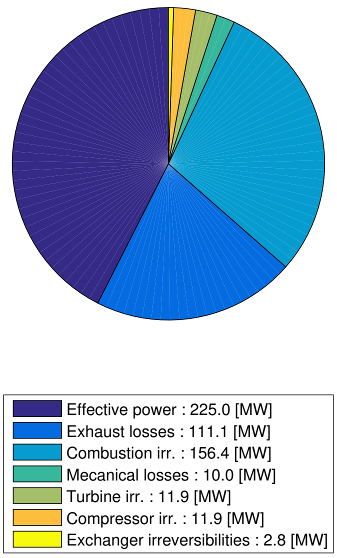

Figure 4.4: Exergy pie-chart of the HRGT

SAGT:

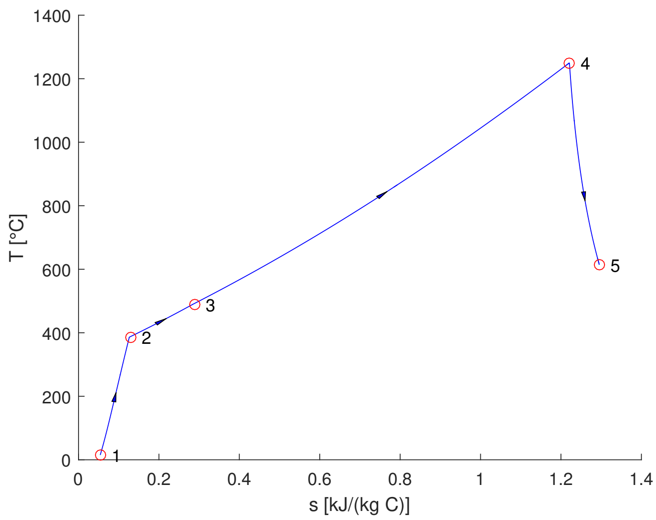

Figure 4.5: T-S diagram of the SAGT

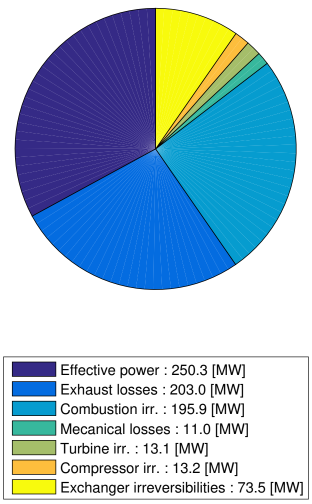

Figure 4.6: Exergy pie-chart of the SAGT

SAHRGT1:

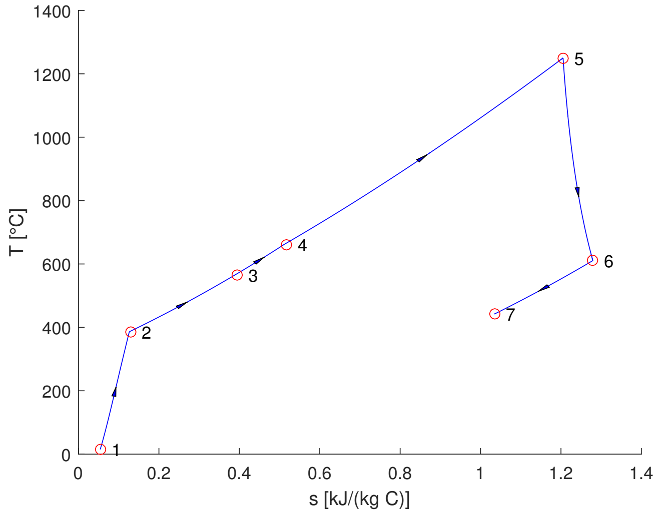

Figure 4.7: T-S diagram of the SAHRGT1. Heat recovery exchanger between 2 and 3. Solar heat exchanger between 3 and 4.

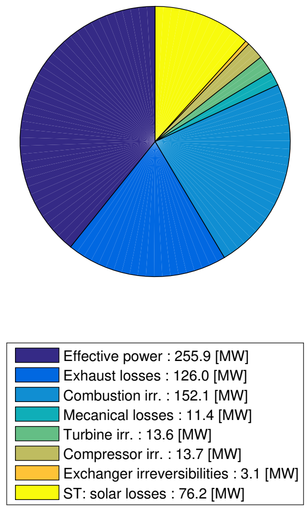

Figure 4.8: Exergy pie-chart of the SAHRGT1

SAHRGT2:

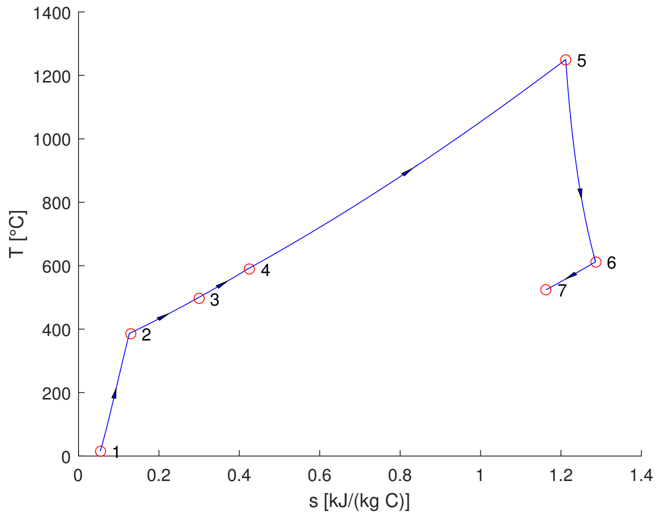

Figure 4.9: T-S diagram of the SAHRGT2. Solar heat exchanger between 2 and 3. Heat recovery exchanger between 3 and 4.

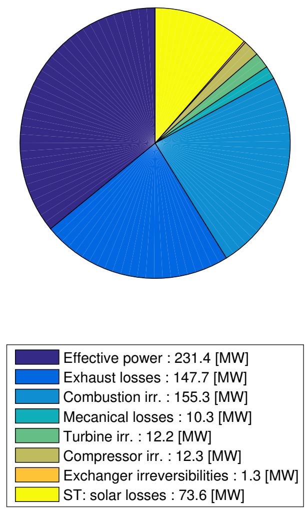

Figure 4.10: Exergy pie-chart of the SAHRGT2

The overall performance of each cycle is then presented in the table below. Mechanical losses and exergetic rotor losses are not shown in the table because they are constant for all cycles. $\eta_{mec} = 0.958$ and $\eta_{rotex} = 0.9075$ (more details about η_{rotex} in [21]).

	NGT	SAGT	HRGT	SAHRGT1	SAHRGT2
$Pe_{SC}\ [MW]$	225	250.3	225	255.9	231.4
$\boldsymbol{\eta_{toten,\,GT}}$	**0.364**	**0.338**	**0.444**	**0.401**	**0.367**
$\eta_{gen,\,GT}$	1	0.929	1	0.903	0.916
$\eta_{cyclen,\,GT}$	0.38	0.38	0.463	0.463	0.419
$\boldsymbol{\eta_{totex,\,GT}}$	**0.349**	**0.329**	**0.425**	**0.392**	**0.359**
$\eta_{gex,\,GT}$	0.684	0.646	0.705	0.65	0.645
$\eta_{cyclex,\,GT}$	0.532	0.532	0.63	0.63	0.582
$\dot{m}_{air}\ [kg/s]$	545	613	555	638	572
$\dot{m}_{fuel}\ [kg/s]$	12	12	10	10	10
$\boldsymbol{\eta_{en,\,sol-rad}}$	/	**0.206**	/	**0.235**	**0.052**
$\eta_{en,\,sol-field}$	/	0.569	/	0.531	0.568
$\eta_{en,\,sol-heat}$	/	0.362	/	0.442	0.091
$\boldsymbol{\eta_{ex,\,sol-rad}}$	/	**0.221**	/	**0.251**	**0.0554**
$\eta_{ex,\,sol-field}$	/	0.359	/	0.381	0.36
$\eta_{ex,\,sol-ex.conv}$	/	0.614	/	0.66	0.154
$A_{coll}\ [m^2]$	/	153728	/	164814	154046
solar share	0	0.102	0	0.121	0.121
$\mathbf{CO_{2,prod}\ [g/kWh]}$	**538**	**484**	**441**	**388**	**429**
$T_{exhaust}\ [^\circ C]$	616.8	614.6	444	442.2	524.3

Table 4.1: Performance summary table

4.4.2 Discussion

The first thing to understand is that the red line in the table separates two groups that cannot be really compared. Indeed, as the power boosting mode has been chosen, the power of the non-hybridized gas turbine is fixed (225 MW) while the fuel consumption of the hybrid is fixed. Therefore, as the gas turbine with heat recovery is more efficient than the standard gas turbine, the fuel consumption of the heat recovery gas turbine is lower than the fuel consumption of the standard gas turbine. That is why the solar share is different to the right and to the left of the red line. Due to this solar share difference, the effects of adding 70 solar MW on the cycle efficiencies cannot be compared. As a consequence, both groups are analysed separately. In addition, it is recommended to look at the table in the same time than reading the discussion about the results.

Without exhaust heat recovery

Nevertheless, the SAGT can be compared with the ISCCs of the previous chapter because the solar share is the same. The table is analysed colour by colour.

- $\eta_{toten,\,GT}$ and $\eta_{totex,\,GT}$ of the SAGT are slightly lower than those of the NGT. Indeed, it is due to the deterioration of $\eta_{gen,\,GT}$ and $\eta_{gex,\,GT}$ because of the low solar field efficiency. In addition, as it can be noticed, $\eta_{cyclen,\,GT}$ and $\eta_{cyclex,\,GT}$ are not impacted by the integration of the solar field into the power plant (contrary to $\eta_{cyclen,\,SC}$ and $\eta_{cyclex,\,SC}$ in the previous chapter). Indeed, this model does not consider a variable turbine polytropic efficiency with respect to the air mass flow, therefore the cycle efficiencies are independent of the power output, thus of the total heat input and thus also of the solar heat flux.
- As a consequence, the solar heat addition results in only increasing the working fluid mass flow, in opposition to the combined cycle hybridization which improves also the specific work of the cycle.

- Concerning the solar performance, it is noticed that $\eta_{en,\,sol-rad}$ and $\eta_{ex,\,sol-rad}$ are low, lower than the combined cycle due to the two effects explained below:

  Firstly, as it is observed in the table, the solar field efficiency is quite high for such a high solar receiver temperature ($495[°C]$). It is due to the fact that the concentration ratio being very high, the solar field efficiency is less dependent on the solar receiver temperature and more on the concentration efficiency (this trend can be observed in the energy pie-charts in the appendices). The energy and exergy solar field efficiencies of the SAGT are lower than the solar field efficiencies of the ISCC2 and 3 but are higher than those of the ISS 4 and 5, due to the solar field parameters and to the solar receiver temperature. As A_{coll} is totally dependent on the solar field efficiency, the same trend is observed for A_{coll}.

  Secondly, it can be seen that $\eta_{en,\,sol-heat}$ and $\eta_{ex,\,ex.conv}$ are lower than those of the previous chapter because the gas turbine cycle efficiencies (cyclen and cyclex) are lower than the bottoming steam cycle efficiencies. in addition, $\eta_{en,\,sol-heat}$ is lower than $\eta_{cyclen,\,GT}$ only because by definition, $\eta_{en,\,sol-heat}$ takes into account the mechanical losses, which is not the case for $\eta_{cyclen,\,GT}$. On the contrary, $\eta_{ex,\,ex.conv}$ is higher than $\eta_{cyclex,\,GT}$ because the solar exergy addition increases the average temperature in the combustion chamber, lowering the irreversibilities in the combustion chamber, thus increasing η_{gex} and Pe_{GT}. Accordingly, this indirect power increase (not directly due to the solar exergy addition) is taken into account in the numerator of $\eta_{ex,\,ex.conv}$ while the denominator takes only into account the exergy gain in the solar heat exchanger and not the indirect exergy gain in the combustion chamber.

- Finally, the CO_2 emissions are decreased with the same factor than the power is increased. Nevertheless, the gas turbine CO_2 emissions remain much higher than the combined cycle CO_2 emissions because of the lower total efficiency of the gas turbine.

With heat recovery

In this subsection the HRSGT, the SAHRGT1 and the SAHRGT2 are compared with each other. The table is still analysed colour by colour.

- Firstly, the hybrid gas turbines performance is lower than the standard heat recovery gas turbine performance due to the degradation of η_{gen} and η_{gex}. η_{cyclen} and η_{cyclex} are the same between the HRGT and the SAHRGT1 for the same reason as explained for the NGT and the SAGT and because the heat flux transferred into the heat recovery exchanger is the same, which is not the case for the SAHRGT2.

  Regarding both hybrids, the SAHRGT1 achieves the highest total energy efficiency because despite a smaller η_{gen} due to the higher solar receiver temperature, the SAHRGT1 gets better benefit from the exhaust heat recovery, as explained in the section 4.3, resulting in a greater η_{cyclen}. From the exergy point of view, η_{cyclex} is higher for the SAHRGT1 due to the higher exergy recovered from the exhaust, as confirmed by the smaller exhaust loss depicted in the exergy pie chart of the SAHRGT1. In addition, despite greater solar losses for the SAHRGT1, η_{gex} is also higher for the SAHRGT1 because the average temperature in the combustion chamber is higher for the SAHRGT1 (as it can be seen in Figure 4.7 and 4.9), and thus the combustion irreversibilities are lower (as it can be seen in Fig. 4.8 and 4.8). As a consequence, η_{totex} is higher for the SAHRGT1.

- The air mass flow is greater in the SAHRGT1 compared to the SAHRGT2 because with the same fuel mass flow, the specific heat load in the combustion chamber of the SAHRGT1 $(h_5 - h_4)$ is smaller (as it can be seen in the Figures 4.7 and 4.9), increasing the air excess coefficient as described by the following equation:

$$\lambda = \frac{LHV - h_5}{(h_5 - h_4)m_{al}} \tag{4.6}$$

More details about this equation can be found in the project report [17] or in the book [21].

- Concerning the solar performance, higher $\eta_{en,\, sol-rad}$ and $\eta_{ex,\, sol-rad}$ are observed for the SAHRGT1 compared to the SAHRGT2 because despite the fact that $\eta_{en,\, sol-field}$ and $\eta_{ex,\, sol-field}$ are lower due to a greater solar receiver temperature, $\eta_{en,\, sol-heat}$ and $\eta_{ex,\, sol-heat}$ are significantly higher thanks to the better heat/exergy recovery performance of the SAHRGT1 compared to the SAHRGT2. Nevertheless, the aperture collector area is greater for the SAHRGT1 because the solar field efficiency is smaller. The solar share of these two hybrids is higher than the solar share of the SAGT because the exhaust heat recovery leads to a lower fuel consumption for the same solar heat flux input, as already explained previously.

- Due to the higher power generated by the SAHRGT1, the CO_2 emissions are lower for the SAHRGT1 than for the SAHRGT2.

As a conclusion, it is obtained that the SAHRGT1 achieves better performance than the SAHRGT2. Nevertheless, this could be not the case with a lower concentration ratio, with a higher $\dot{Q}_{sol}$, with a higher compression ratio or with a higher inlet turbine temperature because it would lead to a faster increase in solar radiation losses for the SAHRGT1 compared to the SAHRGT2.

4.5 Parameter study

The most interesting hybridized gas turbine is the SAGT because the heat recovery gas turbines does not allow high power capacities. Indeed, this system needs very big heat transfer surfaces (50 m^2/MW) [21]. Furthermore, the heat recovery gas turbine cannot be integrated into a combined cycle. Consequently, the parameter study is achieved on the SAGT.

4.5.1 $\dot{Q}_{sol}$

Firstly, the variation of the DNI produces the same trends for η_{toten} and $\eta_{en,\, sol-rad}$ than for the combined cycle hybridization, that is why this parameter variation is not presented in this chapter. Nevertheless, the solar share variation is studied.

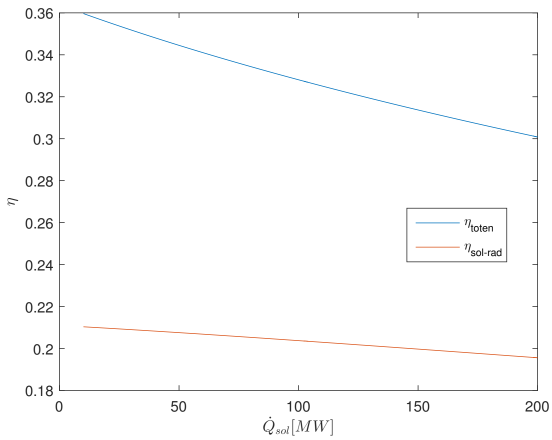

Figure 4.11: Total energy efficiency and solar radiation-to-electrical efficiency with respect to $\dot{Q}_{sol}$

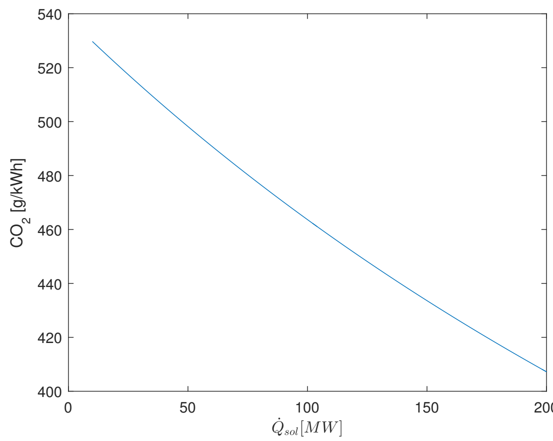

Figure 4.12: CO_2 emissions with respect to $\dot{Q}_{sol}$

As it can be seen in the graphs, contrary to the combined cycle hybridization, the solar radiation-to-electrical efficiency decreases with respect to the solar heat flux because the solar field efficiency decreases. Indeed, higher is $\dot{Q}_{sol}$, higher is the air temperature difference in the solar exchanger and thus higher is the solar receiver temperature. In addition, $\eta_{en,\,sol-heat}$ remains constant. Finally, the CO_2 emissions decrease because the power output increases.

4.5.2 T_H

Furthermore, the influence of the turbine inlet temperature is studied. The temperature range is $[700°C,\ 2500°C]$. The upper temperature 2500 $°C$ is purely theoretical because the turbine materials do not withstand such a temperature but this theoretical temperature range is needed to observe a maximum efficiency.

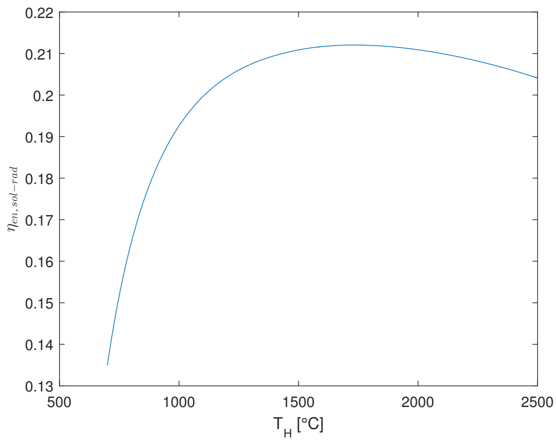

Figure 4.13: Solar radiation-to-electrical efficiency with respect to T_H

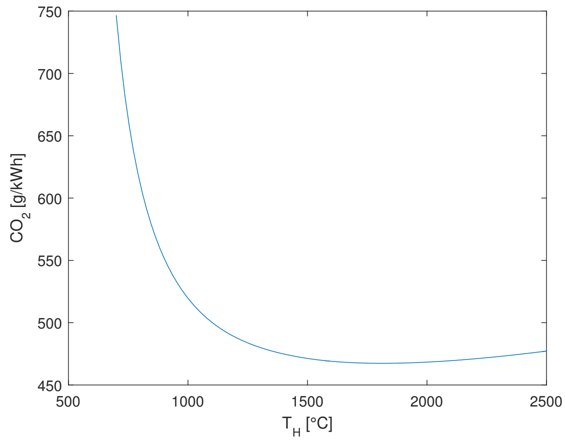

Figure 4.14: CO_2 emissions with respect to T_H

The graphs above show that there is an optimal temperature ($\tilde{1}800°$) for which the solar radiation-to-electrical efficiency is the highest and for which the CO_2 emissions are the lowest. The graph of η_{toten} has the same shape and the same optimal temperature than the graph of $\eta_{en\,sol-rad}$. In fact, low temperatures have the disadvantage to lower η_{cyclen} and thus $\eta_{en,\,sol-heat}$ while high temperatures have the disadvantage to lower the solar field efficiency due to the high radiation losses. As it was seen in the graph 2.5, the optimal temperature relative to $\eta_{en\,sol-rad}$ depends on the concentration ratio. With the selected concentration ratio, the design inlet turbine temperature does not match with the optimal temperature.

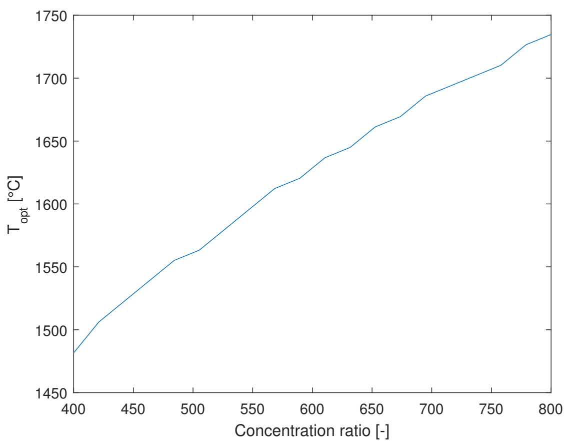

Figure 4.15: optimal turbine inlet temperature with respect to the concentration ratio

Therefore, it is preferable for this case to increase the inlet turbine temperature, if it is possible regarding the thermal resistance of materials. Besides, as the concentration ratio could vary throughout the year, it could be relevant to derive the optimal temperatures for a certain range of concentration ratios (lower than the design value, e.g. [400,800]). It can be seen in the Figure4.15 that the optimum temperatures are big and thus difficult to achieve regarding the resistance of materials.

4.5.3 solar field

Finally, the solar field input parameters are studied. For example, the performance of the gas turbine hybridized with parabolic troughs is analysed. The new solar field parameters are:

$$\eta_{conc} = 0.75 \qquad C = 80$$

The solar field efficiency becomes 0.442 compared to 0.569 for the central tower. This results in lower overall performance. The aperture collector area becomes 198 016 m^2 compared to 153 728 m^2 with the central tower. As explained in the section 4.1, the choice of the solar field type is thus really important for the gas turbine.

4.6 Overall combined cycle hybridization

In this section, three hybrid power plants are compared: the first one is the ISCC2 already analysed. The second one is the hybridized gas turbine of a combined cycle ($SAGT_{cc}$) and the last one is a mix between the first two one ($ISCC2 + SAGT_{cc}$). In fact, 35 solar MW are injected in the gas turbine and 35 solar MW are injected in the bottoming cycle of the combined cycle. The $\dot{Q} - T$ diagrams and the pie charts of the NGCC and the ISCC2 can be found in the chapter 4. The $\dot{Q} - T$ diagrams and the pie charts of the $SAGT_{cc}$ and the $ISCC2 + SAGT_{cc}$ can be found in the appendices.

	NGCC	ISCC2	$SAGT_{cc}$	$ISCC2 + SAGT_{cc}$
$Pe_{tot}\ [MW]$	350.5	384.9	389.4	387.2
$Pe_{GT}\ [MW]$	225	225	250.3	237.7
$Pe_{SC}\ [MW]$	125.5	159.9	139.1	149.5
η_{toten}	**0.567**	**0.524**	**0.525**	**0.525**
η_{totex}	**0.543**	**0.51**	**0.512**	**0.512**
$\eta_{toten,GT}$	0.364	0.364	0.338	0.35
$\eta_{toten,ST}$	0.377	0.349	0.376	0.361
$\eta_{totex,GT}$	0.349	0.349	0.329	0.338
$\eta_{totex,ST}$	0.686	0.548	0.685	0.604
$\dot{m}_{LP}\ [kg/s]$	8	5	9	7
$\dot{m}_{IP}\ [kg/s]$	11	4	12	8
$\dot{m}_{HP}\ [kg/s]$	70	99	78	88
$\dot{m}_{air}\ [kg/s]$	545	545	613	579
$\dot{m}_{fuel}\ [kg/s]$	12.37	12.37	12.37	12.37
$\eta_{en,sol-rad}$	/	**0.295**	**0.317**	**0.308**
$\eta_{en,sol-field}$	/	0.6	0.569	GT: 0.576 ST: 0.6
$\eta_{en,sol-heat}$	/	0.491	0.557	0.524
$\eta_{ex,sol-rad}$	/	**0.316**	**0.339**	**0.33**
$\eta_{ex,sol-field}$	/	0.33	0.359	GT: 0.355 ST: 0.33
$\eta_{ex,sol-ex.conv}$	/	0.958	0.945	0.963

	NGCC	ISCC2	$SAGT_{cc}$	$ISCC2 + SAGT_{cc}$
$A_{coll}\,[m^2]$	/	145 781	153 728	GT: 75 920 ST: 72 890
solar share	0	0.102	0.102	0.102
$CO_{2,prod}\,[g/kWh]$	**346**	**315**	**311**	**313**
$T_{exhaust}\,[°C]$	85.2	71.1	85.5	78.7
$T_{dew\,point}\,[°C]$	44.4	44.4	42.5	43.4

Table 4.2: Performance summary table

By comparing the $SAGT$ performance with the ISCC2 performance, it was expected that the ISCC2 achieves better performance than the SAGT integrated in a combined cycle. Indeed, the solar radiation-to-electrical efficiency is clearly better for the ISCC2 (0.295) than for the $SAGT$ (0.206). However, it is noticed in the table above that the $SAGT_{cc}$ performance is better than the ISCC2 performance. All the main hybrid parameters are better. Actually, it is due to the fact that the total power output is the highest for the $SAGT_{cc}$. Indeed, the gas turbine hybridization has a double effect on the cycle: not only is the power of the gas turbine increased, but the power of the steam cycle is also increased (+13.6 MW). In fact, the air mass flow in the gas turbine is increased by the solar flux addition, therefore the flue gas mass flow entering the HRSG is also increased and thus the power output of the steam turbine is increased. The power difference between the NGCC and the ISCC2 is 34.4 MW while the power difference between the NGCC and the $SAGT_{cc}$ is 38.9 MW. That is why despite that the gas turbine hybridization seemed at the beginning less efficient than the bottoming cycle hybridization, it is finally the contrary.

Finally, it is noticed that the $ISCC2 + SAGT_{cc}$ performance is between the ISCC2 performance and the $SAGT_{cc}$ performance. Below are the graphs of η_{toten} and $\eta_{en,\,sol-rad}$ according to the gas turbine solar heat flux $\dot{Q}_{solg}$, in which the cases between the ISCC2 case and the $SAGT_{cc}$ case are in fact depicted. Indeed, the total solar heat flux remains constant but the distribution of this heat flux between the gas turbine and the bottoming cycle is changed.

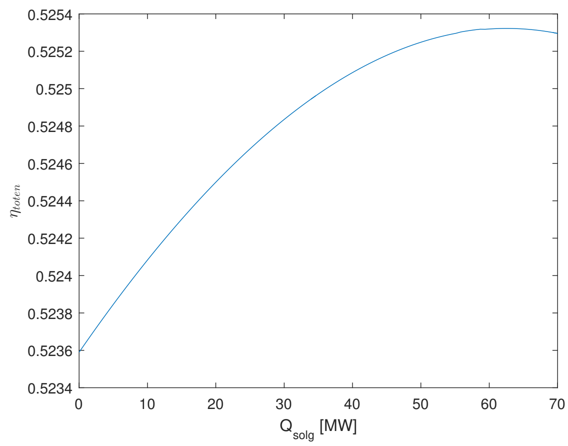

Figure 4.16: Total energy efficiency with respect to $\dot{Q}_{solg}$ by considering $\dot{Q}_{solg} + \dot{Q}_{sol} = 70MW$

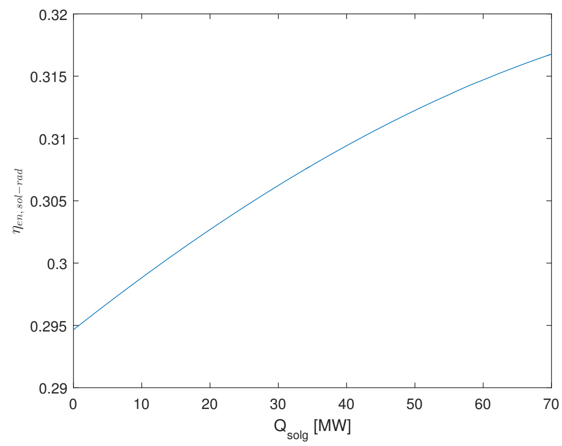

Figure 4.17: Rad. to elec. efficiency with respect to $\dot{Q}_{solg}$ by considering $\dot{Q}_{solg} + \dot{Q}_{sol} = 70MW$

A maximum for η_{toten} is observed at approximately $\dot{Q}_{solg} = 62MW$ because the advantage of the $SAGT_{cc}$ of producing more power is counterbalanced by the disadvantage of achieving greater solar losses. Indeed, solar losses increase with respect to $\dot{Q}_{solg}$ for the SAPG (see Fig. 4.11) while they remain constant for the ISCC2. (see Figure 3.19), as it was previously explained.

Chapter 5

Economic aspects

Besides the thermodynamic aspect, a preliminary economic analysis is conducted in order to find the most profitable hybridization solution. The economic analysis actually allows to gather the main hybrid parameters in a single economic parameter. As it is the parameter that is most taken into account by investors, this assesses also the penetration ability of such hybridization system in the market. The levelized cost of energy (LCOE) is used to link the parameters previously mentioned and the cost of the power plant. It is expressed in \$/kWh. This relation is obtained as follows.

5.1 General expression of the LCOE

First, a distinction is done between the fixed costs, represented by the CAPital EXpenditures (CAPEX), and the variable costs, represented by the OPerating EXpenses (OPEX). Furthermore, no inflation rate and no discount rate are initially taken into account. The discount rate is defined here as the annual income as a percentage of the amount invested[22]. Indeed, the discount rate gives more value to expenses made later than expenses made now because money that has not been spent in the present could be invested in another project and could bring money back. The discount rate is thus equal to the annual investment rate that could be perceived if the money is not spent now in the power plant, and is thus invested in another project. To resume, everybody prefers to incur a \$100 cost later than a \$100 cost now. In addition, the inflation rate enables to take into account the different value between 1 dollars now and 1 dollars one year later. As a consequence, by not considering this inflation rate, the LCOE is expressed in 2018 dollars. This is defined as the nominal LCOE. To begin, the total cost of the power plant is defined as follows [31]:

$$C_{tot} = CAPEX + \sum_{i=1}^{n} OPEX \tag{5.1}$$

with "n" the estimated lifespan of the power plant, C_{tot} and CAPEX expressed in $\$_{2018}$, and OPEX expressed in $\$_{2018}$/year.
Then, the total cost is spread over n years and is expressed according to the annual electricity production (E_{net} in kWh/year).

$$\sum_{i=1}^{n} LCOE_{nom} \cdot E_{net} = CAPEX + \sum_{i=1}^{n} OPEX$$

Concerning the variable costs, as it is preferable to spend money later than now, the LCOE and OPEX of the i^{th} year are discounted by the factor $\frac{1}{(1+r)^i}$, where r is the nominal discount rate.

$$\sum_{i=1}^{n} \frac{LCOE_{nom} \cdot E_{net}}{(1+r)^i} = CAPEX + \sum_{i=1}^{n} \frac{OPEX}{(1+r)^i}$$

The nominal LCOE being defined as a constant, it can be removed from the sum.

$$LCOE_{nom} = \frac{CAPEX + \sum_{i=1}^{n} \frac{OPEX}{(1+r)^i}}{\sum_{i=1}^{n} \frac{E_{net}}{(1+r)^i}} \tag{5.2}$$

This nominal levelized cost of energy is expressed in 2018 dollars. However, a real LCOE expressed in real dollars is wanted. Therefore, as the equivalent cost of 1 $\$_{2018}$ in the i^{th} year will be $1 \cdot (1+e)^i \, \$_{i^{th}year}$, by taking into account the inflation rate e, the real LCOE in $\$_{real}$/kWh becomes:

$$LCOE_{real} = \frac{CAPEX + \sum_{i=1}^{n} \frac{OPEX\,(1+e)^i}{(1+r)^i}}{\sum_{i=1}^{n} \frac{E_{net}\,(1+e)^i}{(1+r)^i}} \tag{5.3}$$

In order to simplify this equation, the inflation rate is included into the nominal discount rate with a view to get the single real discount rate, R. Therefore:

$$1 + R = \frac{1+r}{1+e} \tag{5.4}$$

As "e" is between 0 and 1, the Taylor series approximation achieves a very small error compared to the exact solution. Therefore:

$$(1+e)^{-1} = 1 - e + e^2 - e^3 + ...$$

$$\Rightarrow (1+R) = (1+r)(1-e+e^2+...) = 1 + r - e - e \cdot r + e^2 + \text{ higher order terms } \approx 1 + r - e$$

$$R = 1 + r - e \tag{5.5}$$

The expression of the LCOE becomes

$$LCOE_{real} = \frac{CAPEX + \sum_{i=1}^{n} \frac{OPEX}{(1+R)^i}}{\sum_{i=1}^{n} \frac{E_{net}}{(1+R)^i}} \tag{5.6}$$

In order to further simplify this expression, OPEX and E_{net} are considered constant, which is quite realistic. As a consequence, OPEX and E_{net} can be removed from the sum:

$$LCOE_{real} = \frac{\frac{CAPEX}{\sum_{i=1}^{n} \frac{1}{(1+R)^i}} + OPEX}{E_{net}} \tag{5.7}$$

It is noted that the sum in this equation is a geometric series of common ratio and first term $(1+R)^{-1}$, with "n" terms. Therefore:

$$\sum_{i=1}^{n} \frac{1}{(1+R)^i} = (1+R)^{-1}[1 + (1+R)^{-1} + (1+R)^{-2} + ... + (1+R)^{-n+1}] = (1+R)\,\frac{1-(1+R)^{-n}}{1-(1+R)^{-1}}$$

$$\Rightarrow \sum_{i=1}^{n} \frac{1}{(1+R)^i} = (1+R)\frac{\frac{(1+R)^n - 1}{(1+R)^n}}{\frac{(1+R)-1}{(1+R)}} = \frac{(1+R)^n - 1}{R(1+R)^n} \tag{5.8}$$

Finally, the final expression of the LCOE (confirmed by [30]) taking into account the nominal discount rate and the inflation rate is:

$$LCOE_{real} = \frac{CAPEX \cdot \frac{R(1+R)^n}{(1+R)^n - 1} + OPEX}{E_{net}} \tag{5.9}$$

where the numerator is in [$\$_{real}$/year] and the denominator is in [kWh/year]. The first term of the numerator is thus the investment cost annuity (cost spread over "n" years).

5.2 Detailed expression of the LCOE in the present case

In this section, CAPEX, OPEX and E_{net} are developed and hypotheses are done in order to compute the LCOE. The first hypothesis concerns the lifespan of the power plant, it is fixed to 30 years [18]. In addition, the inflation rate (e) is set to 2% and the nominal discount rate (r) is set to 8 % [22]. Therefore, the real discount rate (R) is approximated to 6%.

5.2.1 CAPEX

First of all, CAPEX is defined as follows:

$$CAPEX = Cost_{sol.f.} + Cost_{cycle} \tag{5.10}$$

where the first term is the solar field investment cost [$] and the second term is the cycle investment cost [$]. The solar field investment cost is different for parabolic troughs and for central tower:

- parabolic troughs [20]: $Cost_{sol.f.} = 310(\frac{\$}{m^2}) \cdot A_{coll}(m^2)$
- central tower [6]: $Cost_{sol.f.} = 225(\frac{\$}{m^2}) \cdot A_{coll}(m^2) + 225(\frac{\$}{kW}) \cdot \dot{Q}_{sol}(kW)$
  where the first term accounts for the heliostats (the mirrors) and the second terms accounts for the central receiver.

The cycle investment cost is also different depending on whether it is a combined cycle or a gas turbine.

- gas turbine [18]: $Cost_{cycle} = 235(\frac{\$}{kW}) \cdot Pe_{tot}(kW)$
- combined cycle [18]: $Cost_{cycle} = 860(\frac{\$}{kW}) \cdot Pe_{SC}(kW) + 235(\frac{\$}{kW})Pe_{GT}(kW)$
  where the first term $Cost_{ST}$ accounts for the steam unit and the second term $Cost_{GT}$ accounts for the gas unit of the combined cycle.

5.2.2 OPEX

Concerning OPEX, the annual operating and maintenance (O & M) cost, it is defined as follows [18]:

$$OPEX = 0.02 \cdot Cost_{sol.f.} + 0.02 \cdot Cost_{ST} + 0.05 \cdot Cost_{GT} + Cost_{fuel} + Cost_{CO_2} \tag{5.11}$$

where:

- $Cost_{fuel}[1] = 6(\frac{\$}{GJ}) \cdot LHV\frac{GJ}{kg}) \cdot \dot{m}_{fuel}(\frac{kg}{year})$ is the fuel cost per year.
- $Cost_{CO_2} = tax_{CO_2}(\frac{\$}{ton}) \cdot \dot{m}_{CO_2}(\frac{ton}{year})$ is the tax on the CO_2 produced.

5.2.3 E_{net}

Finally, the net electricity production per year is computed:

$$E_{net} = (0.8 \cdot Pe_{no\,sol} + 0.4 \cdot \mathit{\Delta} Pe_{sol}) \cdot 364 \cdot 24 \tag{5.12}$$

where $Pe_{no\,sol}$ is the power produced by the combined cycle without any solar heat flux addition (in kW) and $\mathit{\Delta} Pe_{sol}$ is the additional power output due to the solar heat flux addition (in kW). 0.4 and 0.8 are the capacity factors [33, 18]. The capacity factor is defined as the fraction of annual power supplied by a plant relative to its annual design power output [26]. It takes thus into account the DNI variation over a year.

5.3 Results

5.3.1 Bottoming cycle hybridization of the combined cycle

First of all, the LCOE is computed for the different bottoming cycle hybridization options. A first LCOE is calculated without any carbon tax, then a second LCOE is computed with the break-even (BE) carbon tax of the ISCC2, which is the carbon tax for which the LCOE of the non-hybridized power plant is the same than that of the hybridized power plant. This break-even carbon tax, 36$\$/ton_{CO_2}$ corresponds to the french carbon tax, as it can be seen on the carbon tax scale in the appendices (Fig. A.23). [10] The third considered carbon tax is the Swedish carbon tax, 140$\$/ton_{CO_2}$.

	NGCC	ISCC2	ISCC3	ISCC4	ISCC5
LCOE [$/kWh] with Carbon tax = 0 $\$/ton_{CO_2}$	0.04482	0.04542	0.04549	0.04887	0.04881
LCOE [$/kWh] with Carbon tax = 36 $\$/ton_{CO_2}$	0.05726	0.05727	0.05738	0.06075	0.06067
LCOE [$/kWh] with Carbon tax = 140 $\$/ton_{CO_2}$	0.0932	0.09153	0.09175	0.09508	0.09492

Table 5.1: LCOE for different carbon prices

As it can be observed, the LCOEs of the hybridized combined cycles are greater than the LCOE of the natural gas combined cycle due to the high investment cost of the solar field. The ISCC3 and 4 are the less cost-effective power plants because the high radiation losses (due to the high solar receiver temperature) leads to a higher aperture collector area and thus to a higher investment cost compared to the ISCC2 and 3. The best ISCC from the economic point of view is the ISCC2. It can be seen that higher is the carbon tax, higher is the LCOE difference between the ISCCs. Finally, even with a carbon tax equal to 140 $\$/ton_{CO_2}$, ISCC4 and ISCC5 are less cost-effective than the NGCC.

5.3.2 Gas turbine hybridization

Afterwards, the LCOEs of the gas turbines are computed, with the same carbon taxes than for the combined cycle.

	NGT	SAGT	HRGT	SAHRGT1	SAHRGT2
LCOE [$/kWh] with Carbon tax = 0 $\$/ton_{CO_2}$	0.06248	0.06228	0.05178	0.05176	0.05407
LCOE [$/kWh] with Carbon tax = 36 $\$/ton_{CO_2}$	0.08185	0.08062	0.06767	0.06662	0.06973
LCOE [$/kWh] with Carbon tax = 140 $\$/ton_{CO_2}$	0.13783	0.13361	0.11356	0.10956	0.11498

Table 5.2: LCOE for different carbon prices

It can be seen here that even without any carbon tax, the hybridized gas turbine is more profitable than the natural gas turbine. It can be explained by the fact that the gas turbine consumes more fuel per kWh than the combined cycle. Therefore, as the LCOE of the gas turbine is more dependent on the fuel consumption, the positive effect of the hybridization on the gas turbine is greater than that on the combined cycle, despite the fact that the solar field investment cost is higher. However, it can also be noticed that the LCOE of the SAGT is much higher than the LCOE of the ISCCs. In addition, the SAHRGT1 is confirmed to be better compared to the SAHRGT2 by the economical aspect. Indeed, the fuel consumption is higher for the SAHRGT2 due to the lower total efficiency of the cycle.

5.3.3 Overall combined cycle hybridization

In the end, the LCOE of the three combined cycle hybrids described in the section 4.6 are computed and represented in the following table.

	NGCC	ISCC2	$SAGT_{cc}$	$ISCC2 + SAGT_{cc}$
LCOE [$/kWh] with Carbon tax $= 0$ $\$/ton_{CO_2}$	0.04482	0.04542	0.04666	0.04602
LCOE [$/kWh] with Carbon tax $= 36$ $\$/ton_{CO_2}$	0.05726	0.05727	0.05845	0.05784
LCOE [$/kWh] with Carbon tax $= 140$ $\$/ton_{CO_2}$	0.0932	0.09153	0.09249	0.09199

Table 5.3: LCOE for different carbon prices

Even if the energetic and exergetic performance is better for the $SAGT_{cc}$ compared to the ISCC2, the LCOE is lower for the ISCC2 than for the $SAGT_{cc}$. That is due to the bigger solar investment cost of the solar tower compared to the parabolic troughs. As it can be seen in the graph below, by considering a constant total solar heat flux, the LCOE increases linearly with the solar heat flux percentage injected in the gas turbine, $\dot{Q}_{solg}$.

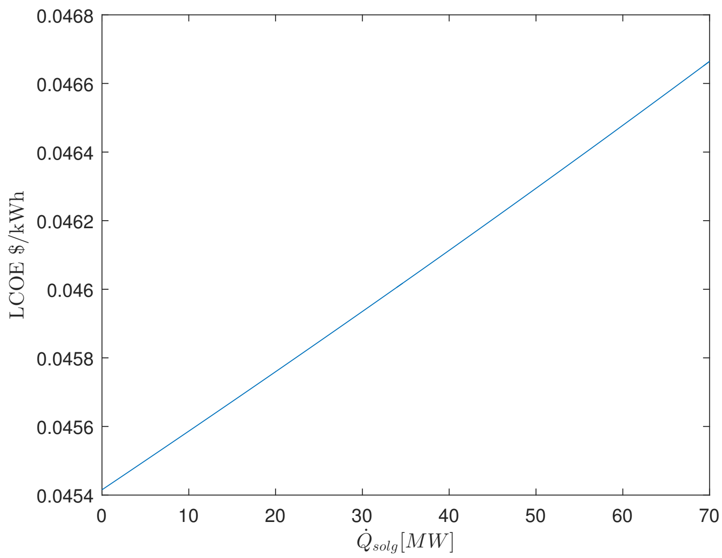

Figure 5.1: LCOE with respect to $\dot{Q}_{solg}$ by considering constant $\dot{Q}_{sol} + \dot{Q}_{solg} = 70\,[MW]$

5.4 Parameter study

As the ISCC2 is the most cost-effective power plant, an economical parameter study is achieved on this cycle. In this section, the LCOE parameter is computed for a CO_2 tax equal to zero.

5.4.1 DNI

Regarding the DNI variation, the graphs allow here to represent the annual change in performance due to the annual solar condition variation at one particular geographical site, compared to the performance at the design DNI (800 W/m^2). With the same hypothesises than in the section 3.7.1, the solar field size is fixed and the LCOE is obtained with respect to the DNI. As it can be noted in the figures below, the LCOE decreases linearly with the DNI because the annual power output increases with respect to the average annual DNI. The LCOE is constant for DNI values below 160 W/m^2 because the DNI is so low that radiation losses are greater than the solar energy impinging the aperture collector area, resulting in no heat flux transferred to the cycle. Therefore, the power output remains constant and thus the LCOE also.
Concerning the break-even CO_2 tax, it was computed thanks to the formula:

$$BE\_CO_2\_tax = \frac{LCOE - LCOE_0}{\frac{\dot{m}_{CO_2,0}}{E_{net,0}} - \frac{\dot{m}_{CO_2}}{E_{net}}} \tag{5.13}$$

where the index 0 refers to the non-hybridized power plant with the same fuel consumption and where $\dot{m}_{CO_2}$ is the annual CO_2 production in ton/year. It can be observed that the break-even CO_2 tax tends to infinity for low values of DNI. Indeed, the solar field efficiency tends to 0 when DNI tends to 160 W/m^2.

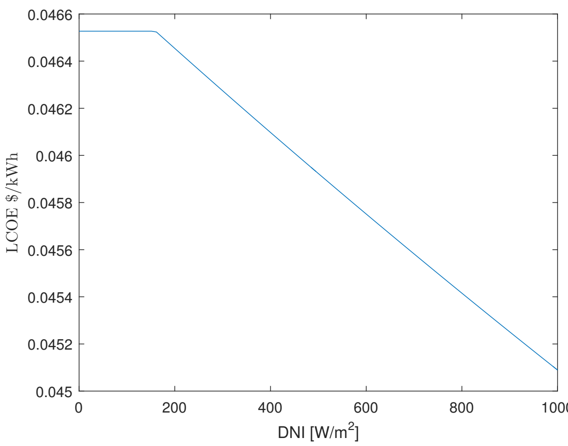

Figure 5.2: LCOE with respect to the average annual DNI

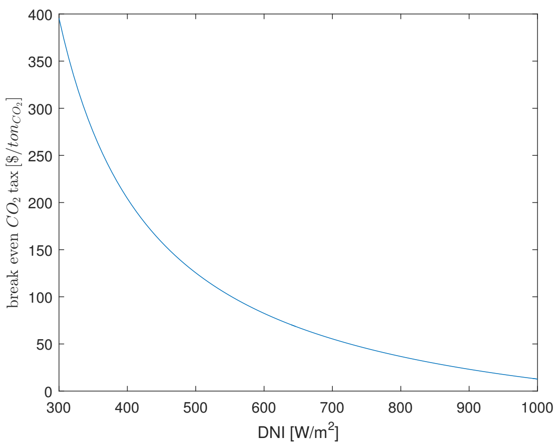

Figure 5.3: break-even CO_2 tax with respect to the average annual DNI

The results of the geographical DNI parameter study can be seen in the appendices (Fig. A.24 & A.25).

5.4.2 $\dot{Q}_{sol}$

Contrary to the DNI variation, the $\dot{Q}_{sol}$ variation induces the increase of the solar field investment cost. This investment cost increase is higher than the decrease in fuel consumption cost and thus the LCOE increases as it can be seen in the figure below.

Moreover, the break-even CO_2 tax remains constant according to $\dot{Q}_{sol}$. Indeed, as the fuel consumption remains constant (due to the power boosting mode), the break-even CO_2 tax variation depends only on the solar field investment cost variation and on the annual power output variation. These two latter parameters are precisely linked by the solar radiation-to-electrical efficiency, which remains constant with respect to $\dot{Q}_{sol}$ as it is observed in the Figure 6.17. That is why the break-even CO_2 tax remains constant.

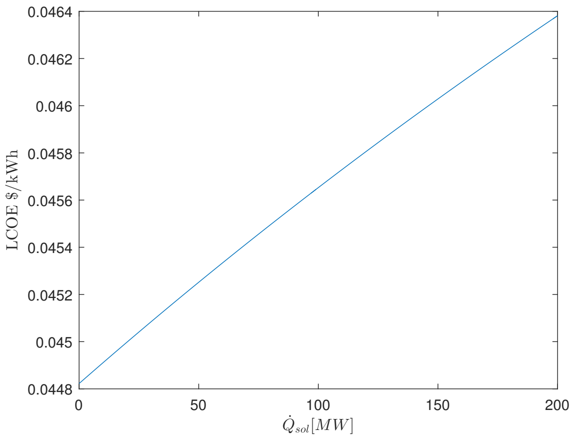

Figure 5.4: LCOE with respect to $\dot{Q}_{sol}$

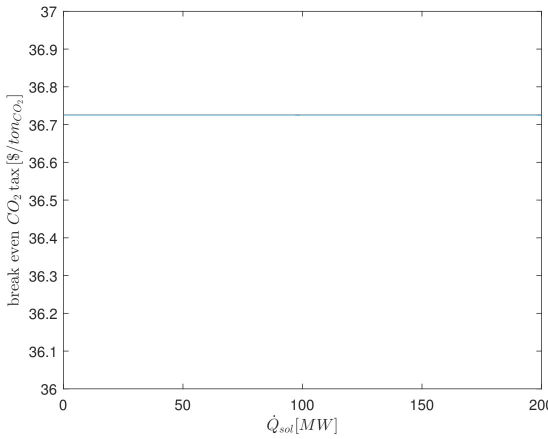

Figure 5.5: BE CO_2 tax with respect to $\dot{Q}_{sol}$

5.4.3 p_{HP}

Concerning the highest pressure of the bottoming cycle, it is observed that the LCOE decreases according to the increase in p_{HP} but tends to a horizontal asymptote. Indeed, the annual power output increase (due to the η_{cyclen} improvement) is counterbalanced by the solar field investment cost increase (due to higher solar radiation losses).

Regarding the break-even CO_2 tax, this not depends any more on only hybrid performance but this also depends on non-hybridized combined cycle performance (respectively the terms without index, and the terms with the index 0 in the formula 5.13). There is an optimal pressure because for low values of p_{HP}, there are not a lot of radiation losses and thus the performance improvement of the hybridized power plant is higher than the performance improvement of the non-hybridized power plant, lowering the break-even CO_2 tax. However, at one point, the solar radiation losses make the performance increase of the ISCC lower than the performance increase of the NGCC, resulting in the increase of the break-even CO_2 tax.

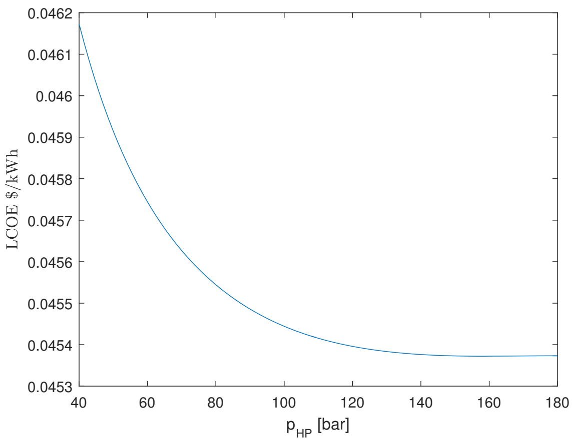

Figure 5.6: LCOE with respect to p_{HP}

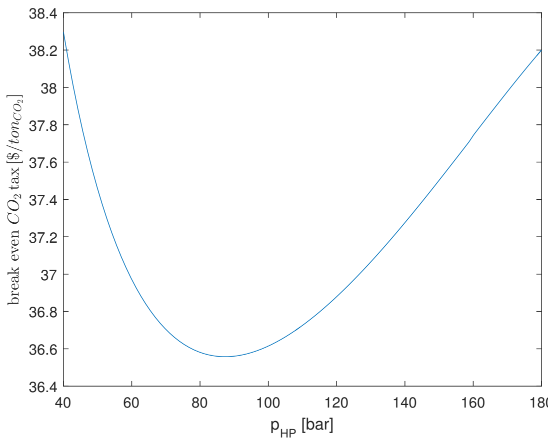

Figure 5.7: BE CO_2 tax with respect to p_{HP}

Chapter 6

Modelling on Thermoflow

The understanding of the problematic being achieved thanks to the Matlab program, it is appropriate to apply the theory to a specific case. In this respect, the modelling of an existent integrated solar combined cycle power plant is performed on a state of the art commercial program, Thermoflow. [1] This was possible thanks to the partnership with Tractebel Engineering, which provided the license in the context of an internship. The modelled power plant concerns in fact a project of the company, the "Duba project".

The modelling on Thermoflow is relevant for this work for many reasons. First of all, it allows to compare the results obtained through the Thermoflow model with the results obtained through the Matlab program. Secondly, the Thermoflow program enabling more features, it is possible to analyse more deeply the solar hybridization, for example the change in performance during one typical day. In addition, it allows to implement the fuel saving mode by enabling iteration on the fuel consumption. Indeed, it is needed in order to match the required power output, depending on the solar conditions, which was difficult to implement in the Matlab program. Generally, the fuel saving mode is valuable for industrialists because it allows to compare the hybrids for a given power output and it allows to analyse for a given power output, the behaviour of the system when the solar conditions change. Indeed, energy regulators impose a power output to the power plant, thus if a constant power output through the day is wanted, the fuel saving mode is required.

However, the fuel saving mode is not really relevant in the context of the proposed project. Indeed, the operators of the power plant have contracts with the gas industry in such a way that they receive a certain amount of gas and they are "obliged" to burn this amount of gaz. Besides, there are yet other incentives for Tractebel Engineering to build a Thermoflow model of the existent power plant. There are three major incentives:

- be able to change some parameters (for example the fuel) of the existent power plant in order to analyse the change in performance.
- better understand the hybridization and find ways to improve the performance of this kind of power plant.
- reuse this model for a future new project.

This chapter presents firstly the modelled power plant, then the modelling methodology used on Thermoflow and finally some valuable results.

6.1 Duba power plant description

First of all, the heat and mass balance flowsheet [12] of the power plant can be found in attached documents (Appendix1). The Duba project is located in Duba. It is a coastal city in the north west of Saudi Arabia. The combined cycle is composed of two different GE (General Electric) gas turbines (7FA.05 and 7F.04) connected to two identical heat recovery steam generators, including in each of them a duct burner. Steam generated in the two HRSGs is sent to a single three body steam turbine. (HP, IP and LP). However, this is a 2 pressure level based combined cycle (only LP and HP evaporators) even if a third pressure is used for the reheat between the HP steam turbine outlet and the IP steam turbine inlet. A single condenser and a single deaerator are part of the cycle. In addition to that, a single solar field is used in parallel with the two heat recovery steam generators in the high pressure circuit. The solar field consists of parabolic troughs with an indirect steam generation (secondary fluid is used to heat water in a solar exchanger).

In fact, water coming from the deaerator is split into two streams, the first one goes to the first HRSG and the second one to the second HRSG. Each stream is pumped to high pressure in a HP pump. Then, HP feed water coming from the HP pump is split into three main streams. The first stream is expanded to low pressure, then evaporated and finally sent back to the deaeretor. The second stream (together with the second stream of the HRSG2) is preheated, evaporated, and partially superheated in the solar heat exchanger. The third stream is preheated but only evaporated in the HRSG. The two latter streams are then mixed and injected in the first HP superheater of the HRSG. After that, an inconsistency was noticed between the heat and mass balance flowsheet given by the vendor [12] and the detailed plans of the heat recovery steam generator. Indeed, according to the flowsheet, there are 2 HP superheaters while 3 HP superheaters are depicted in the plans of the HRSG. In the end, 3 HP superheaters were taken into account in the Thermoflow model. In addition, two reheaters are used to reheat the steam coming from the HP turbine.

6.2 Modelling Methodology

Regarding Thermoflow, it is a mix between an "Application specific" program and a "Fully flexible" program [1] and that is why the program is so powerful. Indeed, the two types of program have advantages and disadvantages. The application specific focuses on one type of power plant and proposes a general model of it. The user can then model a subset of the general model via a guided procedure during which the user is not totally free. The advantage of using this type of program is the robustness as well as the simplicity and the speed of use due to the overall logical structure. However, the user has access to limited features. On the contrary, the "Fully flexible" program allows the user to model any wished system thanks to a library of components that can be connected via a graphical interface. However, the disadvantage of this type of program is the increased probability of inconsistencies and crashes because systems that have never been conceived by the developers have to be handled.

In this respect, three main programs are available in Thermoflow: GT pro, GT master and Thermoflex. The first two ones are mostly "Application specific" and the third one is "Fully flexible". The bigger benefit of Thermoflow is that the three programs are mutually compatible. This allows the use of the two first programs in order to easily create a general model close from the wanted system and then this allows the use of the third program to transform the general model into the specific desired system.

In the context of this work, the goal was firstly to make the thermodynamic properties of the thermoflow model as close as possible from those of the heat and mass balance given by the vendor. Many heat and mass balances exist depending on the weather conditions and the operating conditions. The one that was selected for the model construction provides the highest power output and the highest efficiency. Indeed, both turbines are at full load and winter weather conditions are considered, i.e. the ambient air temperature is 3 $°C$, with a relative humidity of

30 %. Gas turbines are fed with natural gas of LHV=46 406 kJ/kg.

6.2.1 GT pro

The aim was to go as further as possible in the modelling in the GT pro application because this application is the simplest and the most robust one, as explained previously. However, this application is only based on a Thermodynamic design, i.e. the input parameters can only be thermodynamic related parameters. In the thermodynamic design, the component performance is governed by defined thermodynamic characteristics. Furthermore, the configuration possibilities are limited. For example, it is not possible to insert a solar field in GT pro. Therefore, the solar field was firstly modelled as a black box, with water at the inlet and steam at the outlet. The mass flow and the temperature were specified. In addition, it is not possible to select two different gas turbines. Therefore, two 7FA.05 gas turbines (the most powerful) were selected. As it can be seen in the figure below, different input menus had to be filled. The figure below represents the preliminary model of the Duba power plant. All GT pro results are in attached documents (Appendix4).

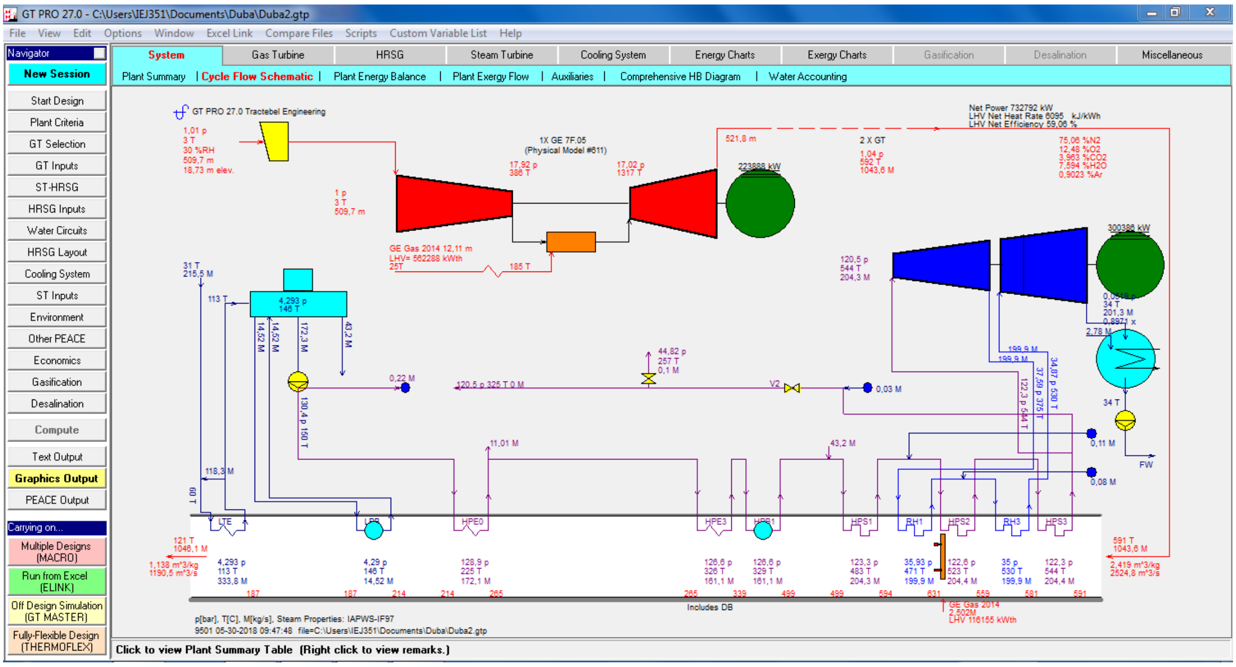

Figure 6.1: Preliminary Duba power plant model in GT Pro

The fully description of all steps is not presented here. Briefly, after all parameters were inserted and after the Thermoflow power plant configuration was the same than the existing power plant, the first tuning was done on the gas turbines because the steam turbine performance depends on the gas turbine parameters. Therefore, the flue gas temperature and the flue gas mass flow were specified in the GT inputs menu. This was performed together with the tuning of the output power by changing the compressor and turbine efficiency. After that, the exchanger performance in the HRSG was tuned in the HRSG inputs menu, in order to produce the correct steam mass flow. Finally, the steam turbine was tuned in the ST inputs menu in order to match the given steam turbine power output.

6.2.2 GT master

After the GT pro model has been completed, the model was run in the GT Master application in order to perform an off design simulation. Indeed, the thermodynamic design in GT pro generates the plant heat balances, the flow schematics and the preliminary hardware designs of the major components, based on the user-input thermodynamic criteria. On the contrary, the off design simulation computes the thermodynamic performance based on the user-input hardware system criteria (size, physical characteristics etc). The values computed in the GT pro application are firstly set by default in GT Master and the user can then change what is needed to be modified. The user can also decide to modify the ambient conditions and the equipment loads in order to analyse the performance under varying operating conditions.

In the context of the Duba project, the complete geometry of the exchangers in the HRSG was implemented in the GT master model, as it can be seen in the figure below representing the hardware design of the last superheater. GT master results are available in attached files (Appendix4).

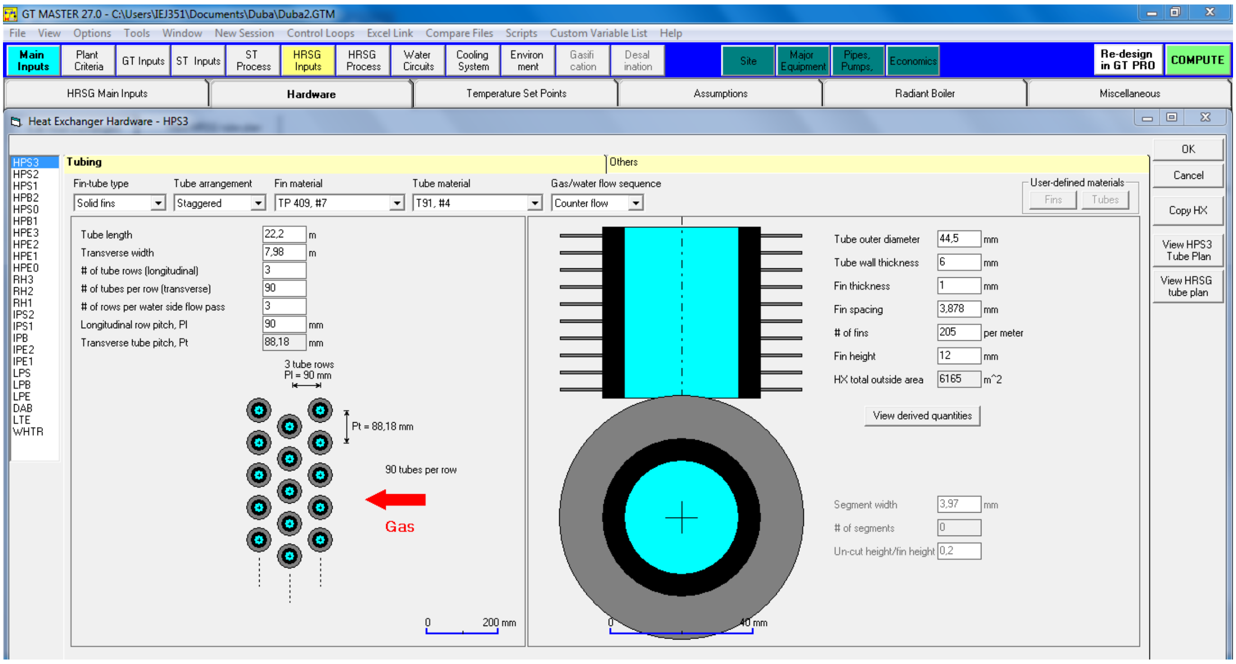

Figure 6.2: HRSG settings in GT Master

6.2.3 Thermoflex

In the end, the GT Master model was imported into the fully flexible application, Thermoflex. The first task in this program concerned the combined cycle in order to make the Thermoflex flow schematic as close as possible to the flowsheet [12] given by the vendor. Afterwards, the solar field was implemented.

Combined cycle

Many modifications of the general design provided by GT Master were performed in order to match the given flowsheet [12]. Only the main changes are described here. One of the two 7FA.05 gas turbines was firstly changed to a 7F.04 gas turbine. Therefore, the new gas turbine was tuned in order to obtain the correct flue gas temperature and mass flow as well as a correct power output. In addition, one deaerator was removed because two deaerators were initially created by GT Master whereas there is only one deaerator in the flowsheet given in data [12]. The LP circuit was also modified in such a way that LP feed water is firstly pumped at high pressure and then expanded before entering the LP evaporator (this was not modelled like that in GT Pro). Finally, pressure losses were specified in the heat exchangers of the HRSG in order to match the pressures of the model with the reality. A representation of the Thermoflex interface is depicted in the figure below. This flowsheet can be seen in detail in attached documents (Appendix4).

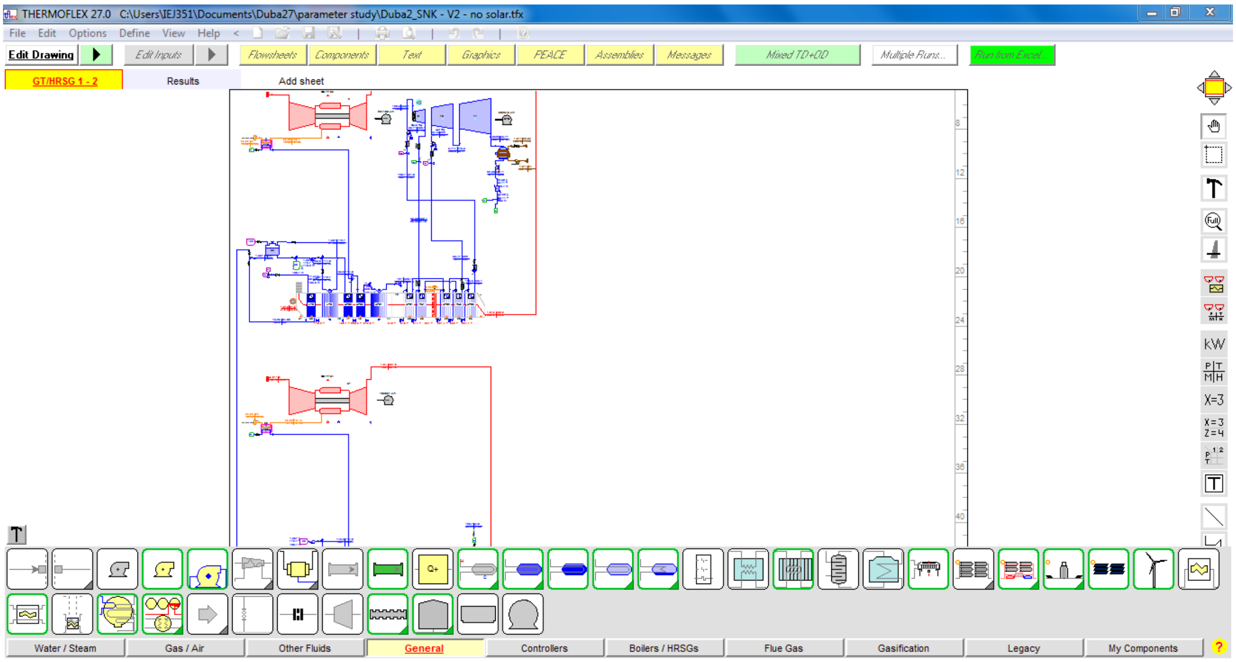

Figure 6.3: Thermoflex graphical interface representing the Duba power plant

Solar field

In a second time, the solar field was implemented in a separated Thermoflex document, according to the document [15] (coming from thermoflex, Appendix2), which provided the detailed flowsheet and some input parameters of the solar field for some specific operating conditions. The aim was firstly to match exactly the thermodynamic variables of the model with those of the given document. This was achieved by means of the thermodynamic design. Once that has been done, the engineering design was used in order to match the water mass flow of the solar field model with the water mass flow of the combined cycle flowsheet [12], that corresponds to other solar conditions. The engineering design is in between the thermodynamic design and the off design. Indeed, the engineering design produces a hardware model of the component at design point using user-defined hardware constraints and heat transfer requirements dictated by the Thermodynamic design. [14]. The design irradiance was set to 800 W/m^2 (same value than for the Matlab model) and the solar fluid "Dowtherm A" was chosen, according to the document [15]. Furthermore, a solar multiple of 1.5 was set (value proposed by default by thermoflex). The solar multiple is the factor by which the design solar field size is multiplied in order to increase the solar capacity factor. Once the solar field model performance matched the combined cycle flowsheet [12] performance, the solar field was switched to off design. This allowed to fix the geometry and the hardware design of the solar field, and to compute the thermodynamic performance depending on the solar conditions. That is how it works in reality. Finally, the solar field was connected to the combined cycle. The Thermoflex solar field model is depicted in the Figure 6.4 and can be observed in detail in attached documents (Appendix4).

As soon as the solar field was connected to the combined cycle, and that the whole integrated combined cycle was switched to off-design mode, a control loop (iterative process that iterates on 1 (or more) parameters in order to control another parameter) was implemented in order to keep the power output constant regardless on the solar conditions. In fact, the fuel mass flows in the two duct burners are adjusted in order to compensate for the intermittency of solar radiation.

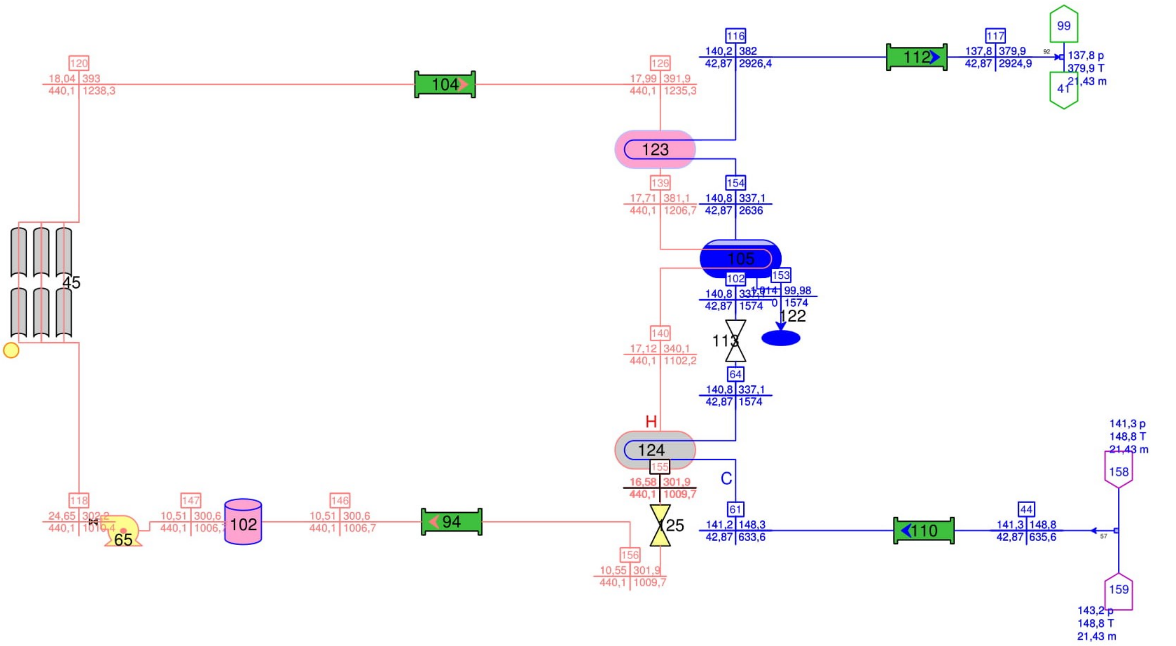

Figure 6.4: Solar field Thermoflex model

6.2.4 Parameter study - E-link

After the Thermoflex model was finalised, parameter studies were achieved. The DNI variation was firstly performed in order to analyse the change in performance with respect to the solar condition variation in Duba. Then the hybridization process was changed. Finally, the $\dot{Q}_{sol}$ variation was analysed. An important point to know is that only the energy analysis was performed because the exergy analysis is unfortunately not available in Thermoflex.

DNI

As the solar field is in off-design mode, the control loops adapt the duct burner (DB) fuel mass flows according to the DNI in order to keep a constant steam production. In fact, the DNI variation leads to solar fluid mass flow variation and thus to solar steam mass flow variation, which has to be compensated by the variation of heat provided by the duct burners. The ideal would have been to implement a second control that adapts the fuel mass flow of the DB1 relative to the fuel mass flow of the DB2 in order to reach the same HRSG exit temperature, but this was not possible (even with the advice of the program designers) because convergence was not reached. In addition, in order to run multiple cases, it is possible to run the Thermoflex model from Excel. An E-link is in fact used to link Excel with Thermoflex. This allows to select the input parameters that must be varied, and the output parameters that are wanted to be analysed.

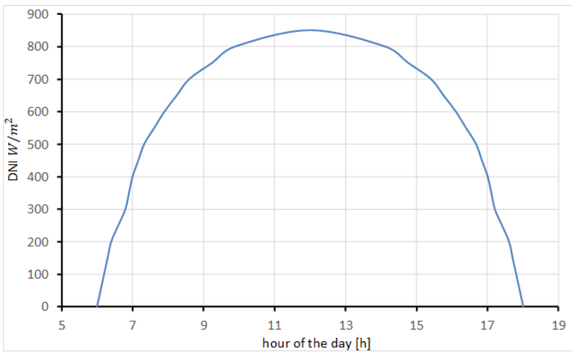

Figure 6.5: DNI variation with respect to the hour of the day in Excel

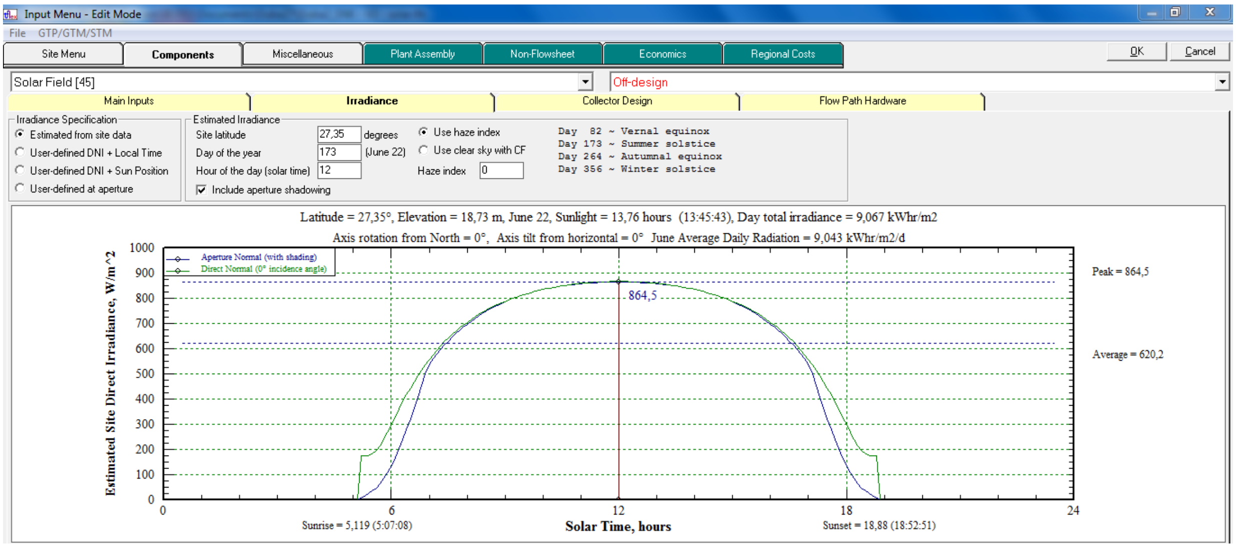

Figure 6.6: DNI variation with respect to the hour of the day obtained in Thermoflex

The DNI variation parameter study can thus be found in the Excel attached documents (Appendix4). Afterwards, a study was done about one typical day. The performance was obtained in relation to the time of the day. Therefore, the graph of the DNI with respect to the time was required. It can be seen on the Figure 6.6 that the latitude of Duba was entered, as well as the day of the year (here the summer solstice) and the program returns a graph of the DNI with respect to the hour of the day (solar time). Then, a similar graph in Excel was built (Fig. 6.5).

Hybridization process

The hybridization process of the Duba power plant (described in the section 6.1) is similar to the ISCC4, which is not the most efficient hybridization system. Therefore, the solar field depicted in the Figure 6.4 was modified in order to only bypass the evaporator (as ISCC2), as it can be seen in the appendices (Fig. A.26). With a view to create this new solar circuit, the solar field was switched back to engineering design. A constant solar share was wanted, thus the solar fluid mass flow was adjusted in order to obtain the same solar heat flux $\dot{Q}_{sol}$ in the solar exchanger. The exit solar fluid temperature of the solar field is also decreased to $383[°C]$ due to the superheater removing. After that, the solar field was switched again to off design mode and the DNI variation in Excel was also achieved on this new integrated combined cycle in order to be able to compare it with the existing integrated combined cycle.

$\dot{Q}_{sol}$

For this parameter study, the solar share is changed and thus the size of the solar field is also changed, but the DNI remains constant. As a consequence, this study is performed with the engineering design in order to be able to change the size and thus the hardware design of the solar field, depending on the solar conditions. There was a problem with this simulation but the problem was solved by replacing the conventional splitter (component that sends arbitrarily half of the stream coming from the HP turbine to each HRSG for the reheat) by a balancing splitter that can regulates the flow distribution. Indeed, the simple splitter was legitimate in the GT pro and GT Master because the heat load in both HRSGs was the same due to two identical gas turbines. However, by replacing one of the two gas turbines (as it was done in Thermoflex), the heat load is not the same anymore and then the balancing splitter is needed. In the end, the $\dot{Q}_{sol}$ parameter study is done only on the existent power plant because the relative effect of the $\dot{Q}_{sol}$ variation is expected to be the same on the other hybridization process for which only the evaporator is hybridized (ISCC2Duba).

6.3 Results

Only the main results are presented in this section, i.e. η_{toten}, $\eta_{sol\,rad}$, the LCOE and the break-even CO_2 tax. Other results can be seen in the Excel attached documents (Appendix4). As the detailed explanations of the phenomena were already presented in the previous chapters, only a comparison between the Thermoflow model and the Matlab model is achieved, except if there is a significant difference between both models. With a view to compute $\eta_{sol\,rad}$, the effective power of the Duba cycle without solar field but with the same fuel consumption must be obtained (according to the formula 2.1). In this respect, the control loop is removed and the DNI is set to 0. For the purpose of computing η_{toten}, the solar contribution $A_{coll}\,DNI$ in the denominator had to be added by hand because the program takes $\eta_{toten} = \frac{Pe_{tot}}{\dot{m}_{fuel}\,LHV}$ as total energy efficiency definition, even with a solar field. The break-even CO_2 tax was also computed "by hand" from the results obtained via Thermoflex because the program does not directly compute this parameter.

6.3.1 DNI variation

First of all, one can notice that by increasing the DNI, the total energy efficiency decreases, as already pointed out in the section 3.7.1. Even if the Duba power plant cannot really be compared with the ISCC2 because the cycles are not the same, the order of magnitude can nevertheless be compared. Therefore, it is observed in the graph 3.17 that the order of magnitude and the shape are exactly the same. It is also confirmed that the ISCC2Duba is globally more efficient than the existing Duba power plant, as it can be seen in the graph 6.7.

Regarding the other main hybrid parameter, the solar radiation-to-electrical efficiency, exactly the same trend as in the section 3.7.1 is observed. Indeed, the shape of the curve is the same, the order of magnitude is also the same, and the asymptotic behaviour as well as the root existence are present in both graphs. In addition, the hybridization of only the evaporator is confirmed to be more efficient concerning the solar performance.

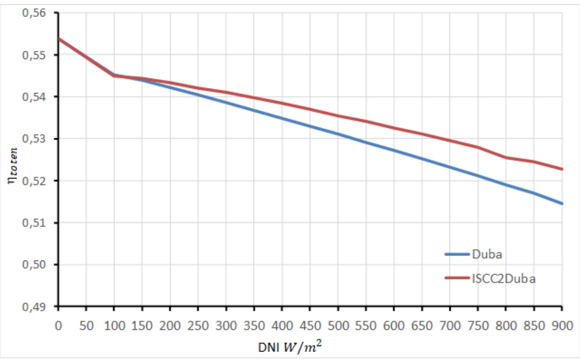

Figure 6.7: η_{toten} with respect to the DNI

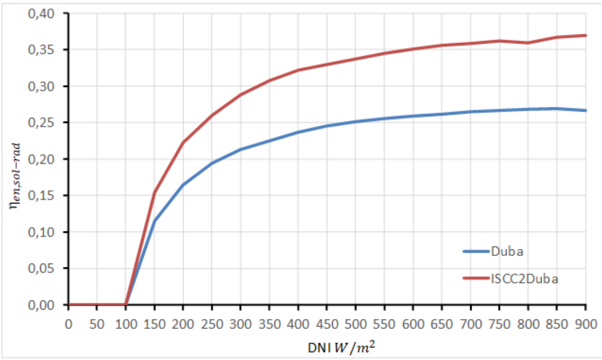

Figure 6.8: $\eta_{en,\,sol-field}$ with respect to the DNI

As it was already said in the section 3.7.1, the solar field efficiency has the same shape than the solar radiation-to-electrical efficiency (because the solar heat-to-electrical efficiency is constant). In addition, the order of magnitude is the same than for the ISCC2 and 3 as it can be seen in the table 3.2 because the solar receiver temperature is similar (not the same than the ISCC4 and 5 because the solar receiver temperature is very different). However, the solar field efficiency is here smaller for the ISCC2Duba compared to the real Duba power plant. That seems illogical regarding the observations done in the section 3.7.1 because the solar receiver temperature of the ISCC2Duba is lower (-14°C), resulting in lower radiation losses. In fact, it is guessed that the solar radiation decrease is supplanted by the heat transfer efficiency decrease (which is not taken into account by the Matlab model). Indeed, for the same solar heat flux transferred in the solar field, the solar fluid mass flow is higher (+484 kg/s) and the solar fluid temperature at the solar field inlet is also higher (+34 °C), resulting in lower heat transfer performance. [19]

Regarding the solar heat-to-electrical efficiency, the shape is a bit different compared to the Matlab model for low DNI values (totally constant in the Matlab model). Indeed, the Matlab model does not take into account the pumping losses in the solar field, thus $\eta_{en\,so-heat}$ does not vary with the solar fluid mass flow and does not depend on the solar conditions. However, in the Thermoflex model, the pumping losses are high at low DNI because a low DNI value means a low solar fluid mass flow and that results in a low pumping efficiency. Indeed, the pumping efficiency is lower at partial load. That is why the solar heat-to-electrical efficiency is lower at low DNI values.

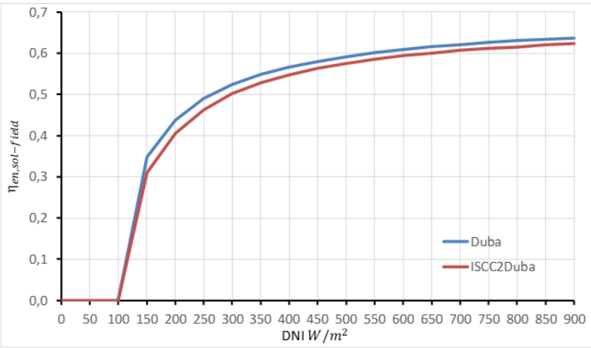

Figure 6.9: $\eta_{en,\,sol-field}$ with respect to the DNI

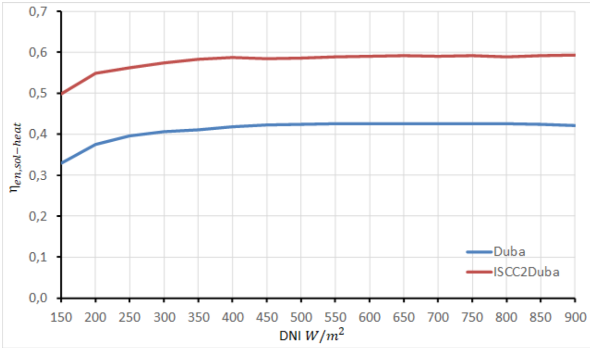

Figure 6.10: $\eta_{en,\,sol-heat}$ according to the DNI

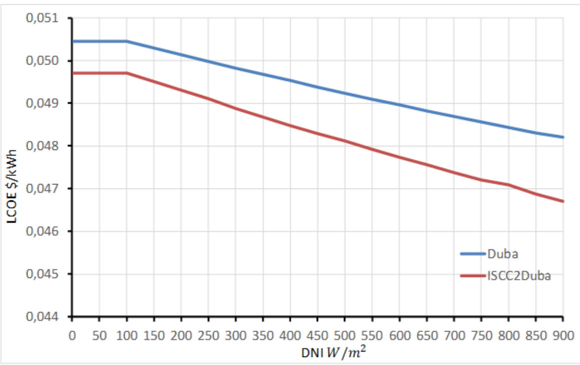

Figure 6.11: LCOE with respect to the DNI

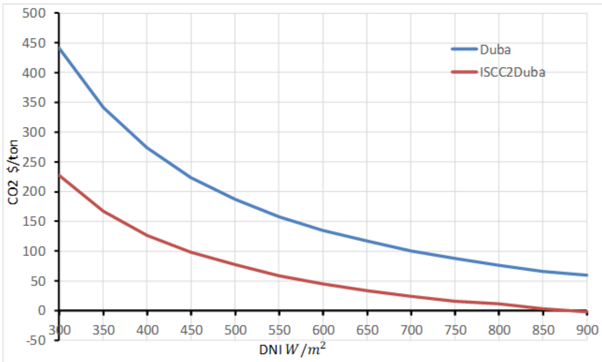

Figure 6.12: BE CO_2 tax according to the DNI

Finally, the two main economical parameters are depicted in the two figures above. The same results than in the chapter 5 are obtained. Indeed, the LCOE decreases linearly with the DNI (as in the Figure 5.2) and it can be noticed that the hybridization of only the evaporator is more profitable. However, with the observations done in the Figure 6.9, it is surprising (only in the case of the Duba project) that for DNI=0, the hybridization of only the evaporator is more profitable. Indeed, as the solar field of the ISCC2Duba is less efficient, more parabolic troughs are needed and thus the solar field installed investment cost is higher (as it can be seen in the attached document Appendix4). Nevertheless, the ISCC2Duba requires only one evaporator in the solar circuit whereas the real Duba power plant requires one economizer, one evaporator and one superheater. That is why the total investment cost of the ISCC2Duba is lower. Finally, it is observed that the LCOE values are in the same order of magnitude than the LCOE values of the chapter 5.

The break-even CO_2 tax is depicted in the figure 6.12. Again, the ISCC2Duba achieves the best performance and it is even noticed that at approximately DNI=900, the break-even CO_2 tax of the ISCC2Duba is negative, which means that the integrated combined cycle is already more profitable than the conventional combined cycle without any CO_2 tax. In addition, the shape of the LCOE curve is the same than that obtained in the previous chapter. The order of magnitude is also the same.

6.3.2 Daily DNI variation

It can be valuable to analyse the change in performance over a day, depending on the solar conditions (represented by the DNI). In addition, as the graph of the DNI with respect to the hour of the day is symmetric, only the morning is depicted in the following figures.
It can seen that the variation of the total energy efficiency is no more a line because the variation of the DNI with the time has a parabolic shape. As a consequence, there is a sharp decrease early in the day and η_{toten} stabilizes at noon.
Concerning the 3 solar efficiencies, it is noticed that they raise sharply during the first hour of the day and that they are almost constant the rest of the day until the last hour of the day.

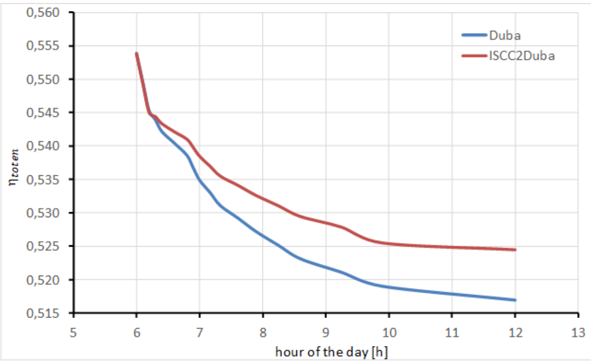

Figure 6.13: η_{toten} with respect to the time

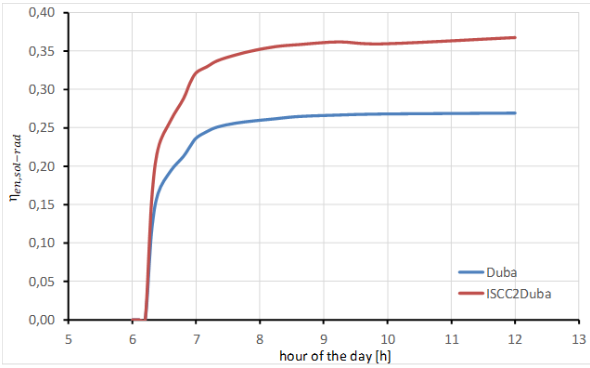

Figure 6.14: $\eta_{en,\,sol-rad}$ with respect to the time

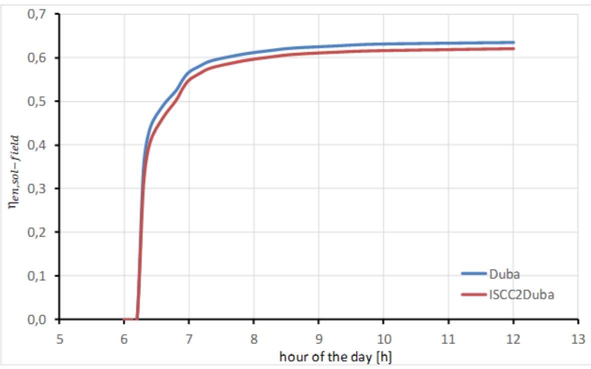

Figure 6.15: $\eta_{en,\,sol-field}$ according to the time

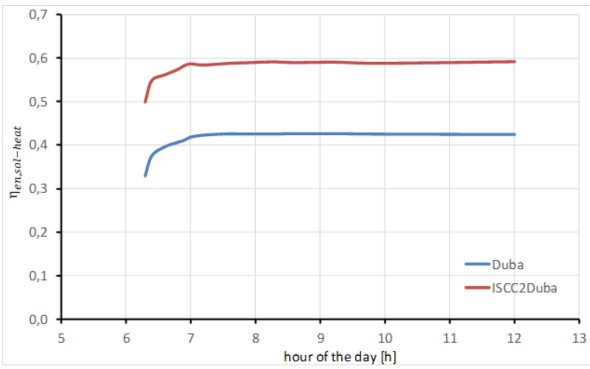

Figure 6.16: $\eta_{en,\,sol-heat}$ according to the time

With regards to the LCOE, there is no sense in analysing the daily variation because the LCOE is computed on an annual basis and because the annual DNI variation is already taken into account in the LCOE by means of the capacity factor (Eq. 5.12). In fact, the LCOE and the break-even CO_2 tax can be interpreted in this case as average annual values. Accordingly, the LCOE and the break-even CO_2 tax are derived from the graphs 6.11 and 6.12 for the design DNI value, which is equal to 800 W/m^2. It can be seen in the table below that the ISCC2Duba achieves better annual performance than the existing Duba power plant.

	Duba	ISCC2Duba
LCOE [$/kWh] with carbon tax = 0 $/t_{CO_2}$	0.0484	0.0471
break-even CO_2 tax [$/t_{CO_2}$]	76.1	11.4
LCOE [$/kWh] with the break-even CO_2 tax	0.0747	0.0509

Table 6.1: LCOE and BE CO_2 tax comparison between the ISCC2Duba and the Duba power plants

6.3.3 $\dot{Q}_{sol}$ variation

As it can be seen in the Figure 6.17, the total energy efficiency decreases linearly with the solar heat flux, which confirms the result obtained in the chapter 3 (Fig. 3.19). The order of magnitude is also the same.
With regards to the solar radiation-to-electrical efficiency, it is almost constant as already explained in the chapter 3. In fact, the solar field efficiency is totally constant and the shape of $\eta_{en,\,sol-rad}$ is thus the same than the shape of $\eta_{en,\,sol-heat}$.

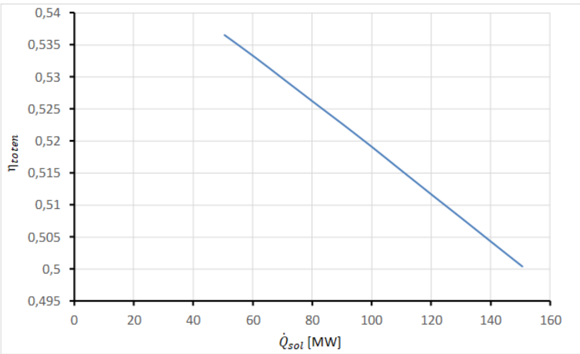

Figure 6.17: η_{toten} with respect to $\dot{Q}_{sol}$

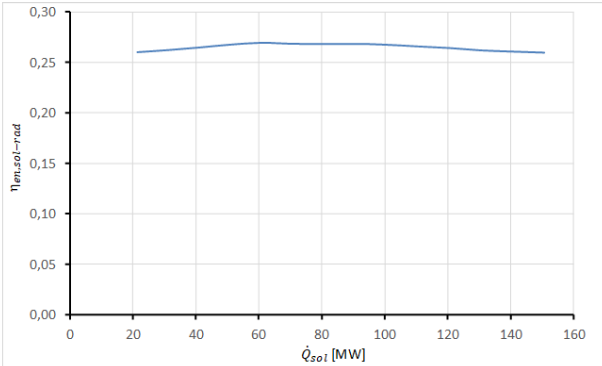

Figure 6.18: $\eta_{en,\,sol-rad}$ with respect to $\dot{Q}_{sol}$

Concerning the LCOE, the result obtained with Thermoflex is the same than the result obtained with Matlab. Indeed, the LCOE increases linearly with the solar heat flux (as in the Figure 5.4) and is in the same order of magnitude.
Nevertheless, the graph of the break-even CO_2 tax obtained here does not follow the same trend than the Figure 5.5. It is due to the different hybridization mode. Indeed, the Matlab model is in power boosting mode which increases the power of the cycle whereas the Thermoflex model is in fuel saving mode which reduces CO_2 emissions. In fact, despite the fact that the LCOE increases due to the increase in solar field investment cost, the decrease in CO_2 emissions makes the break-even CO_2 tax to decrease, as depicted in the Figure 6.20.

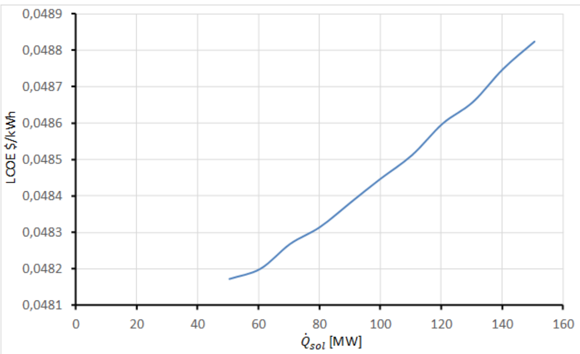

Figure 6.19: LCOE with respect to $\dot{Q}_{sol}$

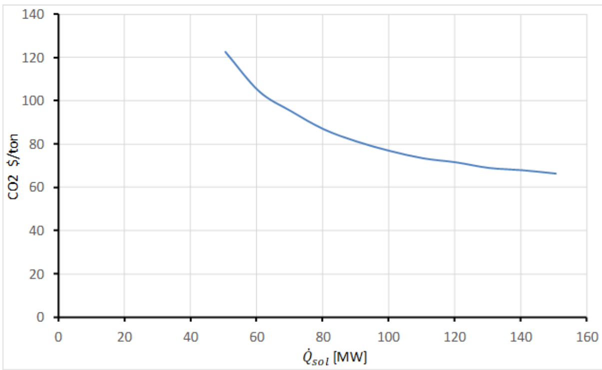

Figure 6.20: BE CO_2 tax with respect to $\dot{Q}_{sol}$

Chapter 7

Conclusion

7.1 Summary of contributions

A quantitative answer to the two main questions asked in the introduction can now be given, relative to the state-of-the-art natural gas power station, the combined cycle.

What are the incentives for CSP power plant of being integrated in a combustion power plant?

From the thermodynamic point of view, it can be summarised by the solar radiation-to-electrical efficiency. While it is only **[10-25%]** for solar only power plants [20], this efficiency reaches **29,5%** (ISCC2)-**35,9%**(ISCC2Duba) for the best integrated combined cycle which has been identified as that based on the hybridization of only the evaporator with parabolic troughs. It has been also established that the solar share has almost no influence on the solar radiation-to-electrical efficiency. Nevertheless, it has appeared that the DNI has a strong influence on this later efficiency. Finally, parabolic troughs have been identified as the more appropriate CSP technology thanks to its high η_{conc} as well as its optimal concentration ratio which is suitable for the solar receiver temperature range relative to the combined cycle. Even better, the solar radiation-to-electrical efficiency reaches **31,7%** for the hybridization of the gas turbine integrated in a combined cycle ($SAGT_{cc}$). In this case, contrary to the ISCCs, the solar share increase results in the solar radiation-to-electrical decrease. Finally, the solar central receiver has been identified as the most relevant CSP technology for the gas turbine hybridization because of its high concentration ratio which is appropriate for the temperature range of the turbine inlet.
From the economic point of view, the hybridization is also highly recommended. Indeed, while the LCOE of the CSP power plants is **[0.17-0.33] $/kWh** [3], the LCOE reaches **0.04666 $/kWh** for the $SAGT_{cc}$ without carbon tax. Even better, the LCOE of the ISCC2 reaches **0.04542 $/kWh** (0.0471 for the ISCC2Duba). Indeed, although the $SAGT_{cc}$ is thermodynamically more efficient, the ISCC2 is more cost-effective due to the lower investment cost of the parabolic troughs compared to the central receiver. In addition, the average annual DNI increase lowers the LCOE whereas the solar share increase raises the LCOE.

What are the incentives for combustion power plants of integrating a solar field?

From the thermodynamic point of view, the hybridization decreases unfortunately the total cycle efficiency. Indeed, it is equal to **0.567** and **0.554** for respectively the NGCC and the NGCCDuba, **0.524** and **0.5255** for respectively the ISCC2 and the ISCC2Duba, and **0.525** for the $SAGT_{cc}$. Contrary to the solar radiation-to-electrical efficiency, the total cycle efficiency decreases with the DNI and the solar share.
Nevertheless, from the environmental point of view, the advantage of the hybridization is clearly emphasised by the CO_2 emissions mitigation. Indeed, the natural gas combined cycle produces

346 g/kWh(NGCC)-**367 g/kWh**(NGCCDuba), while the ISCCs produce **315 g/kWh**(ISCC2)-**338 g/kWh**(ISCC2Duba) and the $SAGT_{cc}$ produces **311 g/kWh**. In addition, the CO_2 emissions decrease continuously with the DNI and the solar share.
Finally, from the economic point of view, the hybridization of the combined cycle has been pointed out to be not profitable without carbon tax. Indeed, the LCOE of the natural gas combined cycle is **0.04482 $/kWh**(NGCC)-**0.0468 $/kWh**(NGCCDuba) while the LCOE of the integrated combined cycles is **0.04542 $/kWh**(ISCC2)-**0.0471 $/kWh**(ISCC2Duba) and is **0.04666 $/kWh** for the $SAGT_{cc}$. Nevertheless, from a CO_2 tax equal to **36** $\$/\mathbf{t_{CO_2}}$(ISCC2)-**11.4** $\$/\mathbf{t_{CO_2}}$(ISCC2Duba) and equal to **101.2** $\$/\mathbf{t_{CO_2}}$ for the $SAGT_{cc}$, the hybridized power plant becomes more cost-effective than the non-hybridized power plant.

To conclude, it is important to choose carefully the geographical site on the earth, the CSP technology, and the combustion power plant parameters (e.g. T_H and p_{HP}) to maximize the hybridization performance. In the end, hybridization of combustion power plants with concentrated solar power is a trade-off between the cheap, efficient, reliable but polluting combustion cycle and the expensive, low efficient, intermittent but environmental friendly solar power plant. Therefore, it allows a faster penetration of renewables in the energy market, especially with the help of a CO_2 tax, which is expected to emerge/increase in the coming years.

7.2 Program comparison

The hybridization was analysed in this work from an innovative point of view. Indeed, this work has been devoted not only to a thermodynamic study but also to an economic study of the problematic. Furthermore, two programs were used with advantages and disadvantages for each. The first study was achieved via a Matlab program (with two graphical interfaces), allowing a real understanding of the problematic. Moreover, It enabled the exergy analysis which is not possible in Thermoflex. It allowed also unlimited possibilities of parameter study because the code is simple and totally open to the user. Then, a state-of-the-art commercial program, Thermoflow, was used with a view to verify the results obtained with Matlab, to perform a daily analysis, to study the fuel saving mode (difficult in the matlab program), and finally to take into account all losses that are not modelled in the Matlab program. Besides, Thermoflow allowed the hybridization performance assessment of another more complex cycle than that used for the Matlab model, which was certainly the biggest advantage of using Thermoflow.

7.3 Further research directions

It is certainly possible to go further in the study of power plant hybridization. Potential extensions are listed below:

- Improvement of the Matlab program. Regarding the solar field model: heat transfer and pumping losses modelling in the secondary solar fluid circuit. Concerning the combined cycle model: modelling of the pressure losses and heat losses in the HRSG as well as the pump irreversibilities. Other parametric studies could also be relevant, e.g. the compression ratio of the SAGT, etc...;
- Implementation of solar energy storage;
- Detailed geographical study of the hybridization performance;
- Hybridization of the Rankine cycle;
- Better economical study by considering variable fuel cost, variable O&M costs etc...

Appendices

A summary of CSP-coal hybrid systems.

Configuration	Solar Collection Temp.	Collector Type	Solar heat collection fluid	Solar fraction	Solar-toelectricity efficiency
Solar Steam Generation					
Molten salt power tower with storage produces steam in parallel with coal boiler [9]	571 °C+	Power Tower	Molten Salt (binary nitrate)	6.1% (max)	27.8%
Direct steam generation in line focus receiver for high pressure superheated steam production [8]	500 °C	Line Focus	Direct Steam Generation	–	38–45%
Direct steam generation in central receiver for high pressure superheated steam production [8]	565 °C	Central Receiver	Direct Steam Generation	–	38–45%
Feedwater Preheating					
PT solar field with VP1 used for boiler feedwater preheating [15]	267 °C	Parabolic Trough	Therminol VP1	–	21.2% (max)
PT solar field with Dowtherm A used for boiler feedwater pre-heating [16]	292 °C	Parabolic Trough	Dowtherm A	–	21% (annual)
PT solar field with Dowtherm A used for boiler feedwater pre-heating [17]	292 °C	Parabolic Trough	Dowtherm A	–	27.3%
PT solar field with thermal oil used for boiler feedwater pre-heating [20]	260 °C (max)	Parabolic Trough	Thermal Oil	10.3% (max)	40.3% (max)
Direct steam generation in parabolic trough combined with turbine extraction steam for BFW pre-heating [10]	398.1 °C	Parabolic Trough	Direct Steam Generation	–	28.5%
Thermal oil-heated in PT for BFW Pre-heating [18]	387 °C	Parabolic Trough	Thermal Oil	5.77%	13.6%
Thermal oil heated in PTC for BFW pre-heating [13]	283 °C	Parabolic Trough	Thermal Oil	–	21% (annual)
PTC used to heat Thermal oil for LP BFW pre-heating [12]	140 °C	Parabolic Trough (or evacuated tube)	Thermal Oil	~30% (max)	11.4%
PTC used to heat Thermal oil for HP BFW pre-heating [12]	282 °C	Parabolic Trough	Thermal Oil	~29% (max)	24.1%
Air Preheating					
Boiler air pre-heating with solid particle receiver [23]	540 °C	Power tower	Air with ceramic particles	7.8%	22.3% (max)
Gasification					
Power tower that makes steam for coal gasification [53]	650 °C	Power Tower	Molten Salt	–	–
Direct heating of gasification reactor before combined cycle [52]	1077 °C	Power Tower + Parabolic Trough	Reactant gases (steam/ CO_2) + Direct Steam Generation	31% (max)	–
Parabolic trough makes steam for gasification and pre-heats CO_2 [54]	142.9 °C (steam) / 198.9 °C (CO_2)	Parabolic Trough	Direct steam generation / supercritical CO_2	22.6%	–
CO_2 Capture					
PTC used to heat Thermal oil for solvent regeneration in CO_2 capture [12]	145 °C	Parabolic Trough/ evacuated tube	Thermal Oil	~29% (max)	15.3%
PT solar field with VP1 to provide heat to stripper in post-combustion CO_2 separation [33]	295 °C	Parabolic Trough	Therminol VP1	27.6%	27%

Figure 1: Summary of CSP-coal hybrid systems [26]

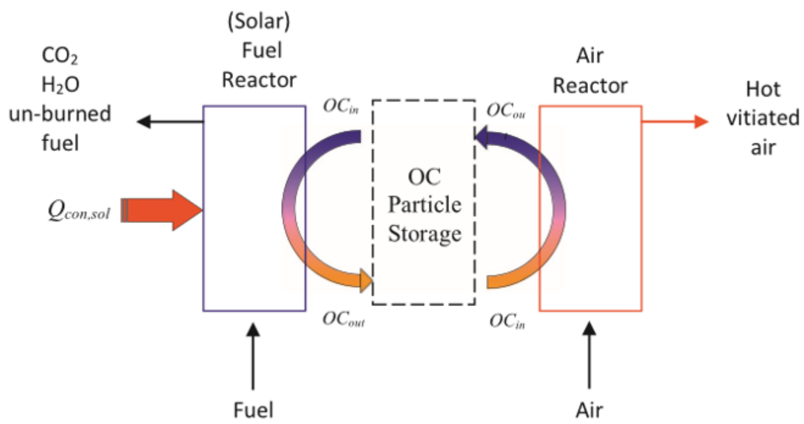

Figure 2: Hybrid solar chemical looping combustion [23]

A summary of CSP-natural gas hybrid systems.

Configuration	Solar Collection Temp.	Collector Type	Solar heat collection fluid	Solar Fraction	Solar-toelectricity efficiency
Air Heating for Gas Turbine					
Power tower pre-heats air at front end of GT with HRSG for cogeneration [71]	~1000 °C	Central receiver	Air	74.2% (31.5% annual)	- (~85% cogen.)
Multiple dish and MGTs in parallel combine outlet air streams to HRSG for steam cycle [62]	900 °C	Parabolic dish	Air	66.4% (max), 32.0% (annual)	- (38.2% power block)
Parabolic dish with micro gas turbine in simple-cycle mode [61]	900 °C	Parabolic dish	Air	52.590.7% (annual)	16.818.4% (annual)
Dish used to directly heat air for recuperated gas turbine with pressurized receiver [63]	900 °C	Parabolic dish	Air	68.7%	- (29.1% overall)
Dish used to indirectly heat air for recuperated gas turbine with atmospheric receiver [63]	780 °C	Parabolic dish	Air	99.5% (at peak)	- (23.4% overall)
Solar and combustion heat used in series to heat closed Brayton cycle via HX [73]	800 °C+	Central receiver	Air	~37%	- (37.8% overall)
Steam Injected Gas Turbine (STIG)					
Solar-aided HRSG generated steam for injection into GT combustor [75]	238.1 °C	Parabolic trough/ linear Fresnel	Direct steam generation	48.9% (max)	15–24%
Solar-aided HRSG generated steam for injection into GT combustor [81]	~200 °C	Parabolic trough	Direct steam generation	31–33%	22–26% (annual)
Solar-aided HRSG generated steam (with latent TES) for injection into GT combustor [76]	200–280 °C	Parabolic trough	Direct steam generation	35.2% (annual)	20.1% (annual)
Solar-aided HRSG generated steam for injection into GT combustor [79])	202.2 °C	Parabolic trough	Direct steam generation	9.341.7% (annual)	11.217.1% (annual)
Integrated Solar Combined Cycle (ISCC)					
PTC with DSG supplements HRSG for cogen [71].	–	Parabolic trough	Direct steam generation	69.9% (24.7% annual)	- (~86% cogen)
Linear Fresnel collector with DSG supplements HRSG for cogen [71].	–	Linear Fresnel	Direct steam generation	70.7% (23.9% (annual)	- (82% cogen)
HYSOL molten salt power tower provides steam for Rankine. GT effluent gas also used for molten salt heating [100,107]	550 °C	Central receiver	Molten salt	45%	- (52% gas- toelectric)
Aux. boiler produces saturated steam in parallel with solar loop. Solar used for superheating [84]	313 °C	Parabolic trough	Therminol VP1 and Behran Oil	~63% in June, ~18% in Jan.	- (20–42% overall)
Power tower/molten salt with gas to reach supercritical steam conditions [85]	700 °C	Central receiver	High temp molten salt	–	- (43.2% overall)
Parabolic trough with oil in ISCC [97]	393 °C	Parabolic trough	Therminol VP1	12.8%	29.7%
Parabolic trough with molten salt in ISCC [97]	454 °C+	Parabolic trough	Molten salt	12.8%	29.2%
Power tower with molten salt in ISCC [97]	565 °C	Central receiver	Molten salt	12.8%	27.5%
Linear Fresnel with DSG in ISCC [97]	454 °C	Linear Fresnel	Direct steam generation	12.8%	26.8%
Methane Steam Reforming					
MSR reaction occurs in parabolic trough. Syngas used for gas turbine power generation [83]	600 °C	Parabolic Trough	Steam reforming reactants/ products	–	–

Figure 3: Summary of CSP-natural gas hybrid systems[26]

A summary of CSP-biofuel hybrid systems.

Configuration	Solar collection temp.	Collector type	Solar fraction	Solar heat collection fluid	Solar-toelectricity efficiency
Solar/Biofuel Steam Generation					
Biomass-fired boiler and MoltenSalt/Power tower boiler used in parallel for steam generation in steam cycle [121]	540 °C	Central receiver	23.9% (annual)	Molten Salt	- (33.4% overall)
Biomass used to superheat steam after being generated by parabolic trough plant [117]	393 °C	Parabolic trough	–	Thermal Oil	27.5%
Biomass furnace and PT with thermal oil used to supply heat to ORC with waste heat providing district heating [123]	305 °C	Parabolic trough	9%	Thermal Oil	– (16% overall electric)
Power tower used to pre-heat air. Syngas/biogas used for HRSG duct burning [118]	700 °C	Central receiver	Up to 50%	Air	11%
Solar/Biofuel Gasification					
IGCC using biomass shares HRSG with molten salt power tower system [133]	565 °C	Central receiver	–	Molten Salt	20%
Power tower Solar biomass gasifier makes syngas for IGCC [135].	877 °C	Central receiver	19.0%	Gasification reactants/ products	21.3% (18.5% annual)
Power tower air heater heats air for combustor. Biomass gasifier in parallel makes syngas. Combined cycle operation [135]	877 °C	Central receiver	19.0%	Air	17.3% (15.1% annual)

Figure 4: Summary of CSP-biofuel hybrid systems [26]

Combined cycle hybridization

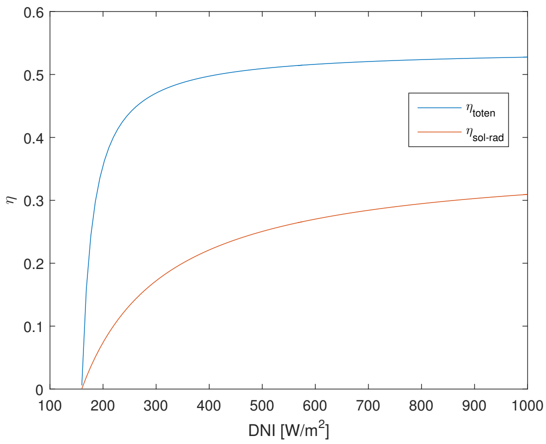

Figure 5: $\eta_{en\,sol-rad}$ and η_{toten} with respect to the geographical DNI

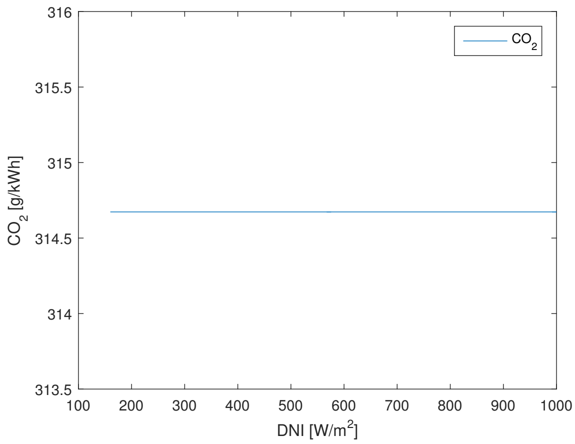

Figure 6: CO_2 emissions with respect to the geographical DNI

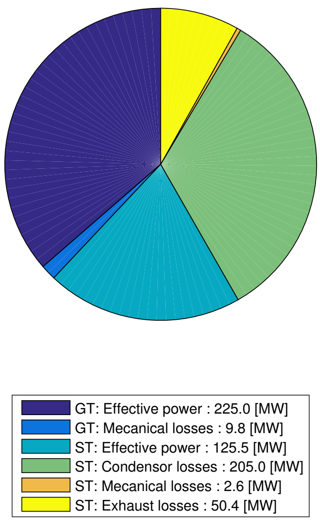

Figure 7: Energy pie chart of the NGCC

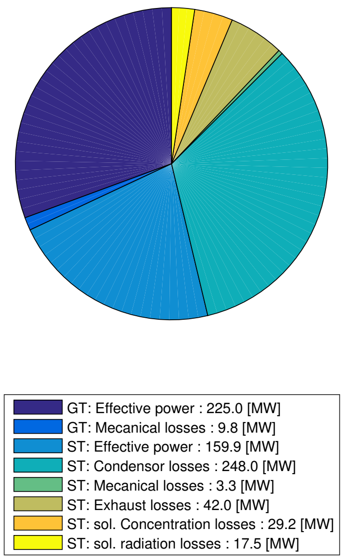

Figure 8: Energy pie chart of the ISCC2

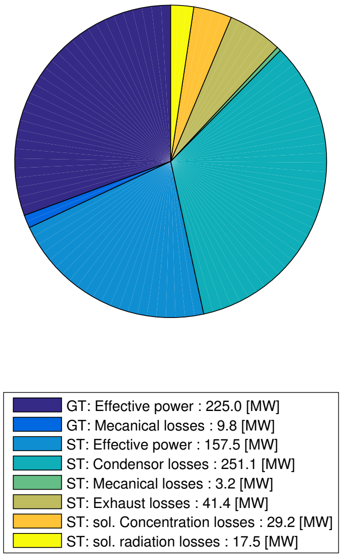

Figure 9: Energy pie chart of the ISCC3

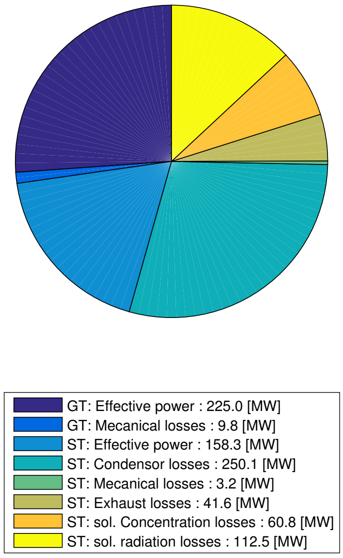

Figure 10: Energy pie chart of the ISCC4

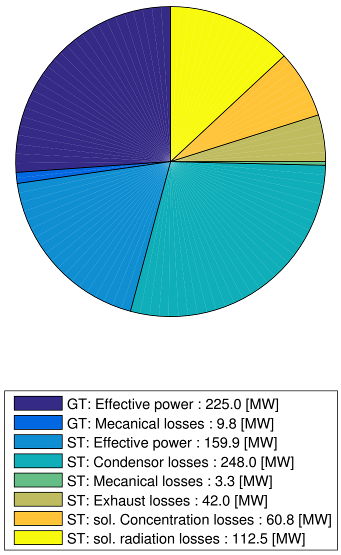

Figure 11: Energy pie chart of the ISCC4

Gast turbine hybridization

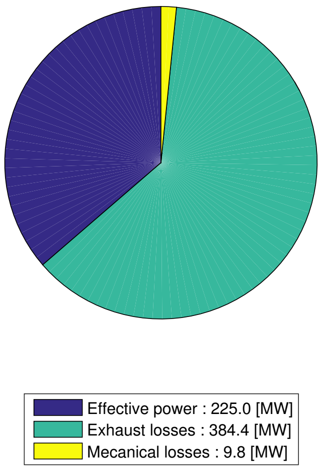

Figure 12: Energy pie chart of the NGT

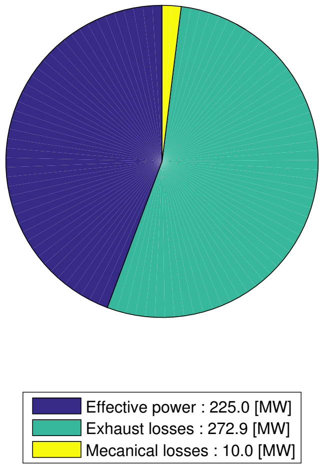

Figure 13: Energy pie chart of the HRGT

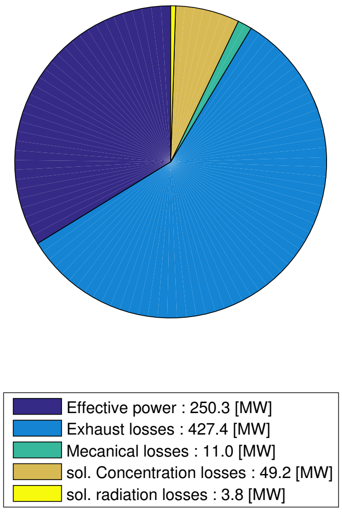

Figure 14: Energy pie chart of the SAGT

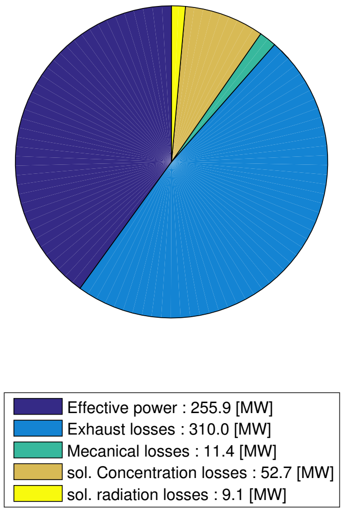

Figure 15: Energy pie chart of the SAHRGT1

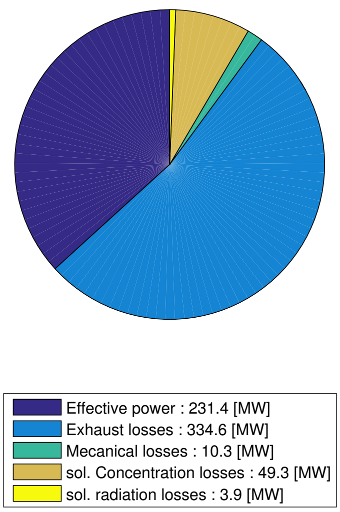

Figure 16: Energy pie chart of the SAHRGT2

Overall combined cycle hybridization

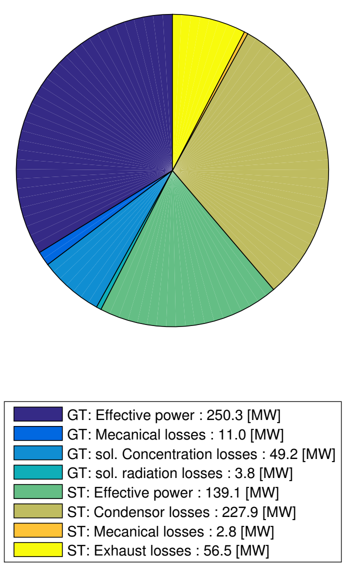

Figure 17: Energy pie chart of the $SAGT_{cc}$

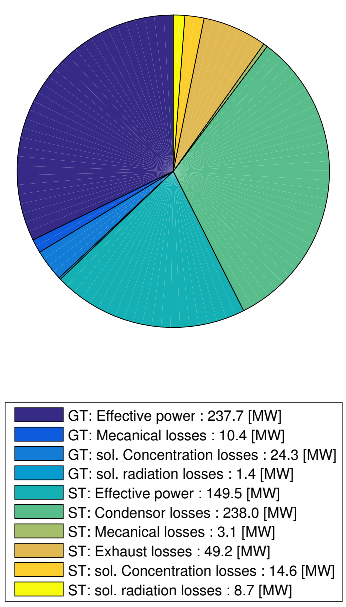

Figure 18: Energy pie chart of the $ISCC2 + SAGT_{cc}$

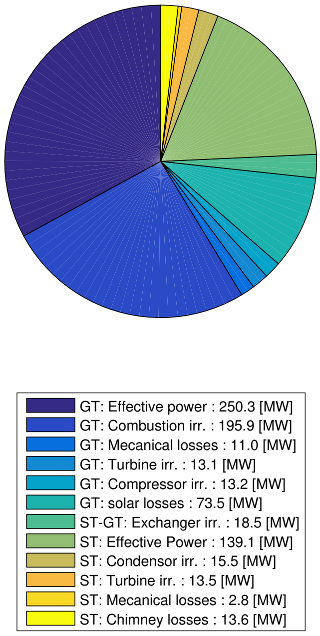

Figure 19: Exergy pie chart of the $SAGT_{cc}$

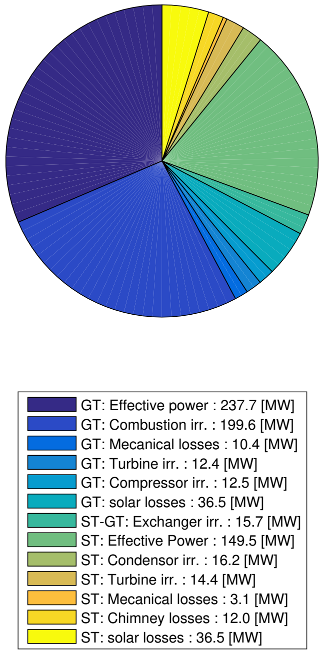

Figure 20: Exergy pie chart of the $ISCC2 + SAGT_{cc}$

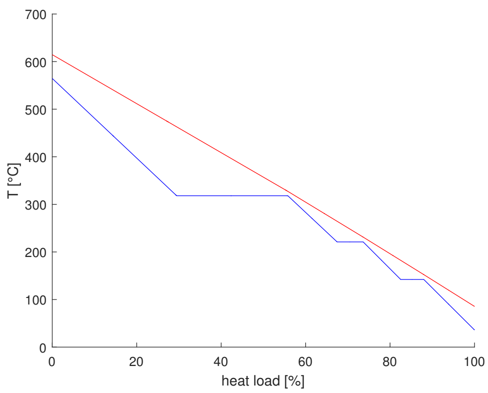

Figure 21: $\dot{Q} - T$ diagram of the $SAGT_{cc}$

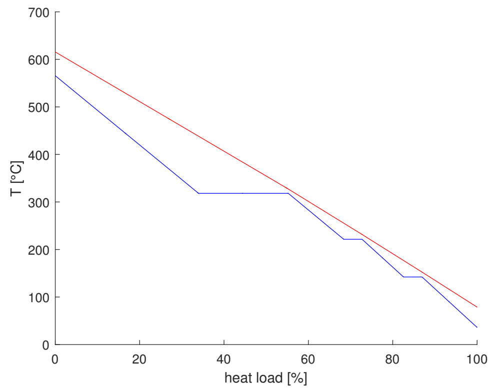

Figure 22: $\dot{Q} - T$ diagram of the $ISCC2 + SAGT_{cc}$

Economical aspect

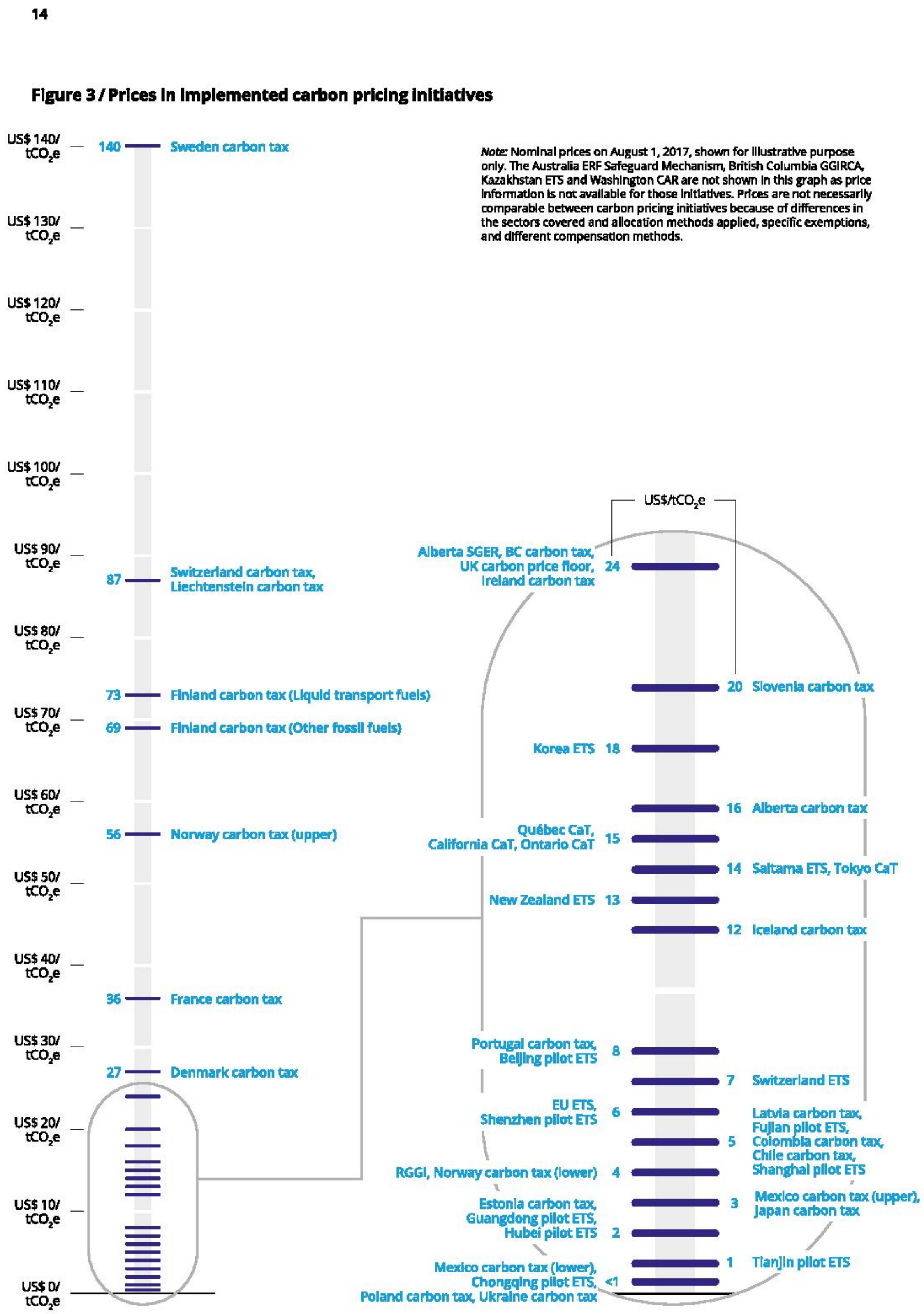

Figure 23: State and Trends of Carbon Pricing 2017 [10]

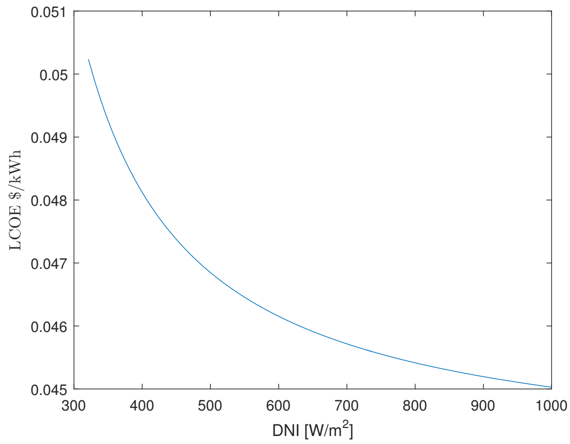

Figure 24: LCOE with respect to the geographical DNI

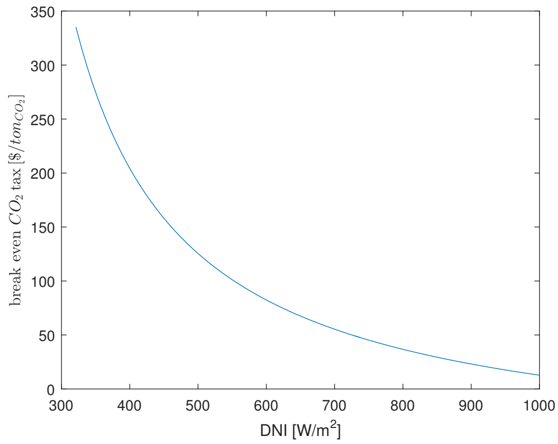

Figure 25: BE CO_2 tax with respect to the geographical DNI

Thermoflow

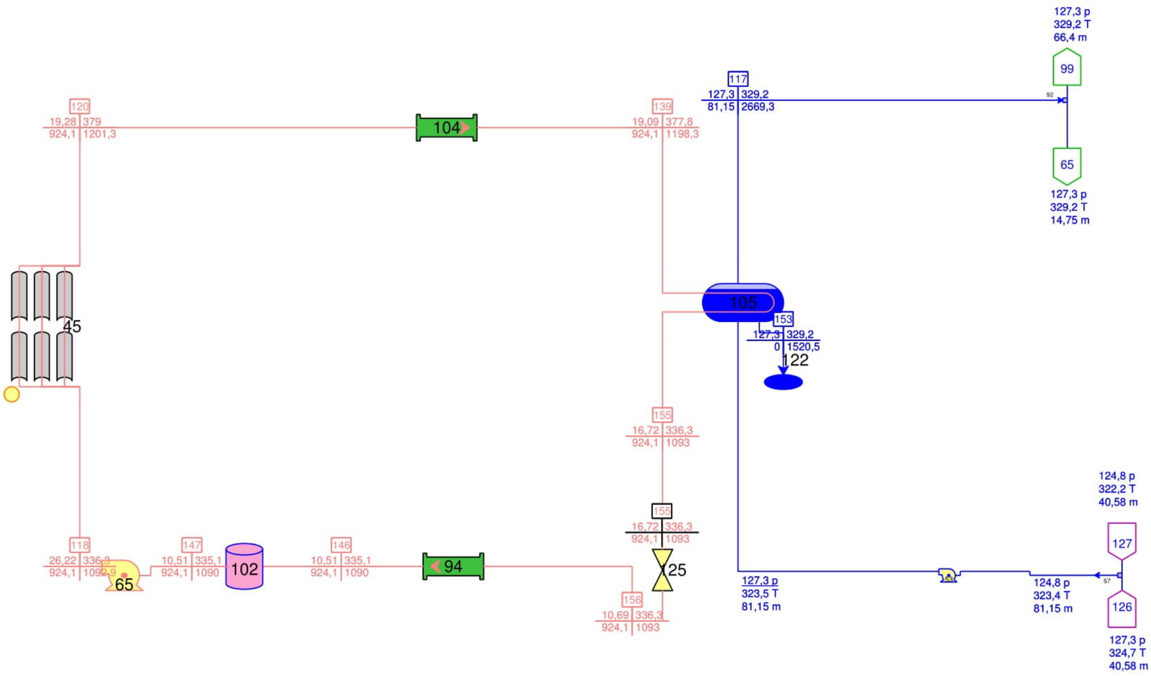

Figure 26: Solar field Thermoflex model for which only the evaporator is hybridized

Matlab graphical interfaces

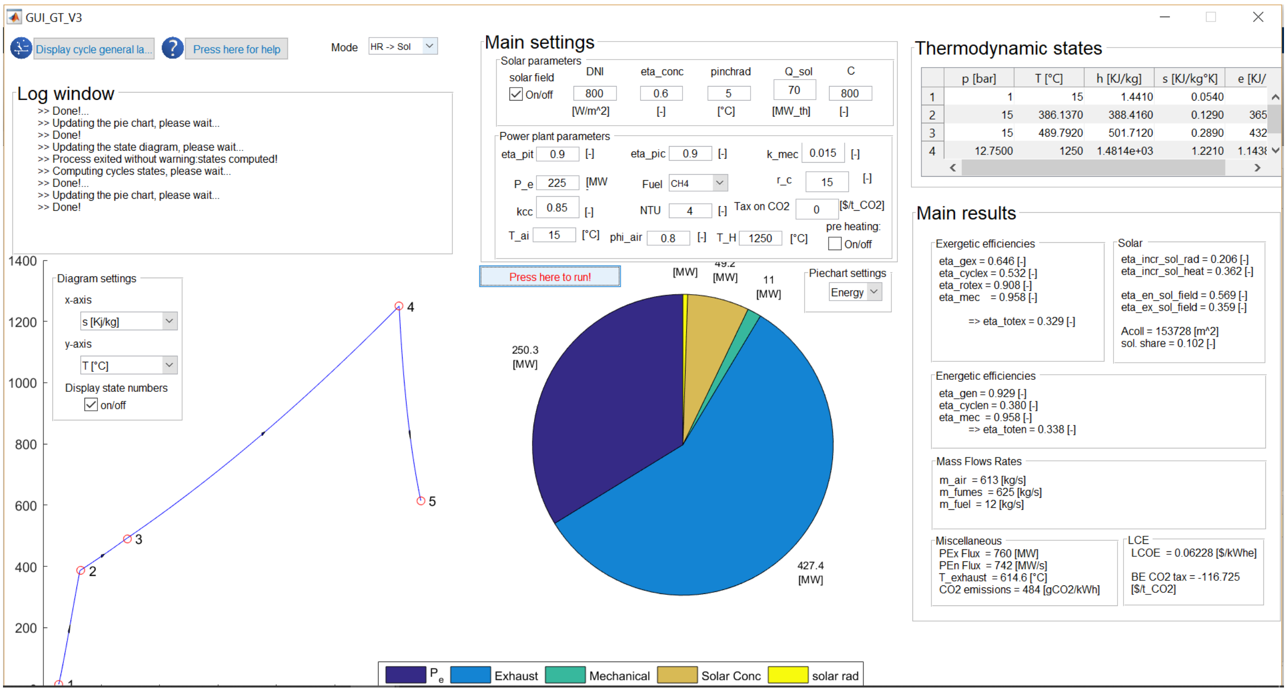

Figure 27: Matlab graphical interface of the gas turbine program

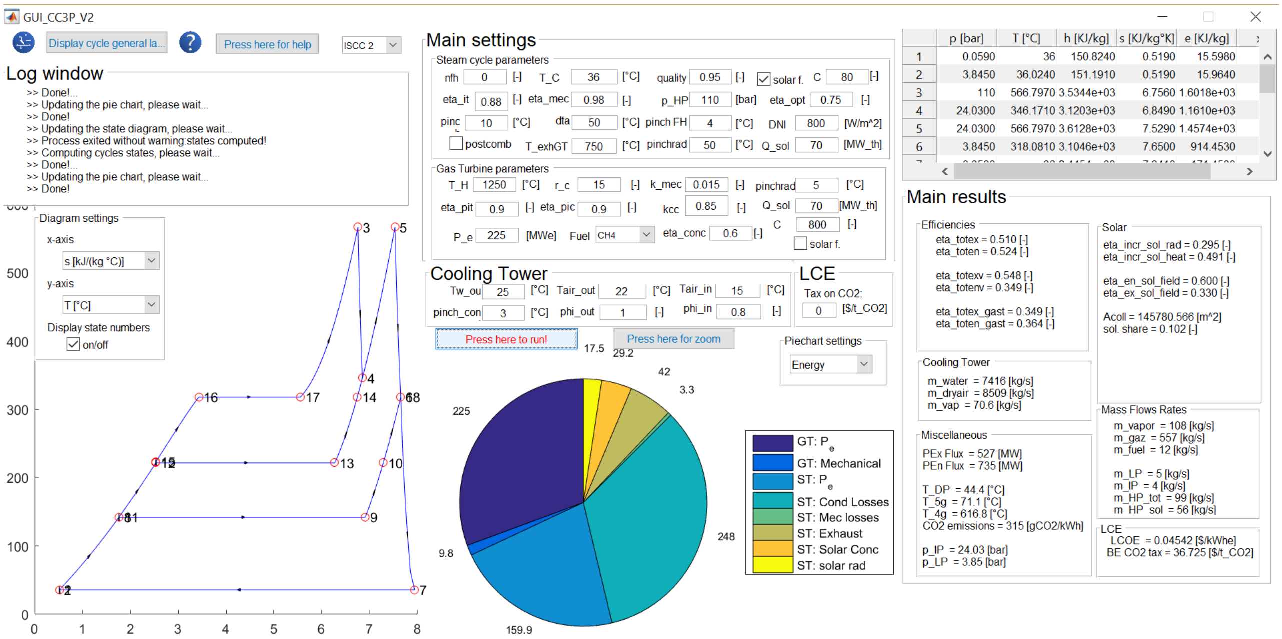

Figure 28: Matlab graphical interface of the combined cycle program

Bibliography

[1] Thermoflow. `https://www.thermoflow.com/index.html`.

[2] Technology roadmap: Concentrating solar power. Technical report, OECD/IEA, 2010.

[3] Renewable power generation costs in 2017. Technical report, International Renewable Energy Agency, Abu Dhabi, 2018.

[4] Lukas Aichmayer, James Spelling, and Björn Laumert. Preliminary design and analysis of a novel solar receiver for a micro gas-turbine based solar dish system. *Solar energy*, 114:378–396, 2015.

[5] Lukas Aichmayer, James Spelling, and Björn Laumert. Thermoeconomic analysis of a solar dish micro gas-turbine combined-cycle power plant. *Energy procedia*, 69:1089–1099, 2015.

[6] Antonio L Avila-Marin, Jesus Fernandez-Reche, and Felix M Tellez. Evaluation of the potential of central receiver solar power plants: configuration, optimization and trends. *Applied energy*, 112:274–288, 2013.

[7] Omar Behar. Solar thermal power plants–a review of configurations and performance comparison. *Renewable and Sustainable Energy Reviews*, 92:608–627, 2018.

[8] FJ Cabrera, A Fernández-García, RMP Silva, and M Pérez-García. Use of parabolic trough solar collectors for solar refrigeration and air-conditioning applications. *Renewable and sustainable energy reviews*, 20:103–118, 2013.

[9] Mattia Cagnoli, Laura Savoldi, Roberto Zanino, and F Zaversky. Coupled optical and cfd parametric analysis of an open volumetric air receiver of honeycomb type for central tower csp plants. *Solar Energy*, 155:523–536, 2017.

[10] Vivid Economics et al. State and trends of carbon pricing 2017. 2017.

[11] F Eddhibi, M Ben Amara, M Balghouthi, and A Guizani. Optical study of solar tower power plants. In *Journal of Physics: Conference Series*, volume 596, page 012018. IOP Publishing, 2015.

[12] General Electric. *document heat balance CCA22915NG: 7F.05 on NG at Base Load. Supp. Firing ON to HP Drum Limit, No Let down. 50 MJ/s of Solar*, May 2016.

[13] Clifford K Ho and Brian D Iverson. Review of high-temperature central receiver designs for concentrating solar power. *Renewable and Sustainable Energy Reviews*, 29:835–846, 2014.

[14] Thermoflow Inc. Matching a vendor's hrsg in thermoflex. `https://www.thermoflow.com/ppt/Vendor\%20Matching/Matching\%20Vendor\%20HRSG\%20in\%20TFX.ppsx`, may 2018.

[15] Initec Energia. *document DUB-04-WTB-BC-IEM-054_2: Solar steam generator*, February 2017.

[16] Bruce Kelly, U Hermann, and M Hale. Optimization studies for integrated solar combined cycle systems. *Solar Engineering*, pages 393–398, 2001.

[17] M. Lejeune and A. Gérard. Modélisation et étude de cycles thermiques via la création d'un outil de simulation informatique, 2016.

[18] Yuanyuan Li and Yamin Xiong. Thermo-economic analysis of a novel cascade integrated solar combined cycle system. *Energy*, 2017.

[19] P. Billuart M. Duponcheel, G. Winckelmans. Lecture notes in fluid mechanics about heat exchangers, 2016.

[20] Giovanni Manente, Sergio Rech, and Andrea Lazzaretto. Optimum choice and placement of concentrating solar power technologies in integrated solar combined cycle systems. *Renewable Energy*, 96:172–189, 2016.

[21] J. Martin and P. Wauters. *Installations thermiques motrices: Analyse énergétique et exergétique*. Cours universitaires. Presses universitaires de Louvain, 2009.

[22] James McCalley. Cost of wind. `home.engineering.iastate.edu/~jdm/wind/CostOfWind.ppt`.

[23] Graham J Nathan, Mehdi Jafarian, Bassam B Dally, Woei L Saw, Peter J Ashman, Eric Hu, and Aldo Steinfeld. Solar thermal hybrids for combustion power plant: A growing opportunity. *Progress in Energy and Combustion Science*, 2017.

[24] Richard Petela. Exergy of undiluted thermal radiation. *Solar Energy*, 74(6):469–488, 2003.

[25] Guy Polonsky and Abraham Kribus. Performance of the solar hybrid stig cycle with latent heat storage. *Applied Energy*, 155:791–803, 2015.

[26] Kody M Powell, Khalid Rashid, Kevin Ellingwood, Jake Tuttle, and Brian D Iverson. Hybrid concentrated solar thermal power systems: A review. *Renewable and Sustainable Energy Reviews*, 80:215–237, 2017.

[27] Santanu Pramanik and RV Ravikrishna. A review of concentrated solar power hybrid technologies. *Applied Thermal Engineering*, 127:602–637, 2017.

[28] T Prosin, T Pryor, C Creagh, L Amsbeck, and R Buck. Hybrid solar and coal-fired steam power plant with air preheating using a centrifugal solid particle receiver. *Energy Procedia*, 69:1371–1381, 2015.

[29] Simone Semprini, David Sanchez, and Andrea De Pascale. Performance analysis of a micro gas turbine and solar dish integrated system under different solar-only and hybrid operating conditions. *Solar Energy*, 132:279–293, 2016.

[30] Thomas TD Tran and Amanda D Smith. Incorporating performance-based global sensitivity and uncertainty analysis into lcoe calculations for emerging renewable energy technologies. *Applied Energy*, 216:157–171, 2018.

[31] Jan Vermeir. explanations about the lcoe.

[32] Qin Yan, Eric Hu, Yongping Yang, and Rongrong Zhai. Evaluation of solar aided thermal power generation with various power plants. *International Journal of Energy Research*, 35(10):909–922, 2011.

[33] HL Zhang, Jan Baeyens, J Degrève, and G Cacères. Concentrated solar power plants: Review and design methodology. *Renewable and Sustainable Energy Reviews*, 22:466–481, 2013.

[34] Maolong Zhang, Xiaoze Du, Liping Pang, Chao Xu, and Lijun Yang. Performance of double source boiler with coal-fired and solar power tower heat for supercritical power generating unit. *Energy*, 104:64–75, 2016.

[35] Yawen Zhao, Hui Hong, Xiaosong Zhang, and Hongguang Jin. Integrating mid-temperature solar heat and post-combustion co2-capture in a coal-fired power plant. *Solar energy*, 86(11):3196–3204, 2012.

Rue Archimède, 1 bte L6.11.01, 1348 Louvain-la-Neuve www.uclouvain.be/epl